A polarimetric study of ETA carinae and the carina nebula

T. F. Carty

A POLARIMETRIC STUDY OF ETA CARINAE

AND

THE CARINA NEBULA

BY

T.F. CARTY

A thesis submitted to the University of Durham for the degree of Doctor of Philosophy

April 1979

ABSTRACT

This thesis contains an account of some of the work undertaken by the author while a member of the Astronomy Group at the University of Durham. The work of the group involves the measurement and interpretation of the linear polarization in nebular astronomical objects.

The initial chapters briefly describe the theory of polarized light and the method of observing linear polarization, along with an indication of the techniques involved when analyzing the data.

Chapter three is a review of recent work on interstellar grains with a summary of the present ideas on the nature of the grains.

The next chapter summarizes the observations of the peculiar object η Carinae and in the following chapter, a polarization map of the nebulosity around η Carinae is presented and a model determined to account for the observed linear polarization. The model involves the assumption of a bipolar type geometry for η Carinae with a size distribution of silicate grains of the form

$$n(a) = \exp\left\{ -\left[a/0.022\right]^{0.85} \right\}$$

and it is found that grains of .15μ contribute most to the scattering at optical wavelengths. Using the same distribution it is found that maximum emission at 10μ can be expected from grains of size .1μ .

The final chapter contains observations of the linear polarization in the Carina Nebula in the region of η Carinae, and the results are interpreted in the light of present ideas concerning η Carinae and its relationship with the Carinae Nebula. It seems that the light from η Carinae is being reflected by clouds in the Carina Nebula.

CONTENTS

INTRODUCTION

"Spurred by discoveries of elliptical polarization, by the combination of photometry and polarimetry, by the introduction of new computers and instruments, including those on spacecraft and by the growing realization of the usefulness of these techniques when supported by well-developed interpretive theories " (Gehrels, 1974) there has, in recent years, been a wave of activity in polarimetry.

With most astronomical problems, there are many parameters to solve. For example, the geometry and aspect of a reflecting object with respect to the light source must be determined or assumed and this may be complicated by a dependence on wavelength as in the case of planetary atmospheres where penetration depends on the wavelength of the incident and emergent light. Also dependent on the wavelength is the complex refractive index and the number of scatterers or optical depth of atmosphere. Distribution of sizes and shapes of particles must also be determined and whether or not they are preferentially aligned.

In order to solve for all these parameters many independant phenomena must be observed. Since the object is extremely remote, solution of the astronomical problem requires that observations of the light emitted or reflected by the body be made in the fullest detail, and hence the need for light scattering theories is obvious.

From the beginning the development of light scattering theories has been linked with astronomy. Computations on the radiation pressure exerted on perfectly conducting spheres were made before 1900 in order to explain the theory of comet tails. Since 1930 much attention has been paid to the optical properties viz scattering and/or extinction of interstellar grains. Later work on scattering by cylinders was aimed at explaining interstellar polarization.

Laboratory work in formulating physical and chemical theories of the properties of such grains in the ambient gas and radiation field have complemented the basic data which should be obtained over as many parameters as possible. Therefore, results of radioastronomy, spectroscopy, photometry, radial velocity studies, and direct photographs and visual observations should be added to those of polarimetry over as large a range of wavelengths and phases as possible.

This is especially important in objects such as the Carina Nebula which present strikingly different appearances at different wavelengths. Also in η Carinae, where previous observations have suggested a particular geometry and grain type as the nature of the scattering particle, present polarimetric observations may allow the determination of a size distribution of grains, but future polarimetric observations along with techniques previously mentioned, at different wavelengths, will be very important in completely determining the nature of this peculiar object.

CHAPTER 1

POLARIZED LIGHT

1.1 WAVE POLARIZATION

Light is a superposition of many electromagnetic waves, each exhibiting transverse, sinusoidal vibrations, and satisfying Maxwell's Equations. The direction and amplitude of each wave is characterized by its electric field vector $\underline{E}$ and its magnetic field vector $\underline{H}$.

C.G. Stokes (1852) was the first to investigate in detail the phenomenon of 'polarized', as opposed to 'natural' light. He defined natural light as :-

> 'Light which is incapable of exhibiting rings of any kind when examined by a crystal of Iceland spar and an analyzer or by some equivalent combination'.

This is equivalent to saying that, on average, natural light has no preferred orientation for the direction of its E vector.

Polarized light, on the other hand, arises when the direction of vibration of the light is restricted in some manner from its natural randomness.

Plane polarization arises when the vibrations are confined to one plane. When the plane of polarization of polarized light rotates with time, and the amplitude of vibration varies, elliptical polarization occurs. If the amplitude of vibration of elliptically polarized light remains the same, the light is said to be circularly polarized. Mixtures of these different polarizations are found in nature.

1.2 THE STOKES' PARAMETERS

The polarization of a beam of light may be completely characterized by four vectors : I, Q, U and V, which were introduced by C.G.Stokes (1852) as follows :-

'When any number of independent polarized streams of given refrangibility are mixed together, the nature of the mixture is completely determined by the values of four constants which are certain functions of the intensities of the streams, and of the azimuths and eccentricities of the ellipses by which they are respectively characterized, so that any two groups of polarized streams which furnish the same values for each of these four constants are optically equivalent'.

An extension of this is the 'Principle of Equivalence' which states that it is impossible by means of any instruments to distinguish between various incoherent sums of electromagnetic waves that may together form a beam with the Stokes' Parameters (I, Q, U, V).

Hence, there is only one kind of natural light with (I, Q, U, V) = (1, 0, 0, 0) which theoretically may be composed of waves in an infinite variety of ways.

The essential property of the Stokes' Parameters is their additivity in the superposition of two independent beams of light, corresponding to the absence of any interference.

The first parameter I represents the flow of energy per unit area, that is, the intensity of the beam. The other parameters have the same dimension.

The second parameter Q is a measure of the horizontal preference displayed by the E-vector. That is, it is a measure of the difference between polarization forms horizontal and vertical ($\leftrightarrow$ - $\updownarrow$). Hence Q will be positive for a preferential horizontal polarization form, negative for the reverse and zero if no preference is shown.

The third parameter U indicates the preference between directions $+45^{\circ}$ and -45° ($\nearrow$ - $\nwarrow$) being positive for polarization forms closer to $+45^{\circ}$ than -45°.

Q and U define an angle θ, relating to the direction of linear polarization, or the azimuth of the major axis of elliptical polarization, such that

$$\tan 2\theta = \frac{U}{Q}$$

The fourth parameter V describes the sense of the elliptical polarization being positive for right-handed forms, negative for left-handed forms, and zero for linear forms.

As measurable intensities refer to a superposition of many simple waves, with independent phases, the Stokes' Parameters of an entire beam of light are given by the sums

$$I = \sum_i Ii, \quad Q = \sum_i Qi, \quad U = \sum_i Ui, \quad V = \sum_i Vi$$

where the index 'i' denotes each simple independent wave.

1.3 THE POLARIZATION ELLIPSE

Consider a plane wave travelling in the z-direction with components of oscillation in the x-and y- directions given by

$$Ex = a_1 \cos(\omega t - \beta z) \tag{1.1}$$

$$Ey = a_2 \cos(\omega t - \beta z + \delta) \tag{1.2}$$

a_1 and a_2 represent the amplitudes of the two vibrations, $\omega/2\pi$ the frequency and δ the phase difference.

Equations 1.1 and 1.2 describe two linearly polarized waves, one polarized in the x-direction, the other in the y-direction.

Combining the two equations vectorially the resultant field is

$$\underline{E} = \hat{x}\, Ex + \hat{y}\, Ey$$

i.e. $$\underline{E} = \hat{x} a_1 \cos(\omega t - \beta z) + \hat{y}\, a_2 \cos(\omega t - \beta z + \delta)$$

At $z = 0$, equations 1.1 and 1.2 reduce to

$$Ex = a_1 \cos\omega t \tag{1.3}$$

$$Ey = a_2 \cos(\omega t + \delta) \tag{1.4}$$

From 1.3

$$\cos \omega t = \frac{Ex}{a_1}$$

which implies that

$$\sin \omega t = \sqrt{1 - \frac{Ex^2}{a_1}}$$

Expanding equation 1.4 and eliminating time gives

$$\frac{Ex}{a_1^2} - \frac{2ExEy}{a_1 a_2}\cos\delta + \frac{Ey^2}{a_2^2} = \sin^2\delta$$

$$\text{or} \quad aEx^2 - bExEy + cEy^2 = 1$$

$$\text{where} \quad a = \frac{1}{a_1^2 \sin^2\delta}, \quad b = \frac{2\cos\delta}{a_1 a_2 \sin^2\delta}, \quad c = \frac{1}{a_2^2 \sin^2\delta}$$

This represents the equation of an ellipse

Therefore,

$$\underline{E} = \hat{x}\, Ex + \hat{y}\, Ey$$

represents the general case of elliptical polarization ; the locus of the tip of the vector $\underline{E}$ describing an ellipse

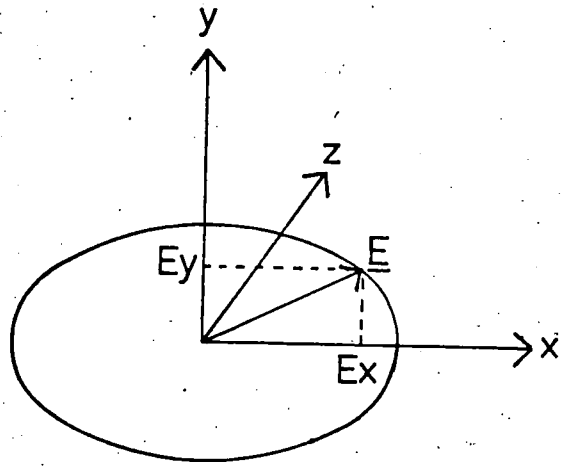

Fig. 1.3 - The Polarization Ellipse

The Stokes' Parameters are defined by

$$I = a_1^2 + a_2^2$$

$$Q = a_1^2 - a_2^2$$

$$U = 2a_1a_2\cos\delta$$

$$V = 2a_1a_2\sin\delta$$

It can be seen that

$$I^2 \geq Q^2 + U^2 + V^2,$$

the equality only being true for completely polarized beams.

1.4 DETERMINATION OF THE STOKES' PARAMETERS

Suppose that a beam of monochromatic light is observed after passing through a polarizer, orientated at an angle θ to the positive x-direction (Fig.1.4).

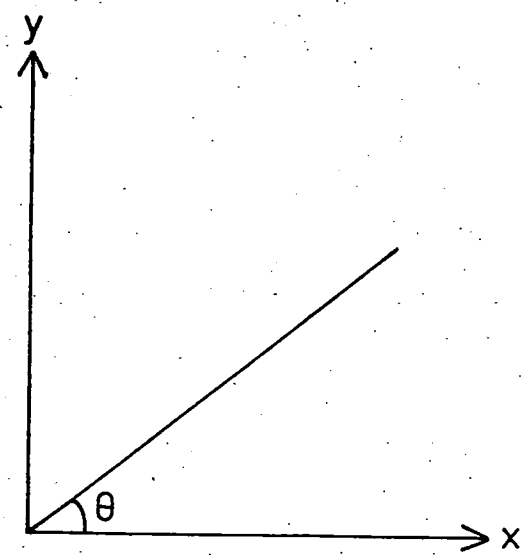

Fig. 1.4 - Illustrating Notation

The component of the electric vector in the θ-direction is given by

$$E(\theta) = Ex\cos\theta + Ey\sin\theta \qquad (1.5)$$

so that

$$I(\theta) = E(\theta) \cdot E^{*}(\theta)$$

i.e. $$I(\theta) = Jxx\cos^2\theta + Jyy\sin^2\theta + Jxy\cos\theta\sin\theta + Jyx\sin\theta\cos\theta \qquad 1.6$$

where $$J = \begin{vmatrix} ExEx^{*} & ExEy^{*} \\ EyEx^{*} & EyEy^{*} \end{vmatrix} = \begin{vmatrix} a_1^2 & a_1a_2e^{i\delta} \\ a_1a_2e^{-i\delta} & a_2^2 \end{vmatrix}$$

These elements may be determined quite simply from a set of convenient measurements for θ. For example, θ = 0°, 45°, 90°, 135°.

Substituting these values for θ in equation 1.6, it may be seen that

$$I\ (0^{o}) = Jxx = a_1^{2}$$

$$I\ (45^{o}) = Jxy/2 + Jyx/2$$

$$I\ (90^{o}) = Jyy = a_2^{2}$$

$$I\ (135^{o}) = -Jxy/2 - Jyx/2$$

Combining $I\ (45^{o})$ with $I\ (135^{o})$:

$$I\ (45^{o}) - I\ (135^{o}) = Jxy + Jyx = 2\ a_1 a_2 \cos\delta$$

The Stokes Parameters may be extracted from these equations thus :

$$I = I\ (0^{o}) + I\ (90^{o})$$

$$Q = I\ (0^{o}) - I\ (90^{o})$$

$$U = I\ (45^{o}) - I\ (135^{o})$$

with the orientation of the polarization vector given by

$$\theta = \frac{1}{2} \tan^{-1} U/Q$$

Consideration of the imaginary parts of Jxy and Jyx arising when the y-component of the light is retarded with respect to the x-component is necessary for the evaluatkon of V. In the present case V = O, and the light is plane polarized.

References:

Axon, D J (1977) Thesis, University of Durham.

Born, M, Wolf E (1965) 'Principles of Optics' (Pergamon Press)

Perrin F (1942) J. Chem. Phys. 10 415.

Shurcliffe W A, 'Polarized Light' (Harvard University Press, Oxford University Press).

Stokes, C G (1852) Trans. Cambridge Phil. Soc., 9.

Van der Hulst, H C (1957) 'Light Scattering by Small Particles' (New York, John Wiley & Sons, Inc).

CHAPTER 2

THE NEBULAR POLARIMETER AND REDUCTION TECHNIQUE

2.1 INTRODUCTION

The data discussed in this thesis was obtained at the f/15 focus of the 3.9m Anglo-Australian Telescope in January 1978 and at the f/15 focus of the 1.0m S.A.A.O. Telescope in July 1978 by Scarrott and Warren-Smith.

Analysis of the states of polarization of the light from an astronomical object by the polarimeter results in the production of a linear polarization map of the object. The information is recorded by an electronographic camera. Sufficient data to produce a complete polarization map is contained in eight exposures or electronographs.

2.2 THE NEBULAR POLARIMETER

The nebular polarimeter, developed by Scarrott, Bingham and Axon, is of the Pickering-Appenzeller kind, having a Wollaston prism and rotatable half-wave plate, based on a design by Öhman (see Axon 1977 for further details)

Light passing through the telescope enters the polarimeter and is divided by means of a Wollaston Prism, into two orthogonal components, polarized perpendicularly to each other. In order that these two orthogonal polarizations may be recorded simultaneously, one half of the field of view of the polarimeter is "blocked out" by a series of grids. The plane of polarization of the light is altered by changing the orientation of the $\lambda/2$ plate, which rotates the plane of polarization by twice its own angle

Figure 2.21 shows the path of a light say through the optical components of the polarimeter, the properties of which are summarized in table 2.2A.

2.3 THE ELECTRONOGRAPHIC CAMERA

The 4cm electronographic image tube was developed by Dr.D.McMullen at the Royal Greenwich Observatory. The main features are shown in figure 2.31.

Figure 2.21 RAY DIAGRAM OF POLARIMETER

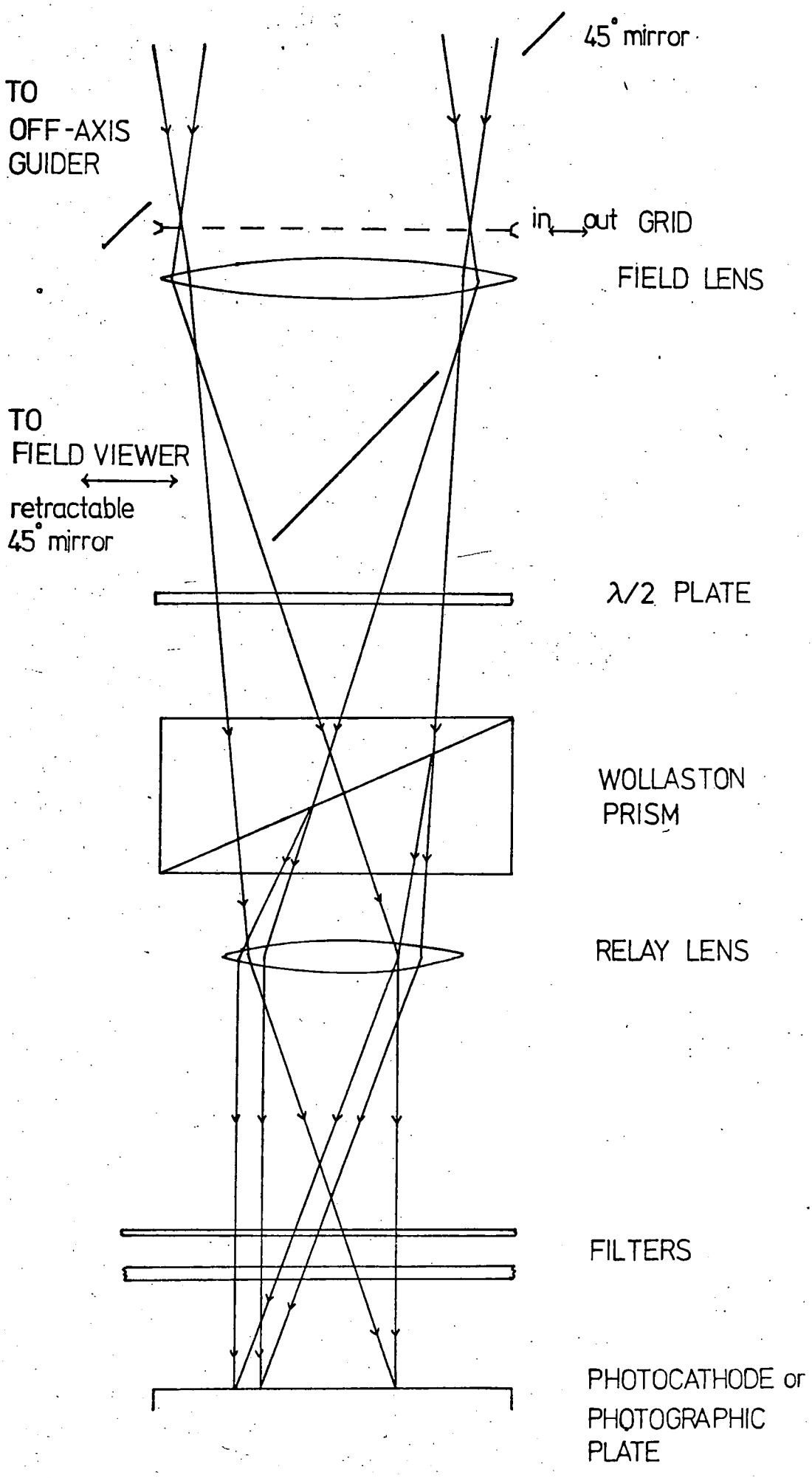

TABLE 2.2A

Function and Properties of the Optical Components of the Polarimeter

Component	Function	Construction/Properties
45° Mirror	Detachable off-axis guider.	Aluminized perspex (used on SAAO telescope)
Grids	To block out one half of the field of view in alternate strips	Black coated perspex which eliminates edge effects
Field lens	To constrain all light to pass through optical system	20 cm focal length f/4 achromatic doublet
Grid viewing mirror	Enables object to be placed centrally in the field	Aluminized perspex
Half-wave plate	Rotates plane of polarization of incident linearly polarized light	Magnesium fluoride and quartz Achromatic in range 4500 - 6800 Å
Wollaston Prism	Separates light into two orthogonal polarizations	Quartz cemented 4 cm width. 1° divergence
Relay lens	Used to focus grids accurately onto photocathode ; introduces 4 x de-magnetization between telescope and photo-cathode and a similar gain in speed	Nikon f/1.4 50 mm bloomed
Filters	To define wavelength range of light reaching photocathode	AAT. Broad V(4800-6400 Å) SAAO. V(5500 ± 500 Å)

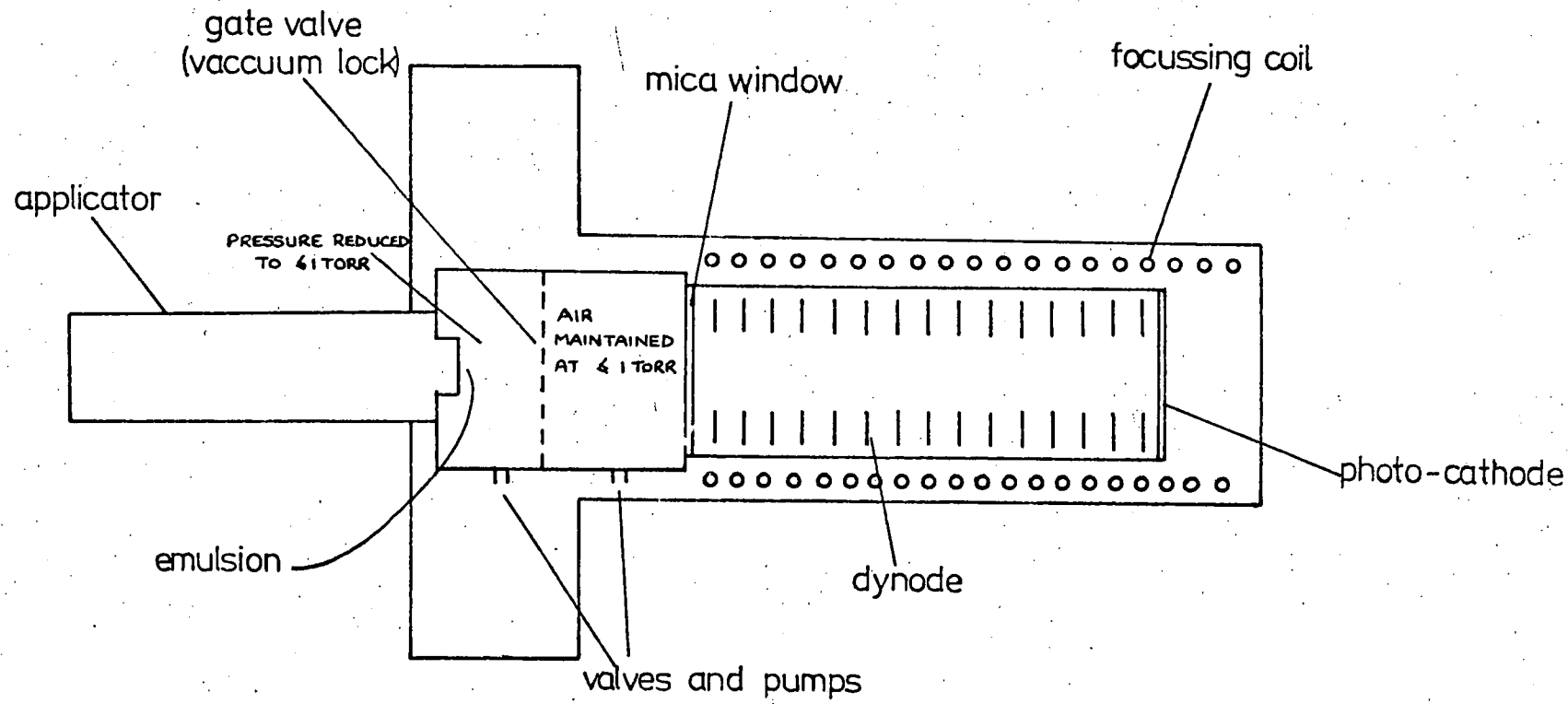

Figure 2.31 THE MAIN FEATURES OF THE ELECTRONOGRAPHIC IMAGE TUBE

Light, passing through the telescope, analyzed by the polarimeter is brought to a focus at the photocathode of the electronographic image tube. Photons, incident on the photocathode eject electrons (with 20% efficiency) which are accelerated down the tube by an assembly of electrodes of uniform potential gradient. A magnetic field brings the electrons to a focus at the nuclear emulsion situated behind the mica window. Reciprocity failure is negligible, and since the emulsion is linear, density being proportional to exposure in the range of interest, calibration of the plates is unnecessary.

Detailed descriptions of the electronographic camera are given elsewhere (McMullen et al, 1972, McMullen 1972).

The air on the output side of the mica window, which is 40mm in diameter and 4μm thick is kept at 1 torr or less by a mechanical pump. The nuclear emulsion on melinex (50μm thick) is mounted in the film holder and brought up to the mica by the pneumatic actuator through the gate valve which acts as a vacuum lock ; the valve is opened only when the pressure on the film side has been reduced to below 1 torr. The emulsion is brought into intimate contact with the mica by pressurizing the space behind the film holder with nitrogen at 10 torr. All the operations viz pumping down the film holder, opening the gate valve, bringing forward the film and pressurizing to 10 torr, are carried out by an automatic electro-pneumatic system. Film can be changed in 2-3 minutes.

2.4 REDUCTION OF THE DATA

In order to obtain a linear polarization map, eight electronographs are necessary for each object, four corresponding to position "grids in" and four to "grids out". The characteristics of the polarization of one half of a field of view (i.e. grids in or grids out) are displayed in figure 2.41.

The plates are digitized in 24 μ pixels with a 25μ step using the PDS microdensitometer at the Royal Greenwich Observatory, forming 512 x 512 matrices of intensities which are stored in the computer. A typical electronograph is shown in figure 2.42.

ORIENTATION OF E-VECTOR WITH ROTATION OF $\lambda/2$ PLATE

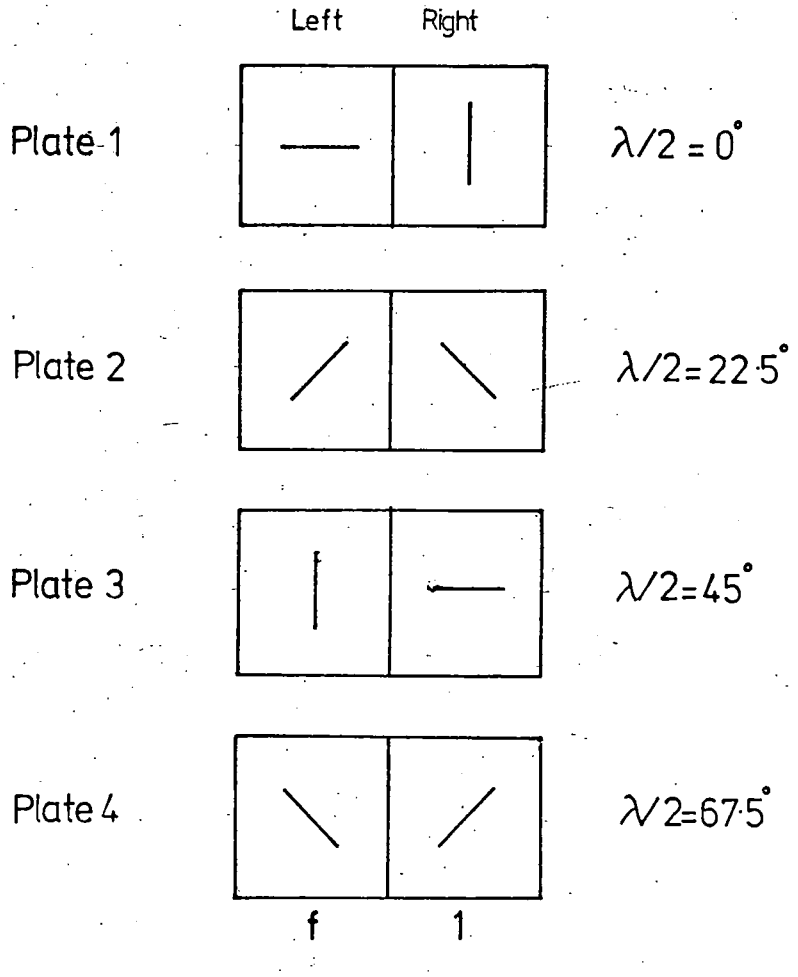

Figure 2.41

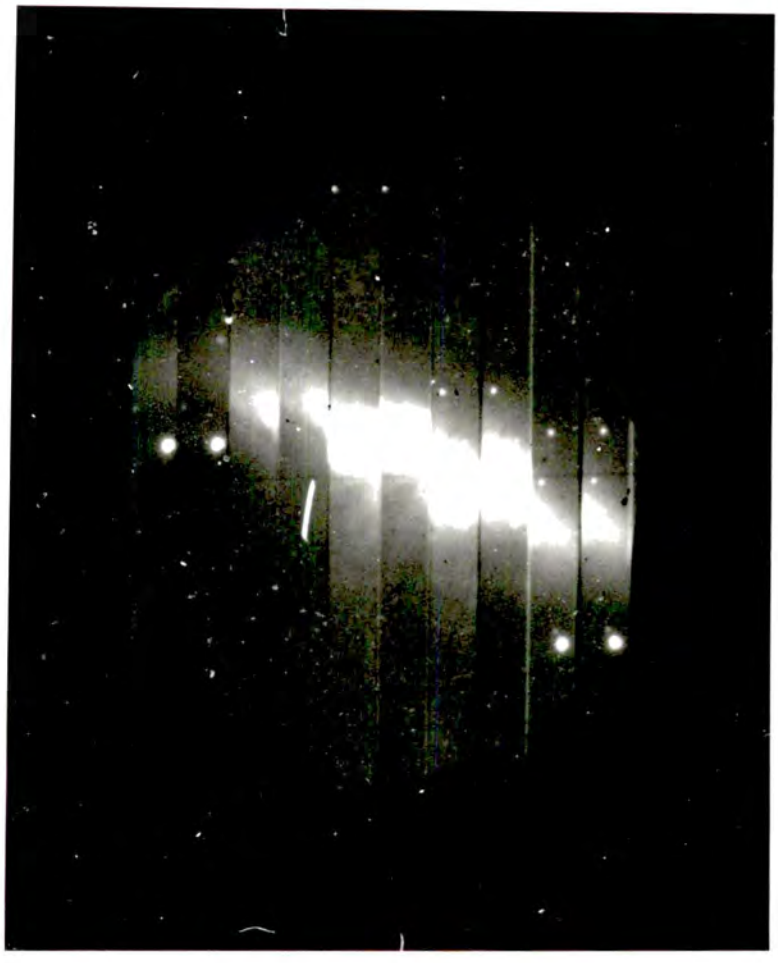

Figure 2.42 A typical electronograph

Full details of the alignments of the plates, the reduction in size of the 512 x 512 matrices, the necessary corrections to be applied to the data and the calculation of the Stokes' Parameters will be found in Warren-Smith's thesis (1979). A brief discussion of the corrections, calculation of polarization, and error estimates, follows.

2.4.1 Clear Plate Subtraction

From figure 2.43 it can be seen that, in order to obtain the signal from an astronomical object alone, it is necessary to subtract a clear plate signal and a sky signal from the data.

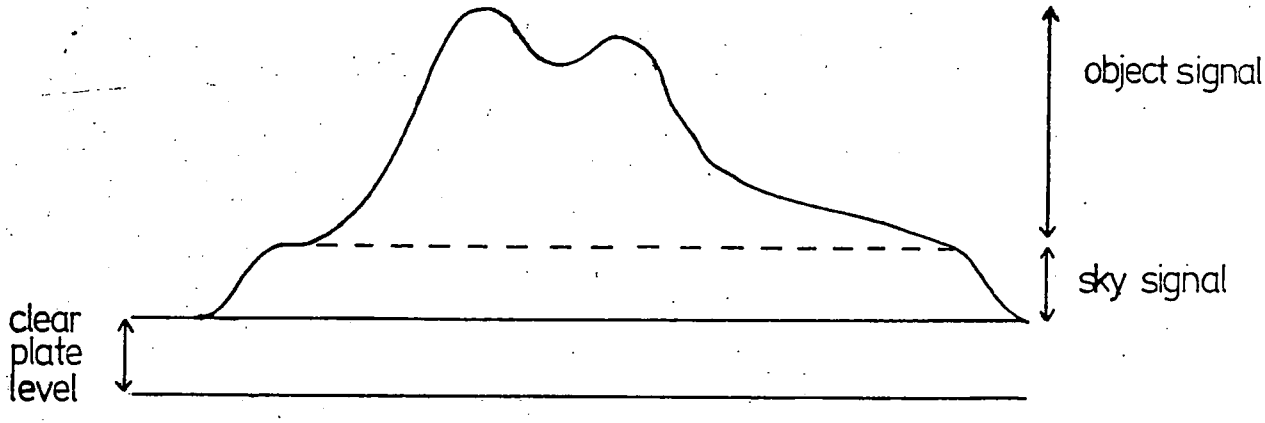

Fig. 2.43 - Intensity Profile from an Electronograph

Upon digitization, the plates are raster-scanned in the x-direction. Hence any fluctuations in the zero level of the microdensitometer will be discernible in the y-direction, the time scale being large compared with that of x-scans.

Traces of the intensity down the plate are obtained for clear plate

either side of the exposed region. The average of the two estimates is subtracted for each y-value.

2.4.2 Photocathode Correction

The effect of the non-uniformity of the photocathode in response to the incoming signal must be removed from the data. This is achieved by investigating the variation in intensity from a uniform source of light, e.g. the night sky, across the field. Four plates are taken, corresponding to the four positions of the $\lambda/2$ plate. The intensities on each plate are first essentially smoothed by normalizing the plates with respect to each other so that equal intensities are obtained. Then the intensity for every point in each left-hand strip is compared with the average intensity for all points in all left-hand strips, a relative sensitivity factor for every point hence being obtained. This is repeated for the right-hand strips. The relative sensitivity factors for the photocathode so obtained are used to correct the object data.

The experimental technique is such that each component of polarized light is measured twice (see figure 2.41). This gives a measure of the consistency of the results and provides not only facility for obtaining the relative response between left-hand and right-hand strips, but also for obtaining the relative exposures between the plates, both of which are again used to correct the data.

2.4.3 Sky Subtraction

Since the sky is recorded simultaneously with the object, the sky intensity may be obtained by finding the average intensity of regions of the plate where there is no signal from the object, for both left and right-hand strips, and may be subtracted accordingly.

2.4.4 Filtering of the Data

The intensities I1 $\rightarrow$I8 may be expressed in the form

$$I_i = I + Q\cos 2\theta + U\sin 2\theta$$

where I_i represents I1 → I8 and I, Q, U, and θ are defined in Chapter 1.

This double sine curve constructed from the intensities I1→ I8 (from the four plates) is now optimized using a "search" programme, until the best fit with the data is obtained. For a particular density, the average dispersion of points from the curve is obtained, and any point with dispersion greater than the average is rejected. This process is repeated iteratively five or six times for each set of eight intensities, i.e. for every pixel.

2.4.5 Calculation of the Stokes' Parameters

Once the data has been filtered the intensities are integrated over x x y pixels with spacings in x and y of Δx and Δy.

A double sine curve is now fitted to these integrated intensities, I1 → I8 and is again optimized to give the most accurate values possible for the Stokes' Parameters. The form of output is shown in the Appendix.

2.4.6 Errors

Ideally, the precision of the polarimetric measurements should be limited only by the quantum noise, i.e. by the fluctuations in the number of incident protons. In practice, however, this is never achieved.

Various systematic errors are produced by the optics of the polarimeter and telescope, the non-uniformity of the photocathode and the imperfections in the nuclear emulsion of the film. Random errors are introduced by the quantum noise and the digitization procedure.

Errors due to the component optics of the system have been shown to be negligible when working at a level of 1% polarization (Axon, 1977) by tests on standard polarized stars.

Systematic errors can be found by comparing the signal recorded on different electronographs since, as noted in section 2.4.2, each component intensity is effectively measured twice.

The random errors on the two-dimensional signal are estimated from the dispersion of individual measurements about a smoothed 2nd order surface

fitted locally to the recorded density (Warren-Smith, 1979).

The errors on the recorded signals lead directly to the errors on the Stokes' Parameters (since the recorded signals after various corrections combine to give I, Q, and U) which in turn transmit them to the degree and angle of polarization.

References:

Axon, D J (1977) Ph.D. Thesis, University of Durham.

Elvius, M (1974) M.Sc. Thesis, University of Durham.

McMullen, D (1972) Proc. ESP/CERN Conference, Geneva.

McMullen, D, Powell, J R, Curtis, N A (1972) Adv. E.E.P. 33A 37.

Serkowski, K (1974) Methods of Experimental Physics, Vol.12. Part 8.

Warren-Smith, R (1979) Ph.D. Thesis, University of Durham.

CHAPTER 3

INTERSTELLAR DUST GRAINS

3.1 INTRODUCTION

As early as 1784, visual recordings of dark and bright nebulae were made by Sir William Herschel who catalogued thousands of nebulae, some of which later were found to be distant galaxies.

Long exposure photographs of the Milky Way revealed conspicuous dark patches and striations against a background of more or less uniform star fields, and a debate as to whether these dark patches were due to obscuring clouds, or to holes in the distribution of stars followed. The answer came in the 1930's when statistical analyses of star counts through dark patches established the existence of optical obscuration.

The determination of the nature of this 'optical obscuration' now known to be in the form of dust grains, still remains an important field of research for astronomers.

3.2 INTERSTELLAR EXTINCTION

The observed intensity of starlight, seen at wavelength λ can be written as

$$I(\lambda) = I_o(\lambda) \exp\left(- N\pi a^2 Q_{ext}(a,\lambda)\right) \qquad (3.1)$$

where $I_o(\lambda)$ denotes the intrinsic intensity of the star, N the grain density, πa^2 the geometrical cross-section and Q_{ext} the efficiency factor for extinction of the grains.

Defining the optical depth as

$$\tau = N\pi a^2 Q_{ext}(a,\lambda) \qquad (3.2)$$

the familiar equation of transfer is obtained

$$I(\lambda) = I_o(\lambda) e^{-\tau} \qquad (3.3)$$

In terms of magnitudes

$$\Delta m(\lambda) = 1.086 \int_0^\infty \pi a^2 Q_{ext}(a,\lambda)\, n(a)\, da \qquad (3.4)$$

where $\Delta m(\lambda)$ denotes the attenuated light at wavelength λ and the grainsize distribution n(a) has now been integrated over.

The absolute magnitude $M(\lambda)$ is defined as the apparent magnitude of a star in the absence of absorption at a distance of 3×10^{19} cm. For a given set of wavelengths λ_i, a set of monochromatic apparent magnitudes $m(\lambda_i)$ may be determined for a star, related to the absolute magnitude $M(\lambda_i)$ by the equation

$$m(\lambda_i) = M(\lambda_i) - 5 + 5 \log_{10} D + A(\lambda_i) \qquad (3.5)$$

where D is the distance of the star in parsecs and $A(\lambda_i)$ is the interstellar extinction in magnitudes at wavelength λ_i. This follows by simply taking account of the inverse square law attenuation together with the extinction.

Colour indices (i-j) are defined as the difference in stellar magnitudes between the two wavelengths λ_i, λ_j. The observed (i-j) colour of a star is then related to the corresponding intrinsic colour from equation (3.5) by

$$(i - j)_{obs} = (i - j)_{intr} + A(\lambda_i) - A(\lambda_j) \qquad (3.6)$$

Colour excesses E_{i-j} are defined by

$$E_{i-j} = (i - j)_{obs} - (i - j)_{intr} \qquad (3.7)$$

From equation (3.6)

$$E_{i-j} = A(\lambda_i) - A(\lambda_j) \qquad (3.8)$$

Hence equation (3.8) corrects measurable colour excesses with interstellar extinction. If $\lambda_i = \lambda_B$, and $\lambda_j = \lambda_V$ using the UBV system (where the filters

used for each of these bands admit radiation in a range of wavelength about 1000 Å wide with central wavelengths of approximately $\lambda_u \approx$ 3650 Å, $\lambda_B \approx$ 4400 Å , $\lambda_v \approx$ 5480 Å), and with λ_α representing some wavelength α, from equation (3.8)

$$\frac{E_{\alpha - v}}{E_{B - v}} = \frac{A(\lambda_\alpha) - A(\lambda_v)}{A(\lambda_B) - A(\lambda_v)} \tag{3.9}$$

Since E_{B-v} is a directly observable quantity for a given star and $A(\lambda_v)$ is not, the determination of the quantity

$$R = \frac{A(\lambda_v)}{E_{B-v}} \tag{3.10}$$

i.e. the ratio of the total to selective absorption is important, both for a knowledge of total extinction in a given case and for making estimates of stellar distances. Various determinations of R are discussed in Wickramasinghe and Nandy (1972).

If A_v can be measured entirely independently, the resultant value of R can be used to set a limit on the density of large particles producing "grey extinction" in visible light (Spitzer, 1968). Values of R, obtained by different methods are tabulated by Crawford and Mandwewala (1976), the average being $R = 3.2 \pm 0.1$.

The extinction curves of Bless and Savage (1972) are reproduced in figure 3.11 from Aannestad and Purcell (1973). The ultraviolet part of the extinction curve was obtained from OAO-2 observations, and the visual and infrared parts are based on measurements by Johnson (1968).

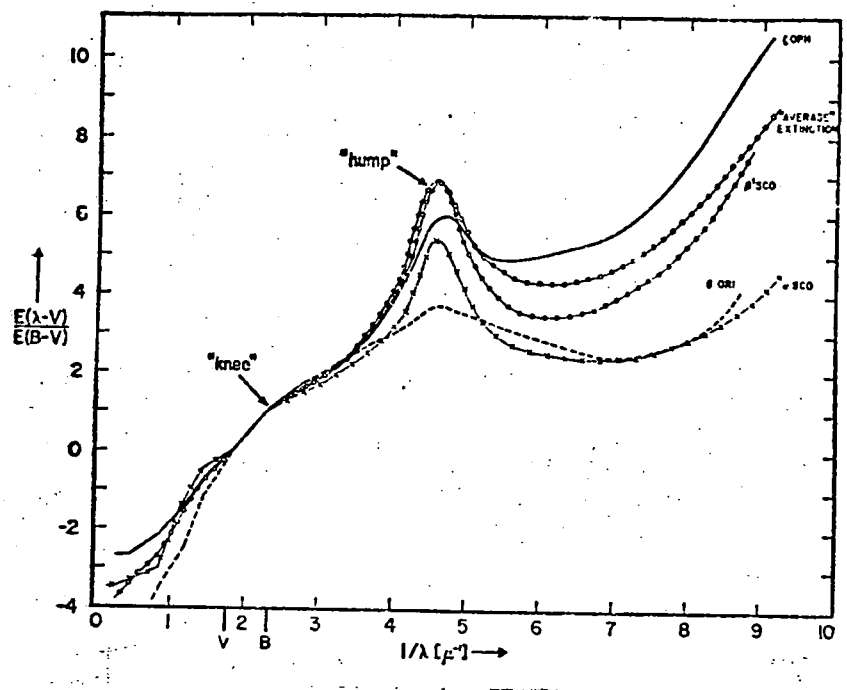

Figure 3.11 Interstellar Extinction Curves from Aannestad and Purcell (1973)

3.2.1 The Ultraviolet Region

From the observations of Bless and Savage (1972) the main features of the ultraviolet extinction curve are found to be : large variations in the ultraviolet extinction from star to star, the greatest variations being in the far-ultraviolet ; a characteristic hump that usually has its maximum at about $4.6\mu^{-1}$, being more pronounced in some objects than in others ; a shallow far-ultraviolet minimum in the region 5,5 - 7.5 μ^{-1} which falls at shorter wavelengths when the far-ultraviolet extinction is smaller ; after the shallow minimum, a rapid rise in the ultraviolet extinction. Nandy et al (1976) have shown that there is no strong variation of the mean extinction curves with galactic position.

3.2.2 Visual Region

In this region, the curve follows a roughly linear $1/\lambda$ law (Stebbins, Huffer and Whitford, 1939). The discontinuity in the slope of the curve at about 2.3 μ^{-1} was first noted by Whitford (1958). Recent observations of Schild (1977) indicate that in no octave of the spectrum is interstellar extinction strictly proportional to $1/\lambda$ and that variations in the interstellar reddening law with galactic longitude are becoming important.

3.2.3 Infrared Region

There are intrinsic differences in the infrared extinction from star to star as indicated in figure 3.11, some of which may imply the presence of circumstellar emission superposed on the stellar contimium. The most important results of the infrared extinction observations have been the discovery of strong absorption bands in the 10μ region and the discovery of the 3.1μ ice-band.

3.2.4 Theoretical Extinction Curves

The existence of a strong absorption peak in the 2200 $\mathring{A}$ region gives great support to the identification of graphite with the ultraviolet extinction hump. Various other types of particle have been proposed, e.g. silicates, quartz, solid hydrocarbons but since silicates are thought to be unlikely due to the severe restrictions on size distribution required to produce the necessary hump, graphite remains the favourite (see Bless and Savage, 1972 and references therein). The most likely cause of the extinction hump is thought to be plasma oscillations in small (mean radius ≃ 0.01μ) nearly spherical uncoated graphite particles. For mean radius > 0.02 μ spherical graphite particles produce broad bumps centred at much larger wavelengths than those observed (Gilra, 1971). If the graphite particles are small compared with the wavelength, then the position of the hump becomes nearly independent of the details of the size distribution of particles which is important because most humps are at $\lambda^{-1} = 4.6\ \mu^{-1}$ and it is unreasonable to suggest that particles have the same size distributions everywhere (Bless and Savage, 1972). However,in other parts of the extinction curve graphite is found to be quite unsatisfactory.

For the optical region, "dirty" ice grains (m = 1.5-0.05i) (see Aannestad and Purcell, 1973), graphite particles surrounded by dielectric ice mantles, mixtures of refractory particles (Wickramasinghe and Nandy,1972) and dielectric whiskers with mantles of polyformaldehyde (Wickramasinghe and Cooke, 1976) have all variously fitted the extinction curve.

In the infrared region the 10μ absorption feature has been identified with silicates although Wickramasinghe (1975) has suggested a possible identification of the 10μ band with polyoxymethylene whiskers.

Dirty ice grains, of radii ∿0.12μ , although fitting the visual extinction cannot reproduce the ultraviolet extinction hump nor the amount of far ultraviolet extinction. Calculations for a two-component size distribution of infinite dielectric cylinders as well as for dirty ice with a small percentage of molecules and metallic compounds give only slight improvements and it seems that dirty ice grains of various shapes, sizes and refractive indices, can be ruled out as the main contributor to interstellar extinction in the ultraviolet. However, combining their own infrared spectrophotometric observations from 2-4μ and 8-13μ , Merrill, Russell and Soifer, (1976) show that ices are common in the interstellar medium, but with small abundances compared with silicates, being confined mainly to molecular cloud regions. From their observations of a heterogeneous group of infrared sources, they conclude that conditions of unshielded interstellar medium do not favour ice growth. These results are in agreement with Knacke et al (1969) whose observations revealed that interstellar grains contain very little ice. Graphite-core and ice-mantle grains again do not give satisfactory agreement in the ultraviolet region of the extinction curve (Wickramasinghe and Nandy, 1972).

As far as mixtures are concerned, extinction calculations performed by Gilra (1971) for a mixture of graphite, meteoric silicate and silicon carbide have proved the "best" fit to the extinction curves, but have the shortcoming of the sensitivity of the extinction hump to variations in the sizes or shapes of the graphite components. Also, it does not embody a realistic wavelength dependent refractive index for the silicate component in the far ultraviolet.

Mixtures of graphite grains of radii 0.065μ and silicate grains of 0.07μ give good agreement with the available extinction data as do mixtures

of graphite, silicate and iron particles of radii 0.05μ , 0.15μ and 0.02μ respectively, using various size distributions (Wickramasinghe and Nandy,1972).

Calculations based on enstatite show that silicate cannot be responsible for the observed visual extinction unless other components different in either composition or size are included (see Aannestad and Purcell, 1973). However, as a result of ultraviolet determinations of optical complex indices of refraction for various silicates, meteoric and iron-sulphide materials, Egan and Hilgeman (1975) suggest the plagioclase felspar bytownite as a suitable material for the interstellar medium having a distribution of particle radii ranging from 0.1 - 0.001 μ.

Day (1976) has produced an amorphous magnesium silicate which could simultaneously account for both infrared and optical extinction. Far infrared properties of these materials suggest that they could supply a significant amount of far-infrared emission observed in such sources as the Orion Nebula.

Wickramasinghe (1975) suggests that, since interstellar formaldehyde has been identified by its 6 cm radio absorption line in over 100 dust clouds, much larger amounts of H_2CO may be present in solid state polymer form as polyoxymethylene whiskers and condensed on interstellar dust grains, and that a significant fraction of all interstellar oxygen and carbon may be locked up as polyoxymethylene. With the exception of H_2 and CO, H_2CO is probably the most abundant gaseous molecule in the interstellar medium. Hence (Wickramasinghe and Cooke, 1976) the case for polymerization and the formation of mantles of polyformaldehyde is as strong as that for the formation of ice-mantles on refractory grains. Apparently whiskers of radii 10^{-5} cm would explain the available data on interstellar extinction in the waveband range 3500 $\mathring{A}$ - 1 μ , and a comparable mass of smaller uncoated graphite and silicate grains is needed in the far ultraviolet.

In general, the gross features of the extinction curve may be easily but not uniquely reproduced by a mixture of grains of which small graphite particles are one component, but where otherwise only a bimodal distribution

of dielectric grains is needed. The larger grains may account for extinction in the visible and infrared regions, whilst the smaller grains cause increasing extinction in the ultraviolet (Aannestad and Purcell, 1973).

3.3 INTERSTELLAR POLARIZATION

Since the discovery of interstellar polarization by Hall (1949) and Hiltner (1949), there has been a massive accumulation of polarimetric observations (see Aannestad and Purcell 1973 for a review of observations).

The results of the survey by Mathewson and Ford (1970) are generally interpreted in terms of a galactic magnetic field, aligning elongated dust grains by the Davis-Greenstein mechanism. Polarization arises because extinction is greatest for the vibration of the electric vector of the light in the plane parallel to the long axis of the cylinder. Since the grains are oriented such that their long dimension is transverse to the field, the implication is that the plane of polarization of the light will be parallel to the galactic magnetic field, which has proved to be the case (Mathewson and Ford 1970).

The results of surveys by Serkowski, Mathewson and Ford (SMF) (1975) and by Coyne, Gehrels and Serkowski (CGS) (1974) indicate that the interstellar polarization curve as a function of wavelength for all stars can be fitted by a unique function with one free parameter - the wavelength of maximum polarization (λ_{max}). The values of λ_{max} are found to be concentrated within the range 5000 Å - 6000 Å, λ_{max} for a few stars being greater than this. SMF suggest that λ_{max} is proportional to the average size of interstellar dust grains producing both extinction and polarization. λ_{max} is in fact found to be proportional to the mean grain size, multiplied by (n-1) where n is the refractive index of the grains (Cohen 1977). CGS find that models of dielectric cylinders, with Davis-Greenstein orientation mechanism fit the results.

It has been suggested that Davis-Greenstein alignment in the interstellar medium is not efficient enough unless the grains possess special

properties such as ferromagnetism (see Aannestad and Purcell 1973). Purcell (1975) has proposed a "pinwheel theory" in which surface "rockets" spin the grains up to high speeds, so that more complete alignment is achieved in a weak magnetic field. In fact, direct observational evidence from 10μ polarization measurements in Orion (Dyck and Beichmann 1974) indicates that ordinary silicate grains can be aligned, but recent calculations by Elsasser and Staude (1978) indicate shortcomings in the model of Dyck and Beichmann and show that scattering by circumstellar dust and electrons distributed non-spherically can account for the large polarizations observed in a variety of young stellar objects, as opposed to the need to invoke a magnetic field.

In the case of stars with long λ_{max}, SMF suggest that larger than normal grains exist. Further investigations by Cohen (1977) show that it is possible for the grains to grow by accreting mantles from the gas rather than by coalescence of previously existing grains. Since only 1% by weight of the interstellar medium is in the form of grains and since elements heavier than helium are only 1% of total cosmic abundance by weight, Cohen concludes that the mantles which accrete in dense regions have different chemical compositions from grain cores, preferably involving as much hydrogen and as little of the heavier elements as possible.

Most of the stars with long λ_{max} are located in dark cloud complexes where grain growth might reasonably occur because of high density and ultraviolet shielding. Water ice is certainly a possibility for the mantle and the fact that infrared absorption bands of water ice have been observed in dense molecular clouds, lends support to the hypothesis of a different chemical composition in grains in the densest regions of the interstellar medium (Cohen 1977).

Aligned grains cause linear dichroism of the interstellar medium, and in general they must also cause linear birefringence, i.e. a difference in the real part of the refractive index for the medium for waves polarized parallel and perpendicular to the direction of grain alignment. Thus arises

the possibility of observing a small component of circular polarization in the light from a linearly polarized source, that has traversed a region where the grains are aligned in some direction,neither parallel nor perpendicular to the polarization vector of the source.

Martin (1972) shows how optical observations of circular polarization yield valuable information about the grain material. He demonstrates that the wavelength of circular polarization is sensitive to the imaginary part of the complex refractive index of the grain material and hence provides a powerful tool in determining the nature of interstellar dust grains. He proposes the following materials for interstellar grains with refractive indices $m = n-ik$:

(1) Ice, with $n \sim 1.3$ which is dielectric even when impurities raise k to 0.05 ("dirty ice").

(2) Silicates with $n \sim 1.7$ with k ranging from 0 to $\sim .3$. The non-absorbing variety are dielectric but those with large k would have a more "metallic" behaviour.

(3) Iron with $k \sim n$ which is metallic.

(4) Graphite which is optically anisotropic (see Martin 1972)

(5) Silicon carbide, again optically anisotropic.

Shapiro (1975) demonstrates that flat, platelet grains of magnetite can account for the observed wavelength dependence of linear and circular interstellar polarizations. Given conditions of perfect alignment they can also account for the amount of polarization whilst locking up in magnetite grains only a relatively small fraction of the total iron present in the interstellar medium. Hence much magnetite dust would only contribute a small amount to the observed interstellar extinction, thus allowing the extinction curve to be explained by other types of dust. If perfect alignment is not achieved, it is necessary only to put more iron into the magnetite grains and in turn account for a large fraction of the total extinction.

However, a determination of the interstellar birefringence by McMillan and Tapia (1977) yields results consistent with nearly pure dielectric material. This revision therefore removes, according to them, all observational evidence for materials such as magnetite, which have a measureable k.

The few ultraviolet polarization observations that exist (Gehrels 1974) and those in the infrared (Dyck 1974) show behaviour which is in general consistent with that expected for dielectrics (Martin 1975).

3.4 FAR INFRARED OBSERVATIONS

Many galactic HII regions are associated with far infrared sources of heated dust which appears to be present both inside the HII region, and outside in the neutral gas (Emerson and Jennings, 1976). Recent observations (see Aannestad, 1976 and references therein) show that in some cases, the far infrared maps correlate closely with the radio continuum maps, indicating that the dust in these cases is mixed with the ionized gas within the nebulae.

Emerson and Jennings interpret the results of their observations of far infrared sources in terms of emission from dust clouds heated by hot stars, grains (or grain mantles) of ice, fitting the data well. Greenberg (Emerson and Jennings, 1976 - discussion) however, suggests a mixture of core-mantle particles in the 0.1μm size range and a large number of much smaller core particles (probably silicates) in the 0.005 μm size range as the dust composition.

Observations of the three most observed HII regions viz. Orion A, W3 and M17, have been modelled successfully by Aannestad (1976) in terms of dusty HII regions containing olivine-core and ice-mantle grains. The refractory component of the dust, withstanding high temperatures much better than the mantle material, will be subject to evaporation mainly in the immediate vicinity of the exciting star. Further from the central star, the temperature may be low enough for the grain to maintain its mantle. The distribution of such grains is thus limited, but is still possible in a

substantial portion of an HII region. In terms of sizes of the grains, Aannestad has taken a core size of 0.05 μm and a mantle size of 0.15 μm.

Rowan-Robinson (1976) has constructed models of optically thick dust clouds fitted to the spectra of galactic (Orion and W3) and extra-galactic (M82 and NGC 253) sources from 3 μm - 1 mm. He finds that if the grains are composed of ice or silicates, then radii greater than 10μm are required and that grant grains appear to be a general feature of sources peaking in the far infrared.

Multiply branched whiskers in the form of "snow-flakes" which may be expected to grow very rapidly under suitable conditions, can also enhance infrared and far infrared emissivities (Edmunds and Wickramasinghe, 1976) and Narliker, Edmunds and Wickramasinghe (1976) suggest that it is possible to explain the cosmic microwave background in terms of thermalization of radiation from sources such as galaxies by somewhat exotic graphite whiskers of radii 10^{-6} - 10^{-5} cm and of lengths $\sim$ several hundred μm.

3.5 COMETARY DUST

Comets are believed to be the remnants of the most primitive material in the solar system. Because their reflected light and thermal emission are seen uncontaminated, by the light of any illuminating star, they can be studied in greater detail than any other source of interstellar dust and hence are very important.

The silicate signature has been observed in Comet Bennett, Comet Kohoutek, and Comet Bradfield (see Ney, 1977 and references therein). The comet data also indicates that the material responsible for the 10 μm feature is very refractory, with grains surviving at temperatures of 1000^{o} K (Ney, (1977)).

Observations of Comet West (Ney and Merrill, 1976) yield scattering phase functions best fitted by dielectric materials (where $1.3 \lesssim n \lesssim 2.0$ and $n >> k$) such as dirty ice or silicates with $6 \lesssim x \lesssim 15$ (where $x = \frac{2\pi a}{\lambda}$ is

the size parameter of the grains).

Recent analysis of the 10 μm and 18 μm bands in Comets Bennett and Kohoutek (see Cooke and Wickramasinghe 1976) indicates the presence of materials such as polyformaldehyde. Both these bands and the underlying infrared continium are depressed by a factor of 10 in intensity a few days after perihelion when the radiative temperature is only $\sim 500^{\circ}$ K, consistent with the evaporation of formaldehyde but not with that of silicate grains where temperatures > 1400° K are necessary.

The detection of polyformaldehyde in the Allende carbonaceous chondrate (Breger, Zubrovic, Chandler, 1972) increases the evidence for it, as a constituent of interstellar dust grains.

3.6 SUMMARY

Martin (1977) has reviewed the nature of the recent investigations into interstellar dust properties and also emphasizes the importance of new areas and techniques of investigation.

Studies of interstellar extinction, albedo (from diffuse galactic light data) and polarization (both linear and circular) are found to be consistent with a 3-component grain model. Wickramasinghe (1976) summarizes these results:

(i) Extinction and polarization observations in the waveband 10,000-3000 Å demand a predominantly dielectric grain model ; partially aligned dielectric needles of refractive index m = 1.5 with radii $\sim$ .15 μm are consistent with these data.

(ii) Extinction, phase function and albedo data in the 3000-1800 Å waveband require the dominance of a predominantly absorbing (low-albedo) grain population. The grain population must provide an explanation of the 2200 Å interstellar absorption band. If graphite is responsible for the extinction in this waveband, the particles must be nearly spherical with radii $\lesssim$ 0.02 μm, the 2200 Å band being a small particle resonance in graphite.

(iii) Extinction and albedo data at wavelengths $\lesssim$ 1800 Å require a dielectric grain population with radii $\lesssim$ 0.01 μm.

According to Wickramasinghe (1977) all the data can be accounted for in terms of a mixture of small spherical graphite particles, radii $\lesssim$0.02 μm, small dielectric spheres, radii < 0.01 μm and larger elongated dielectric particles, radii $\sim$ 0.15 μm, with the mass density of all three populations roughly comparable. At present, it is thought that silicate grains probably make up the smaller sized dielectric component, and icy grains, probably with silicate cores the larger sized component.

Interstellar column density derivations, e.g. by Snow (1975) indicate that all elements in interstellar clouds are underabundant with respect to hydrogen, lending support to the hypothesis of Routly and Spitzer (1952) that these"missing" elements are bound up in interstellar grains. Hence there is general support (see Wickramasinghe, 1977,for further references) for the idea that the bulk of the elements Mg, Si, Fe is condensed in grains or grain cores as iron, silicon carbide and silicate particles, and that the CNO elements are also locked away in grains, presumably as grain mantles, but to a lesser extent (Wickramasinghe, 1977).

References

Aannestad P A, 1975, Astrophys J. 200, 30.

Aannestad P A, 1976, Far Infrared Astronomy, ed. M Rowan - Robinson (Pergamon Press).

Aannestad P A, Purcell, E M, 1973, Ann. Rev. Astron. Astrophys 11, 309.

Bless R C, Savage B D, 1972, Astrophys J. 171 293.

Breger I A, Zubrovic P, Chandler J C, 1972, Nature 236 155.

Crawford D L, Mandwewala N, 1976, Publ. Astron. Soc. Pacific 88 917.

Cohen J G, 1977, Astrophys J. 214 86.

Cooke A, Wickramasinghe N C, 1976, Far Infrared Astronomy, ed.M Rowan - Robinson (Pergamon Press).

Coyne G V, Gehrels T, Serkowski K, 1974, Astron. J. 79 581.

Day K L, 1976, Astrophys J 210 614.

Dyck H M, 1974, Planets, Stars and Nebulae studied with photopolarimetry ed. T Gehrels (Univ. Arizona Press).

Dyck H M, Beichman C A, 1974, Astrophys J 194 57.

Edmunds M G, Wickramasinghe N C, 1976, Far Infrared Astronomy, ed. M Rowan - Robinson (Pergamon Press).

Egan W G, Hilgeman T, 1975, Astron J. 80, 587.

Elsässer H, Staude H J, 1978, Astron. & Astrophys 70 L3.

Emerson J P, Jennings R E, 1976, Far Infrared Astronomy. ed. M Rowan - Robinson (Pergamon Press).

Field G B, 1974, Astrophys J 187 453.

Gehrels T, 1974, Astron. J 79 590.

Gilra D P, 1971, Nature 229 237.

Hall J S, 1949, Science 109 166.

Hiltner W A, 1949, Science 109 165.

Johnson H L, 1968, Stars and Stellar Systems 7 Nebulae and Interstellar Matter ed. Middlehurst, Aller (Chicago Press).

Knacke R F, Cudaback D D, Gaustad J E, 1969, Astrophys J., 158 151.

Knacke R F, Gaustad J E, Gillet F C, Stein W A, 1969, Astrophys J., Lett. 155 L189.

Martin P G, 1972, Mon. Not. Roy. Astron.Soc., 159 179.

Martin P G, 1975, Astrophys J. 202 389.

Martin P G, 1977, Astrophys & Space Sci. Lib. 70 Topics in Interstellar Matter. ed. H Van Woerden (D. Reidel Publ.Comp).

Mathewson D S, Ford V L, 1970, Memoirs Roy Astron.Soc. 74 139.

McMillan R S, Tapia S, 1977, Astrophys J. 212 714.

Merrill K M, Russell R W, Soifer B T, 1976, Astrophys J 207 763.

Nandy K, Thompson G I, Jamar C, Monfils A, Wilson R, 1976, Astron. Astrophys 51 63.

Narliker J V, Edmunds M G, Wickramasinghe N C, 1976, Far Infrared Astronomy. ed. M Rowan-Robinson (Pergamon Press).

Ney E P, 1977, Science 195 541.

Ney E P, Merrill K M, 1976, Science 194 1051.

Purcell E M, 1975, The Dusty Universe. ed. G B Field, A G W Cameron (NWAP, New York).

Routly P M, Spitzer L, 1952, Astrophys J 115 227.

Rowan-Robinson M, 1976, Far Infrared Astronomy. ed. M Rowan-Robinson (Pergamon Press).

Schild R E, 1977, Astron J. 82 337.

Serkowski K, Mathewson D S, Ford V L, 1975, Astrophys J. 196 261.

Shapiro P R, 1975, Astrophys J 201 151.

Snow T P, 1975, Astrophys J. Lett. 202 L87.

Stebbins J, Huffner C M, Whitford A E, 1939, Astrophys J. 90 209.

Whitford A E, 1958, Astron J. 63 201.

Wickramasinghe N C, 1975, Mon. Not. Roy. Astron. Soc. 170 11P.

Wickramasinghe N C, 1977, Astrophys. and Space Sci. Lib. 70. Topics in Interstellar Matter. ed. H Van Woerden (D. Reidel Publ. Comp).

Wickramasinghe N C, Nandy K, 1972, Rep. Prog. Phys. 35 157.

CHAPTER 4

ETA CARINAE

4.1 EARLY HISTORY

4.1.1 The Light Curve

The earliest recorded observations of η Carinae are summarized in Table 1A. There is no mention of the star in the oldest catalogues (Ptolemy) and since the earliest records of observations of the η Carinae region at the end of the 16th century (v. Houfmann, Bayer) do not include the star,it is reasonable to assume that at the time of Ptolemy the star was fainter than 4th magnitude and may possibly have been increasing in magnitude over the centuries (Innes 1903).

Observations were made by various people until 1834 when Sir John Herschel began his own series of observations at the Cape of Good Hope which lasted until 1838. During these years η Carinae fluctuated between 2nd and 1st magnitude.

When first observed by Sir John Herschel in 1834 it "appeared as a very large star of the 2nd magnitude, or a very small one of the first and so it remained without apparent increase or change up to nearly the end of 1837...."

It was on 16th December, 1837, that Herschel's "astonishment was excited by the appearance of a new candidate for distinction among the very brightest stars of the first magnitude....". After a "momentary hesitation", the "natural consequence of a phenomenon so utterly unexpected", he satisfied himself that it was his "old acquaintance", η Argûs as the star used to be called. Its light was nearly tripled.

From this time on its light continued to increase until it attained maximum brightness on 2nd January, 1838, when it was almost as bright as

TABLE 4.1A

Earliest Recorded Observations of the Magnitude of η Carinae.

DATE	AUTHORITY	MAGNITUDE
1677	Halley	4
1751	Lacaille	2
1811-1815	Burchell	4
1822	Fallows	2
1822-1826	Brisbane	2
Feb. 1 1827	Burchell	1 = α crucis
Feb.29 1829	Burchell	2...1
1829-1833	Johnson	2
1832-1833	Taylor	2
1834-1837	Herschel	1...2
Jan. 2 1838	Herschel	> 1 very nearly = α centauri
March 19 1842	Maclear	< 1 inferior to α crucis
April 1843	Maclear	> 1 nearly equal to Sirius
Apr.11-14 1843	Mackay	1 fully bright as Canopus

magnitude of α crucis = 1.0

magnitude of α centauri = -0.3

magnitude of Canopus = -0.7

α centauri ($-0^m.3$). By 20th January, it was "visibly diminished" and continued to fade beyond 14th April, 1938, after which time Herschel's own observations of η Carinae ceased.

η Car's subsequent increase "in lustre" was observed by the Rev. W S Mackay, at the General Assembly's Mission, Calcutta, in March 1843. During March, the brightness of the star was oscillating and at maximum brightness rivalled Canopus ($-0^m.7$), its minimum being somewhat less than the magnitude of α Crucis ($1^m.0$).

By 1857, η Car had faded to a first magnitude star, by 1860 a 3rd and after 1868 faded considerably.

Another small, but relatively well-defined maximum occurred in 1889, but by the end of the century η Car had faded to 8th magnitude.

Figure 4.31 shows the Light Curve of η Car.

4.1.2 Early Spectroscopic Observations

The earliest available spectroscopic observations were made by Le Sueur (1870) and Clerke (1888). Le Sueur describes the spectrum as being "crossed by bright lines" and identified the lines Hα, He I λ5876, and Fe II λλ 5169, 5018. These observations, during the latter part of the decline of the great 1843 maximum, indicate that the spectrum may have had a similar appearance to today's. Le Sueur also states that "occasionally there is an appearance as if of a multitude [of dark lines] over the spectrum generally, but they refuse to be seen separately and certainly". It is possible that a very rich spectrum of weaker emission lines, like the present one, could have been mistaken visually for an absorption one.

Clerke too says that "indications of dark shadings are perceptible" in the spectrum of η Carinae, but detected no bright lines. It is uncertain whether relatively weak emission lines could have been detected if present, since the observations of both Le Sueur and Clerke were pre-photographic

descriptions.

From 1892 onwards, 40 plates (the Harvard Plates) of the spectrum of η Car were taken with the Boyden 13-inch telescope in Arequipa, Peru.

Bok (1930) has reviewed these early spectra taken by Cannon and describes η Carinae as having an absorption spectrum with superimposed hydrogen emission and a spectral classification of $C\frac{F5}{F3}$. However, an examination of the 1892 and 1893 plates by Hoffleit (1933) shows that an emission spectrum existed before the absorption spectrum of 1893. The main features of the 1893 spectra are : very intense Balmer lines ; faint Fe II lines ; and very strong forbidden lines.

A plate taken in 1895 shows a spectrum much more like the present one. There is still some faint absorption but the emission spectrum is prominent. The Balmer lines are still the strongest but more than 20 other emission lines due to ordinary and forbidden Fe II are clearly visible. Hoffleit detects conspicuous absorption components on the violet sides of the stronger lines, which are later absent.

The next spectrum, observed by Gill in 1899, revealed a bright line spectrum closely resembling that of Nova Aurigae. Baxandall (1919) has suggested that since Gill detected no absorption lines, in agreement with later observers (e.g. Moore and Sanford (1913)) then perhaps the Harvard observers had in some way misinterpreted some of the intervals between bright lines as dark lines, and measured them as such. The most likely explanation is that the spectrum was still undergoing its change, i.e. decreasing intensity of absorption spectrum was accompanied by a strengthening of permitted Fe II lines relative to Balmer lines and by the appearance of very strong forbidden Fe II lines.

Hoffleit (1933) concludes that the spectral changes were probably correlated with the light variation of η Car at this time, the change from

absorption to emission spectrum having taken place whilst the star was rapidly decreasing in brightness from $7^m.5$ in 1892-3 to $8^m.3$ in 1895. The Harvard spectra after 1900 show the usual emission spectrum with perhaps a faint continuous background. Intensities of Balmer lines and Fe II and [Fe II] are of the same order.

These observations, both visual and photographic, provide evidence that η Car underwent at least two major spectral transformations during the second half of the last century. (Walborn and Liller (1977)). Hence the absorption spectrum of 1893 was not necessarily related to the great light maximum of 1843 but probably to the minor one of 1889, i.e. the absorption spectrum of 1893 arose in an expanding shell ejected shortly before.

4.2 THE STRUCTURE OF ETA CARINAE

Eta Carinae has been characterized by, for example, Thackeray (1956) as essentially a scattering nebula, illuminated by a central object. Walborn (1976) considers the three principal components of η Car to be the nucleus, the Homunculus (after Gaviola) and the outer shell. η Car presently has a magnitude of $6^m.2$ and is associated with OB stars at a distance of 2.8 kpc (Walborn and Ingerson 1977).

4.2.1 The Nucleus

The very bright central object in η Car is often referred to as the "central star" but in fact this nucleus is non-stellar. Radiation from this central object is effectively scattered from the "halo".

4.2.2 The Homunculus

With the 61 inch reflector at Bosque Alegre Gaviola (1953) observed a shape resembling a "homunculus", "with its head pointing NW, legs opposite and arms folded over a fat body". This area, oval in shape, is reasonably well defined and of dimensions 12" x 17". The surface brightness is relatively high and it manifests itself as a reddish-orange nebulosity, with a complex internal structure. Gaviola's Homunculus is reproduced in Fig. 4.21.

The objects, formerly thought to be components of a multiple star system, were discerned by Gaviola to be condensations moving radially outwards with speeds ranging from 3".2 to 7".5 per century. The rate of expansion suggested ejection by the central nucleus around 1843 or later.

The light from the nebula was found by Thackeray (1956) to be polarized, the polarization being as great as 40% at the head of the Homunculus. By observing both the polarized and unpolarized lines in the head, Thackeray demonstrated that the head of the homunculus is moving away from the nucleus at the rate of 630 $km\,s^{-1}$ approximately in a direction inclined 70^{o} to the line of sight. Using Gaviola's measured expansion rate, and assuming the head to have originated in the second eruption, in the 1890's, Thackeray obtained a distance of 2,000 LY for η Car.

Measurements of Gaviola's condensations on recent plates (Gehrz and Ney 1972) show that the knots have continued to move outwards and that between 1944 and 1972 there has been a 1.25-fold increase in the pattern's size. This increase implies that ejection occurred around 1835 $\pm$ 10 yrs but since the expansion factors for various parts of the nebula vary, 1.25 being the average increase, it seems likely the material was ejected over a wide range of time. For example, the observations of the head of the homunculus imply ejection in 1862.

4.2.3 The Outer Shell

The surface brightness of the outer shell is distinctly lower than that of the homunculus, but it possesses an intricate structure which is progressively revealed by increasing exposures ; the most distant features extend to at least 25" from the central object.

The principal features of the outer shell have been identified by Walborn (1976) on a composite sketch, reproduced in figure 4.22, and are described by him as follows : (1) the southern (S) ridge, well separated from but perfectly parallel to the homunculus, containing near its western

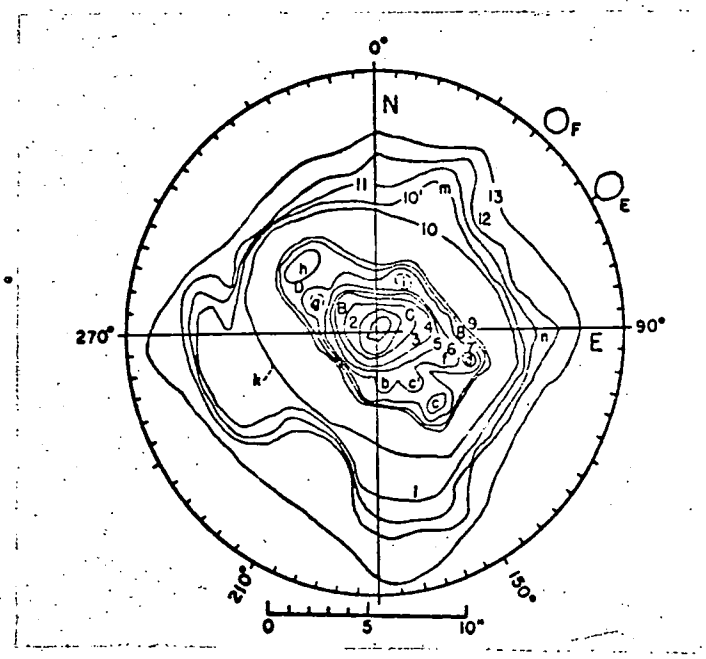

Figure 4.21 The Homunculus (reproduced from Gaviola, 1953)

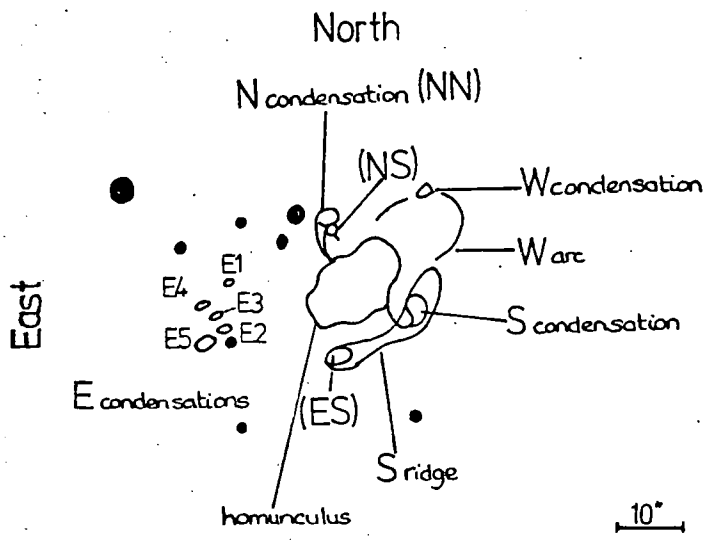

Figure 4.22. Composite sketch of the nebulosity of η carinae reproduced from Walborn (1976) and showing notation of Walborn, Thackeray and Blanco (1978) in parentheses.

end the brightest feature of the entire outer shell, the Southern (S) condensation ; (2) the northern (N) condensation which is a close double ; (3) the western(W) arc, which curves towards the western (W) condensation ; and (4) the five eastern (E) condensations the largest of which (E5) is the most distant well defined feature from the central object (about 25" away). The main body of the outer shell, exclusive of outlying condensations and prominences, is elongated in approximately the same sense as the Homunculus and has dimensions 21" x 29" the ratio of which is essentially identical to that of the homuncular oval dimensions.

Comparison of Walborn's (1976) photographs with those of Thackeray (1949-1950) reveals the N and brightest E condensation have increased their radial distances from the central object. Walborn estimates the displacements to be 1".5 - 2".0 for the quarter century interval implying angular velocities near the upper limit of those derived for features within the homunculus by Gaviola (1950) and Ringuelet (1958).

A consideration of the proper motions of these condensations by Walborn, Thackeray and Blanco (1978) reveals that all motions are outward and radial with respect to the central object, that the velocities of NN and NS condensations are greater than any observed within the Homunculus and that the W and E1-5 condensations have motions similar in magnitude to those in the Homunculus and the south ridge, despite the much greater separations of the former from the central object. This observation supports the idea that W and E1-5 may have been ejected from η Car at the much earlier epoch implied by the assumption of uniform motion.

However, the unknown derivatives of the observed motions introduce a basic uncertainty but if it is assumed that all the observed nebulosity is related to the activity of the last century, it follows that the most outlying features must have been sharply decelerated.

On the assumption of predominantly uniform motions, the suggestions

of Walborn, Blanco and Thackeray about the relationships of the condensation ejections with the light curve of η Car, are summarized in Table 4.2B.

TABLE 4.2B

Relationship of Condensation Ejections with Light Curve (from Walborn, Blanco, and Thackeray, 1978).

Gaviola-Ringuelet Condensation	Walborn Feature	Light Maximum
B, C, b, g		1889
	NN, NS	1870-1872
C, d, h, and	H, S	1830-1840
	W, E1-5	15th century ?

Walborn (1976) indicates some intriguing apparent relationships between structural details of the homunculus and the outer shell. The most striking is the alignment of the "arms" on either side of the homunculus with the N and S condensations. Curved filaments are observed to connect these condensations to the regions of the homuncular arms. The western arc may be a closed loop which, together with the western condensation, bears an analogous relationship to the head of the homunculus, itself a looped structure. Walborn suggests that some mechanism may be operating in η Car which spatially aligns ejections at different epochs, or with very different velocities. A magnetic field is one possibility since this is synonymous with curved and looped structures.

4.3 MODERN LIGHT CURVE MEASUREMENTS

Modern light curve measurements have been made by De Vaucouleurs and

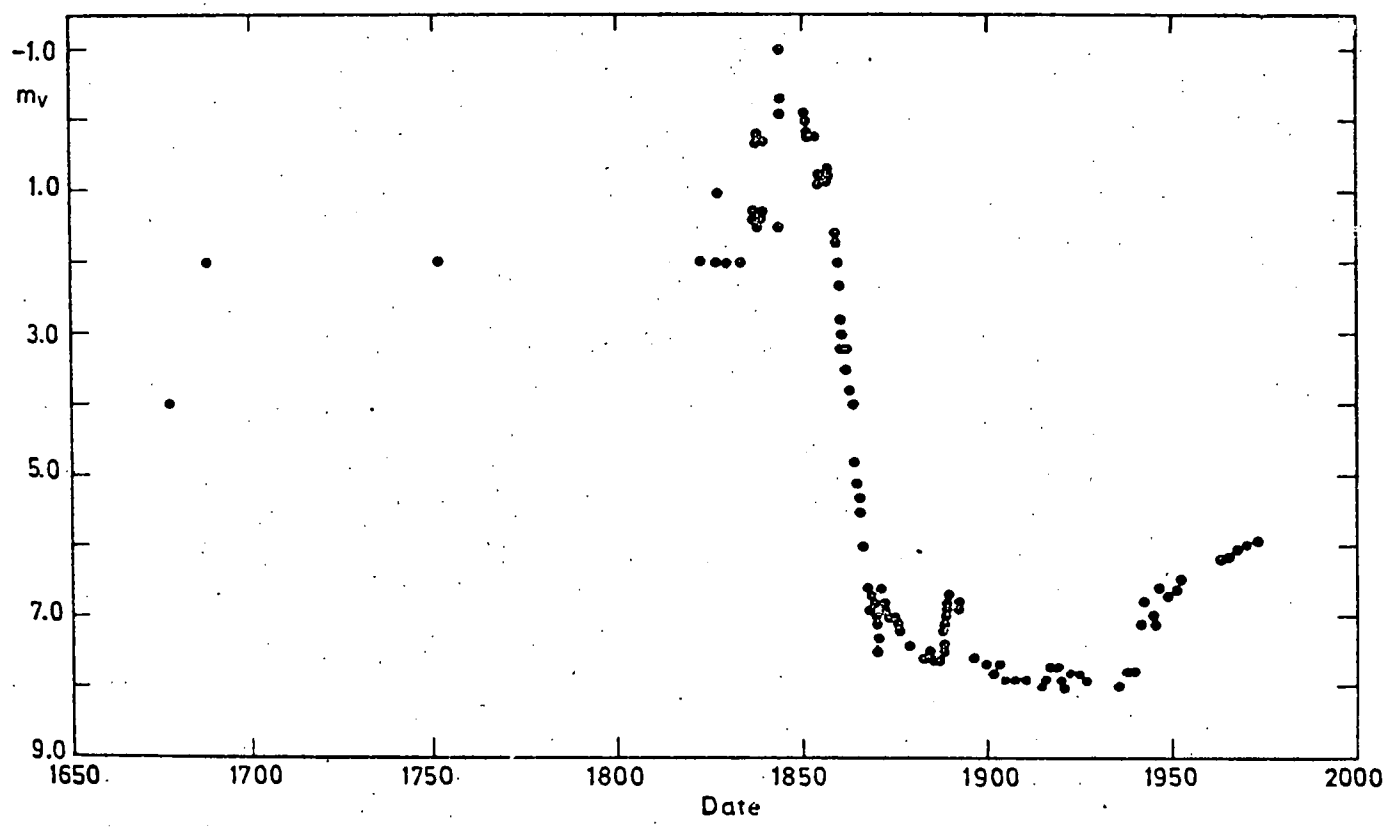

Figure 4.31 The Light Curve of η Carinae (reproduced from Feinstein & Marraco, 1974)

Eggen (1952), O'Connell (1956), Feinstein (1967) and Feinstein and Marraco (1974).

From around 8th magnitude at the turn of the century, O'Connell found that η Car had considerably increased in brightness by 1941 to a magnitude of about 7.4. In 1952 De Vancouleurs and Eggen obtained a magnitude of 6.5 and recent measurements by Feinstein and Marraco (1974) indicate that η Car is still increasing in brightness. Figure 4.31 shows the complete light curve of η Car, reproduced from Feinstein and Marraco (1974).

Feinstein and Marraco have obtained a period of about 1100 days for the variation of light from η Car. However, their data are not well enough distributed in time to be certain of this result and Walker (1972) who has made frequent, evenly spread observations of the light variation suggests that his results indicate irregular rather rapid brightenings, followed by slow declines. He also observes that the overall rate of increase in brightness seems to have slowed somewhat.

Thackeray (1953 a) suggests that since the contribution of the nucleus to the integrated intensity cannot be greater than 25% at most, then the increase in magnitude in recent years must mean that the halo has brightened.

4.4 OPTICAL SPECTRUM

The optical spectrum of η Carinae now consists of a multitude of emission lines superimposed upon a background continium. Detailed descriptions of the spectrum have been given by Thackeray (1953 b) and Gaviola (1953), the most characteristic features being the numerous and very strong forbidden lines due to quadrupole transitions of Fe II.

The emission lines are found to be multiple (Gaviola 1953) consisting of 2, 3, or more components with the red component considerably the strongest (Thackeray 1953). A small number of lines are sharp whilst others range from nebulous to very nebulous.

The strongest line by far is Hα which gives η Car its visual colour. The main component is over 2 Å wide, having a comparatively sharp violet edge and a nebulous red edge. The position of the Hα line corresponds to a radial velocity of +20 km s^{-1}. Other components of Hα on average have radial velocities of several hundred km s^{-1}. The other Balmer lines are also present, the multiple structure, nebulosity and radial velocities varying from line to line.

The main components of [Fe II] λ4287, [Fe II] λ4359 are found to be brighter than the main components of Hβ although the integrated light of Hβ (lines plus continium) forms the second brightest feature of the spectrum (Gaviola 1953). The bright metallic lines show in general a multiplet structure, with a continuous background. The main components have a violet shift of about -28 km s^{-1}, but the radial velocity shifts of all the components do not fall within narrow limits. The near components often have shifts in the range ±140-200 km s^{-1} ; those of the further components may lie between ±250-350 km s^{-1}.

The forbidden lines [N II] , [S II] , [Fe II] , [Ni II] have identical radial velocities to the major components of the hydrogen recombination series (Rodgers and Searle 1967) suggesting that they must originate in the same regions of η Car.

Changes in the spectrum were observed by Gaviola (1953) during his 1948 observations. He found that the general continium had become stronger with respect to the emission lines ; that the sharp [He I] λλ5876, 4471 lines had practically disappeared and that the [N II] , [Ne III] , [Fe II] lines had faded in intensity. His plates of 1949 showed that the spectrum was slowly coming back to 'normal', although the continuum remained enhanced.

Rodgers and Searle (1967) observed similar fadings of [He I] [Ne III] and [Fe III] in the period between March 1964 and March 1965.

Gaviola has detected the early absorption spectrum (P-cygni corresponding to F5 supergiant) measured on the early Harvard plates but partially obscured by the present emission spectrum.

The strongest lines in η Car are accompanied by diffuse absorptions shifted to the violet by about 450 km s^{-1}. The absorption components appear only weakly on dense exposures and as with the emission components the velocities are larger for the stronger members of the Balmer Series.

Pagel (1969) suggests that, rather than being due to scattered radiation from a hot central star, which has never been clearly identified visually, the visual continuum is due to two photon emission by hydrogen in the 2s state. Apparently the spectral distribution and intensity of the continuum relative to Hα and certain other emission lines can be accounted for in this way (see Pagel 1969 and references therein).

Observations of the spectra from the different parts of the nebula are difficult to obtain because the light coming from the nucleus, especially in bad seeing is too strong at distances of only a few seconds, but in general the surrounding shell shows the same kinds of lines as the core but with different intensities, suggesting that the shell shines by core radiation that has been scattered in the shell. This interpretation is supported by absorption features in the shell.

According to Thackeray, the permitted lines which are found to be polarized, are exclusively due to light from the nucleus being scattered by the shell whilst the unpolarized forbidden lines arise in the halo or shell itself.

The principal morphological conclusions to be drawn from the spectroscopic observations are summarized by Walborn, Blanco, Thackeray (1978) as follows :

(1) The emission lines from the central object have sharp cores, but there are diffuse absorption features shifted by about -450 km s^{-1}

relative to the emission.

(2) The homunculus has diffuse emission lines (widths up to nearly 800 km s^{-1}) with generally positive velocity shifts as high as + 850 km s^{-1} for the permitted lines in feature 'h'. There are also blue shifted diffuse absorptions as in the central object.

(3) The emission lines from the E2-5 condensations of the outer shell are relatively narrow and have negative velocity shifts in the range -100 to -200 km s^{-1}.

(4) The emission lines from the outer shell features NN, NS (Gaviola's 'm') and ES (Gaviola's '1') have extremely complex disturbed profiles extending to very high velocities.

(5) In the central object and homunculus the intensity of Hα > [N II] λλ6548, 6583 but throughout the outer shell [N II] > Hα.

4.5 INFRARED MEASUREMENTS

Eta Carinae is the brightest object known at 10μ and 20μ with the exception of objects within the solar system (Westphal and Neugebauer 1969).

The steep rise of the visual continuum towards the infrared was originally observed by Rodgers and Searle (1967), and subsequent measurements e.g. Neugebauer and Westphal (1968), Westphal and Neugebauer (1969), Sutton, Becklin, Neugebauer (1974) and Robinson, Hyland, Thomas (1973) have confirmed the strength of the infrared continuum in η Carinae.

The slope of the continuum in the optical and near infrared is critically dependant on the correction made for differential extinction by interstellar dust. Initially, Neugebauer and Westphal corrected their data using a value of $E_{B-V} = 0.6$, with the visual absorption $A_V = 1.8$ giving $R = 3$. They obtained an increase in the slope of the continuum incompatible with that from a hot star, and in any case difficult to explain. However, by comparing the relative intensities of [Fe II] lines in the spectrum of η Car at different wavelengths, Pagel (1969) has obtained a value of $E_{B-V} = 1.2$,

which replaces the increase in slope of the continuum towards the infrared with a decrease, compatible with the continuum from a hot star.

The existence of the silicate emission peak in the 8-13 μ range has been established by Robinson, Hyland and Thomas (1973). However, the lack of oxygen lines in the spectrum of η Car (Thackeray 1953 ; Rodgers and Searle 1967), indicating a deficiency of oxygen poses a problem since silicate emissivity peaks are only expected to be found in the energy distributions of oxygen-rich stars. Robinson, Hyland and Thomas suggest that the true oxygen deficiency is only marginal and that the apparent deficiency arises due to oxygen atoms becoming bound in molecules and silicate grains.

The infrared continium is now generally accepted as being due to thermal emission by grains (Westphal and Neugebauer 1969 ; Robinson, Hyland, Thomas 1973 ; Pagel 1969) as opposed to synchrotron emission (e.g. McCray 1967).Various single shell and multiple shell models have been developed to account for the infrared energy distribution (Apruzese 1975 ; Mitchell and Robinson 1978 ; Robinson, Hyland, Thomas 1973). Multiple shell models are appropriate because, at each optical maximum, matter which is ejected and moves radially outward, eventually reaches a radius such that the temperature is below the vaporization temperature of the grains, hence the formation of grains occurs and since there have been several optical maxima, the dust grains are likely to be distributed in the form of several concentric shells, (Robinson, Hyland, Thomas 1973). Invoking a model based on various details of the spectrum of η Carinae, and the assumption that the infrared spectrum is due to thermal re-emission from dust surrounding an ionized region Davidson (1971) portrays η Carinae as a very massive star whose surface temperature is about 30,000° K, photoionizing a compact H II region which is surrounded by dust.

4.6 THE NATURE OF ETA CARINAE

In a detailed study of the present condensation process of solid

material around η Car, Andriesse et al (1978) interpret the light curve in terms of a model of time evolution of the dust envelope, which accounts for the wavelength dependent extent of the infrared source. They show that η Car, a high luminosity star ($5 \times 10^6 L_\odot$) with a mass of 160 $M_\odot$ has been losing mass since 1840 at the rate $\dot{M} = 8 \times 10^6 L_\odot$, which may account for the intrinsic fading by 1 magnitude since 1840, and also that since 1856 dust has been condensing from the circumstellar gas at distances greater than 3.7×10^{14} m from the star, initially at the rate $\dot{M}d = 1 \times 10^{-4} M_\odot y^{-1}$ and presently at a somewhat higher rate.

With a surface temperature of the order of 30,000° K (Davidson 1971) η Carinae appears to be well above the main sequence. Hence η Carinae may be either a very massive star approaching the main sequence, or one which has perhaps evolved away from it and become pulsationally unstable.

Since the process of contraction to the main sequence has a smaller time scale than that of evolving away from it, the latter hypothesis seems more likely and variations in brightness, extensive envelope and mass ejection all suggest that the star is showing signs of instability. Hence η Carinae may fall into the category of stars which are mildly, but not yet seriously unstable being much further along its evolutionary path than other known massive stars, and possibly being beyond the point at which the core is exhausted when 60-70% of the total hydrogen has been burned. If the star is rapidly exhausting its supply of nuclear fuel, and with its evolutionary state speeding up very rapidly, η Carinae may possibly undergo a supernova outburst (Burbidge 1962).

Davidson (1971) supports this view of Burbidge, although not necessarily predicting a supernova outburst, and suggests a hypothetical series of events as follows : initially the star was as it is at present day, but without the circumstellar dust it was 4th magnitude rather than

6th. Then some instability caused the sudden ejection of material which formed a shell, giving the appearance of a bright star when the shell had expanded to the point where most of its radiation was at visual wavelengths. As dust grains began to form it seemed to fade and when the expanding envelope became optically thin for some form of scattering, but visually opaque because of the dust, η Carinae assumed its present appearance.

Because η Carinae seems to be a member of a stellar association in Carina, Gratton (1963) suggests that the star is a very young object and that the phenomena shown by it could be those accompanying the formation of a (massive) star or perhaps a group of stars.

As regards η Carinae being in the process of gravitational contraction, it seems that very massive proto-stars are prone to become pulsationally unstable and that in fact the true upper limit to stellar masses may be set by the instability of more massive proto-stars, which may eject material or destroy themselves completely whilst moving towards the main sequence. If this is the case, η Carinae may now be at its high luminosity phase and further evolution may lead to either a catastrophe or a minor re-adjustment, the inner part contracting normally to the main sequence and the outer shell being ejected (Burbidge, 1962).

Zwicky classifies η Carinae as a Type V Supernova, the only other analogous object in the class being in NGC 1058. However, with a difference of only 9 magnitudes between maximum and minimum luminosity, as opposed to 17 magnitudes in a normal supernova, with a spectrum resembling that of normal novae, and with an absence of non-thermal radio emission, η Carinae cannot really be classified as a true supernovae. Thackeray (1956) suggests that η Carinae belongs to a new class of supernova, that of 'ultra-slow supernovae' corresponding to the birth of an expanding association - an event far rarer than an ordinary nova or supernova.

With a maximum luminosity intermediate between that of novae and supernovae, η Carinae may well be "representative of a small group of ejection variables that attain high luminosity", (Payne-Gaposchkin, 1957). The high luminosity, blue colour index and intermediate F-type spectra associates η Carinae with the group of Hubble-Sandage variables, (Warren-Smith et al 1978) the brightest irregular variables in M31 and M33. Hence η Carinae may be an equivalent Hubble-Sandage Variable in our own galaxy.

References

Aller L H, 1970 Sky and Telescope 39 368.

Andriesse C D, Donne B D, Viotti R, 1978 Mon.Not.R.Astr.Soc. in print.

Appenzeller I, 1970 Astron. Astrophys. 5 355.

Apruzese J P, 1975 Astrophys. Journ. 196 753.

Baxandall F E, 1919 Mon.Not.R.Astr.Soc. 79 619.

Bok B J, 1930 Popular Astronomy 38 399.

Burbidge G R, 1962 Astrophys. Journ. 136 304.

Clerke A M, 1888 Observatory 11 429.

De Vaucouleurs G, Eggen O J, 1952 Publ. A.S.P. 64 185.

Davidson K, 1971 Mon.Not.R.Astr. Soc. 154 415.

Feinstein A, 1967 Observatory 87 287.

Feinstein A, Marraco H G, 1974 Astron. Astrophys. 30 271.

Gaviola E, 1950 Astrophys. Journ. 111 408.

Gaviola E, 1953 Astrophys. Journ. 118 234.

Gehrz R D, Ney E P, 1972 Sky and Telescope 44 4.

Gill Sir D, 1901 Mon.Not.R.Astr. Soc. 61 (appendix) 66.

Gratton L, 1963 Star Evolution. Proceedings of the International School of Physics Enrico Fermi (Academic Press).

Herschel Sir J F W, 1847 Results of Astronomical Observations made during the years 1934-38 at the Cape of Good Hope (London : Smith, Elder and Co).

Hoffleit D, 1933 Harvard Bulletins 893 11.

Innes R T A, 1903 Ann. of the Cape Observatory 9 75B.

Le Sueur A, 1870 Proc. Roy. Soc., 18 245.

Lovi G, 1972 Sky and Telescope 43 306.

Mitchell R M, Robinson G, 1978 Astrophys. Journ. 220 841.

McCray R, 1967 Astrophys. Journ. 147 544.

Moore J H, Sanford R F, 1913 Lick Obs. Bull. 8 55.

Neugebauer G, Westphal J A, 1968 Astrophys Journ. 152 L89.

O'Connell D J K, SJ 1956 Vistas in Astronomy 2 1165.

Pagel B E J, 1969 Nature 221 325.

Payne-Gaposchkin C, 1957 The Galactic Novae (North Holland).

Ringuelet A E, 1958 Z Astrophys. 46 276.

Robinson G, Hyland A R, Thomas J A, 1973 Mon.Not.R.Astr.Soc. 161 281.

Rodgers A W, Searle L, 1967 Mon.Not. R.Astr. Soc. 135 99.

Schlovsky I S, 1975 Supernovae (Wiley and Son Ltd).

Sutton E, Becklin E E, Neugebauer G, 1975 Astrophys. Journ. 190 L69.

Thackeray A D, 1949 Observatory 69 31.
1953a Mon.Not.R.Astr. Soc. 113 237.
1953b Mon.Not.R.Astr. Soc. 113 211.
1956 Observatory 76 103.
1961 Observatory 81 102.
1967 Mon.Not.R.Astr.Soc. 135 51.

Walborn N R, 1976 Astrophys. Journ. 204 L17.

Walborn N R, Liller M H, 1977 Astrophys Journ. 211 181.

Walborn N R, Blanco B, Thackeray A D, 1978 Astrophys. J. 219 498.

Walker W S G, 1976 Southern Stars 26 217.

Warren-Smith R F, Scarrott S M, Murdin P, Bingham R G, 1978 preprint.

Westphal J A, Neugebauer G, 1969 Astrophys. Journ. 156 L45.

CHAPTER 5

A DUST SCATTERING MODEL OF THE ETA CARINAE NEBULA

5.1 THE DATA

The Eta Carinae nebula was observed at the f/15 focus of the 3.9m Anglo-Australian Telescope on 17th January 1978, by Scarrott and Warren-Smith. The data was reduced by Warren-Smith and interpreted by Warren-Smith,Scarrott, Murdin and Bingham (1979), henceforth referred to as Paper I.

The polarization map of the Homunculus, corrected for an interstellar polarization of 2.4% at position angle 108° (as given by Visvanathan 1967) is shown in figure 5.22. Each vector represents the degree and position angle of the polarization at that point. Representative errors on the polarization are shown in figures 5.21 which show the spatial variation of polarization. The Stokes' parameters for each point on the map are listed in Appendix 1, along with the polarized intensity, percentage polarization and position angle of polarization. Measurements have been made using an integration bin of 0.7 x 0.7 arcsec with a separation of 0.7 arcsec.

5.1.1 Seeing on the AAT

The AAT is susceptible to changes in the seeing. Since the integration bins are of the order of the seeing disc ($\sim$ 0.8 arcsec FWHM), it is important that the seeing remained constant over the four exposures. (Only four exposures were necessary because the lateral extension of the Homunculus was no more than one grid width, so grids "out" were unnecessary). Profiles of the same star from each plate in x and y are shown in figure 5.11, along with the standard deviation for each distribution. Since the integration bin is composed of 2 x 2 of these intensity bins σ is well within the required accuracy range, and the seeing is constant over the four exposures,

PROFILES OF THE SAME STAR ON PLATES 1,2,3 & 4.
(y above, x below)

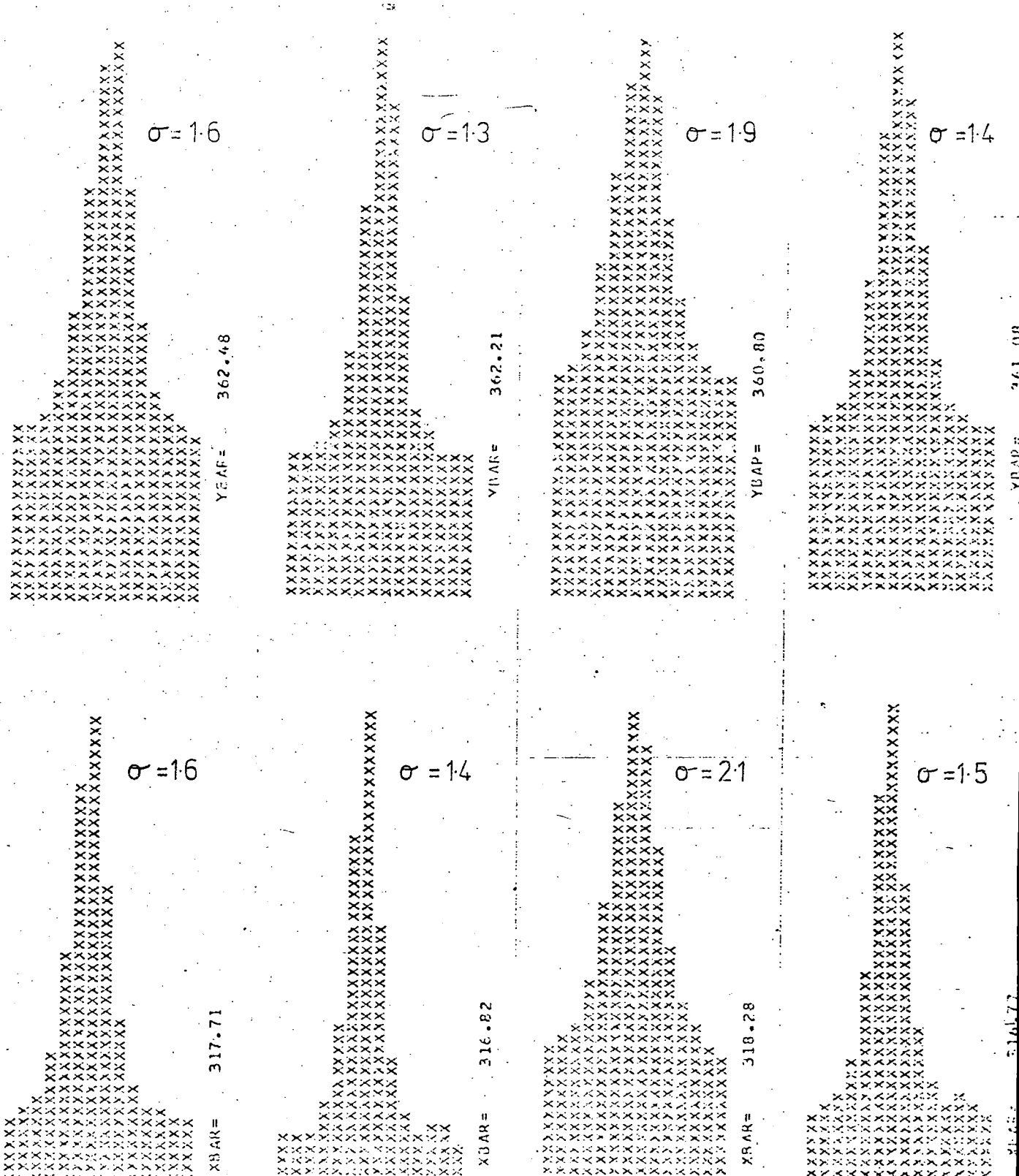

Figure 5.11

with the exception perhaps of plate 3. Plate 3 was found to be extremely noisy and hence was rejected in the production of the polarization map. The reduction technique was carried out as in Chapter 2 except that the filtering stage was necessarily omitted. It was found that a smoother map was obtained using three plates without filtering, than using the set of four plates plus filtering (Warren-Smith, private communication). The errors, normally calculated during the filtering stage were now calculated as a function of noise on the plate.

5.2 THE POLARIZATION MAP

The polarization map of the Homunculus, shown in figure 5.22 is discussed in detail in Paper 1.

5.2.1 Geometry of the Homunculus

The main feature of the generally centro-symmetric polarization pattern is the asymmetry to the NW and SE where the polarizations are 35% and 25% respectively.

The general similarity between this polarization pattern and that of the nebula M1-92 (Schmidt, Angel, Beaver, 1978) has led Warren-Smith et al to postulate a similar geometry. M1-92 is described as being "bipolar", that is, essentially symmetric about an axis passing through two lobes and the central star, also with an optically thick equatorial dust torus. In the case of the Homunculus, this torus is considered to be luminous. If the nebula is inclined at 20° to the plane of the sky (Thackeray, 1961), then to the N, where the torus is before the nebula, it will manifest itself as a sharp drop in polarization due to increased optical depth and hence multiple scattering effects. This is shown in figures 5.21. To the S, where the ring is behind the nebula, the rise in polarization to the extremities of the nebula is uniform, (see geometry in figure 5.23). Both the ring and η Car contribute to the scattered light. The asymmetry in polarization is explained in terms of the scattering processes operating in the Homunculus.

Figure 5.21

EFFECT OF LUMINOUS RING ON THE PERCENTAGE POLARIZATION

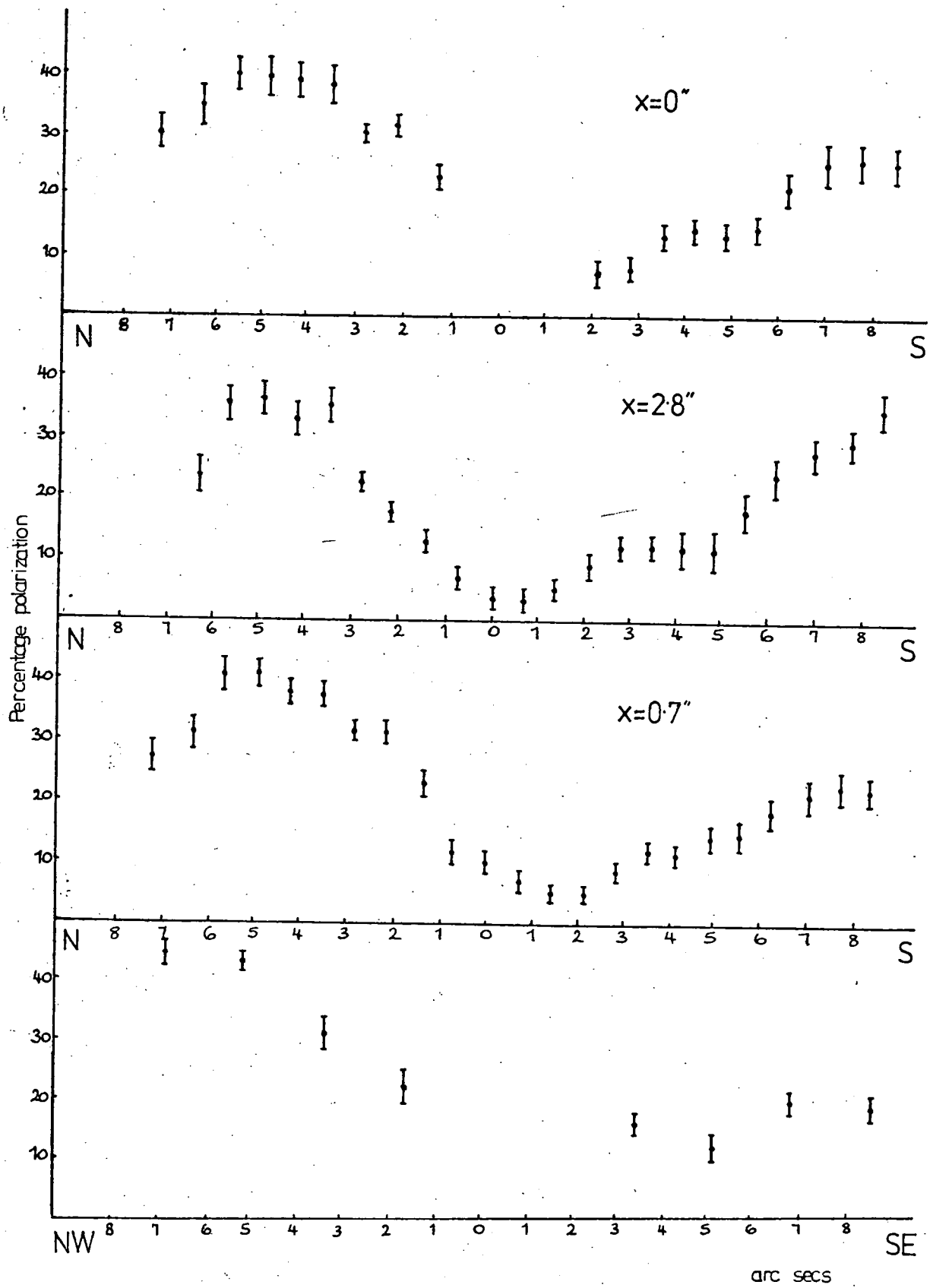

Traces of percentage polarization are taken at distances x" arc from centre of η carinae

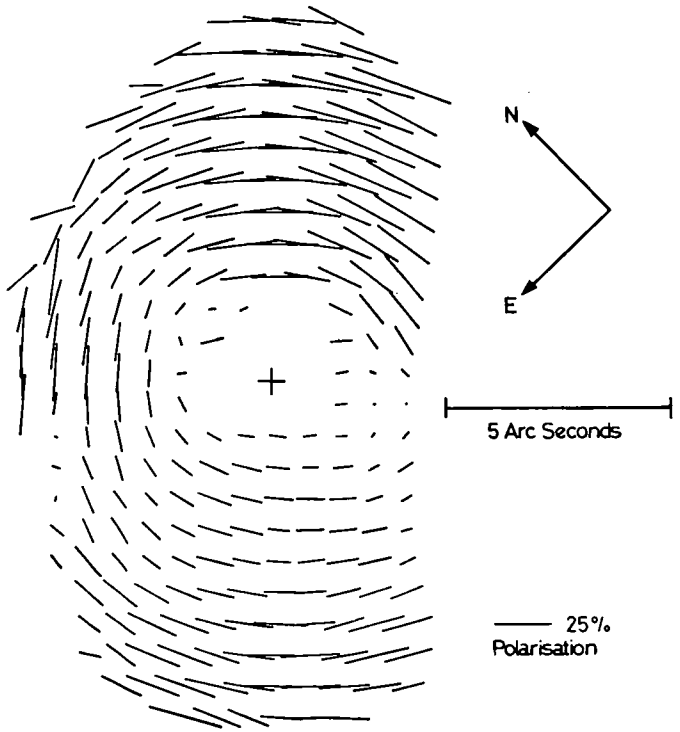

Figure 5.22
Polarization of the Homunculus

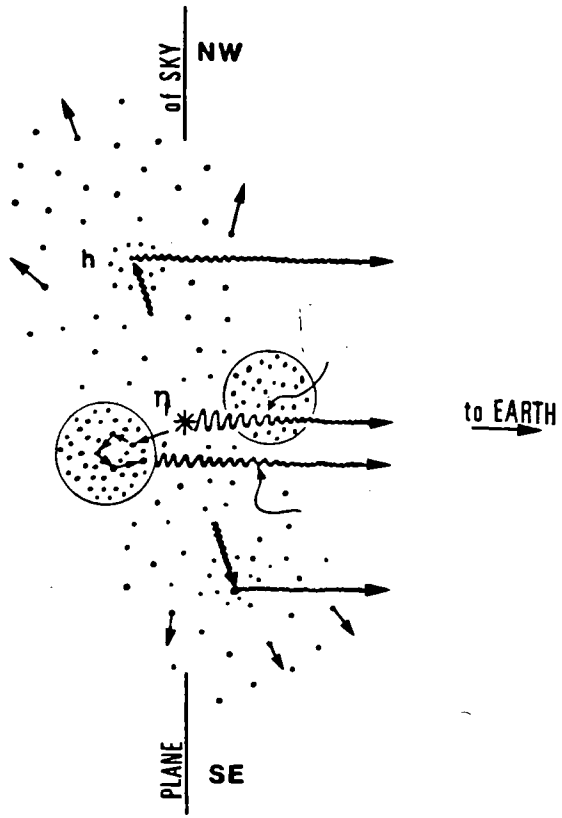

Figure 5.23
Geometry of the Homunculus

5.2.2 Conclusions

Warren-Smith et al postulate that, like with bipolar nebulae (Cohen and Kuhi,1977), η Carinae originated in a nova explosion in which an initially spherical expanding envelope interacts with a disk. Ejection, free along the poles of the disk, is constricted by swept-up disk material in the direction of the disk's equator. They explain the origin of the disk-like circumstellar cloud as an "ex-cretion" disk generated by overflow from the outer Lagronian points of a close binary star and suggest that η Carinae belongs to a class of Hubble-Sandage Variables (Hubble and Sandage 1953) intermediate in magnitude between novae and supernovae.

5.3 THE MODEL

The large polarizations measured in the Homunculus are thought to be due to the scattering of light, from the central source, by dust grains. There is substantial support for the existence of dust grains in η Carinae (Pagel, 1969; Davidson, 1971; Westphal and Neugebauer 1969 ; Gehrz and Ney, 1972). Other mechanisms capable of producing polarization such as Rayleigh scattering and electron scattering can be ruled out due to the absence of the characteristic λ^{-4} component in the continuum,characteristic of Rayleigh scattering,and because the optical depth of electrons is insufficient to produce the necessary electron scattering (Craine, 1974). The asymmetry in the polarization about 90° could be produced by Mie scattering where the grainsize $\sim \lambda$ and where the polarization depends on the nature of the dust particle (characterized by a complex refractive index) and a size.

Evidence for the existence of silicate grains comes from the observations of Neugebauer and Westphal (1968),and Robinson,Hyland and Thomas (1973) amongst others, who identified the 10μ feature attributable to silicates in the infrared emission. Refractory grains, with melting points in the range 1500 K to 2000 K are obvious candidates for the components of dust which must withstand temperatures in the range 200 K to 1500 K (Davidson 1971) as opposed

to volatile substances such as ice with melting points in the range 100 K to 200 K.

Previous models of the Eta Carinae Nebula have consisted of extended spherical circumstellar dust shells (Mitchell and Robinson,1978 ; Aprúzese 1975) based on measurements of infrared emission. Mitchell and Robinson find that a mixture of silicate, corundum and iron grains satisfy the observations, with the silicate grains having a size of .1μ.

Radiative transfer calculations by Apruzese require rather larger particles and in a detailed investigation of the dust around η Carinae, Andriesse (1978) concludes that the dust consists of silicate grains of radius 1μ.

The present model of the Homunculus takes the geometry described in section 5.2.1 with a size distribution and seeks to reproduce the polarization produced by scattering on the major axis at the extremeties of the Homunculus. At these scattering angles viz. 110° to the NW and 70° to the SE, the polarization is found to be 35% and 25% respectively (see figures 5.31 and 5.32). These asymptotic values are assumed to arise where the nebula is optically thin and the scattering geometry is not significantly changing. Between these regions and η Carinae, the polarization drops off considerably due to the effects of increase in optical depth, changes in scattering geometry and the presence of the equatorial ring. The dust is assumed to consist of silicate grains.

5.4 METHOD OF COMPUTATION

The angular scattering functions for the silicate particles are computed by Mie theory (using the formalism given by Wickramasinghe 1973) as a function of complex refractive index

$$m = n - ik = \sqrt{K - 2i\sigma\lambda/c} \qquad (5.1)$$

where n corresponds to the real (refractory) and k the imaginary (absorbing) part of the refractive index, K is the dielectric constant and σ the

Figure 5.31 ASSYMPTOTIC VALUES OF POLARISATION

(Percentage polarisation averaged over 3 bins in x)

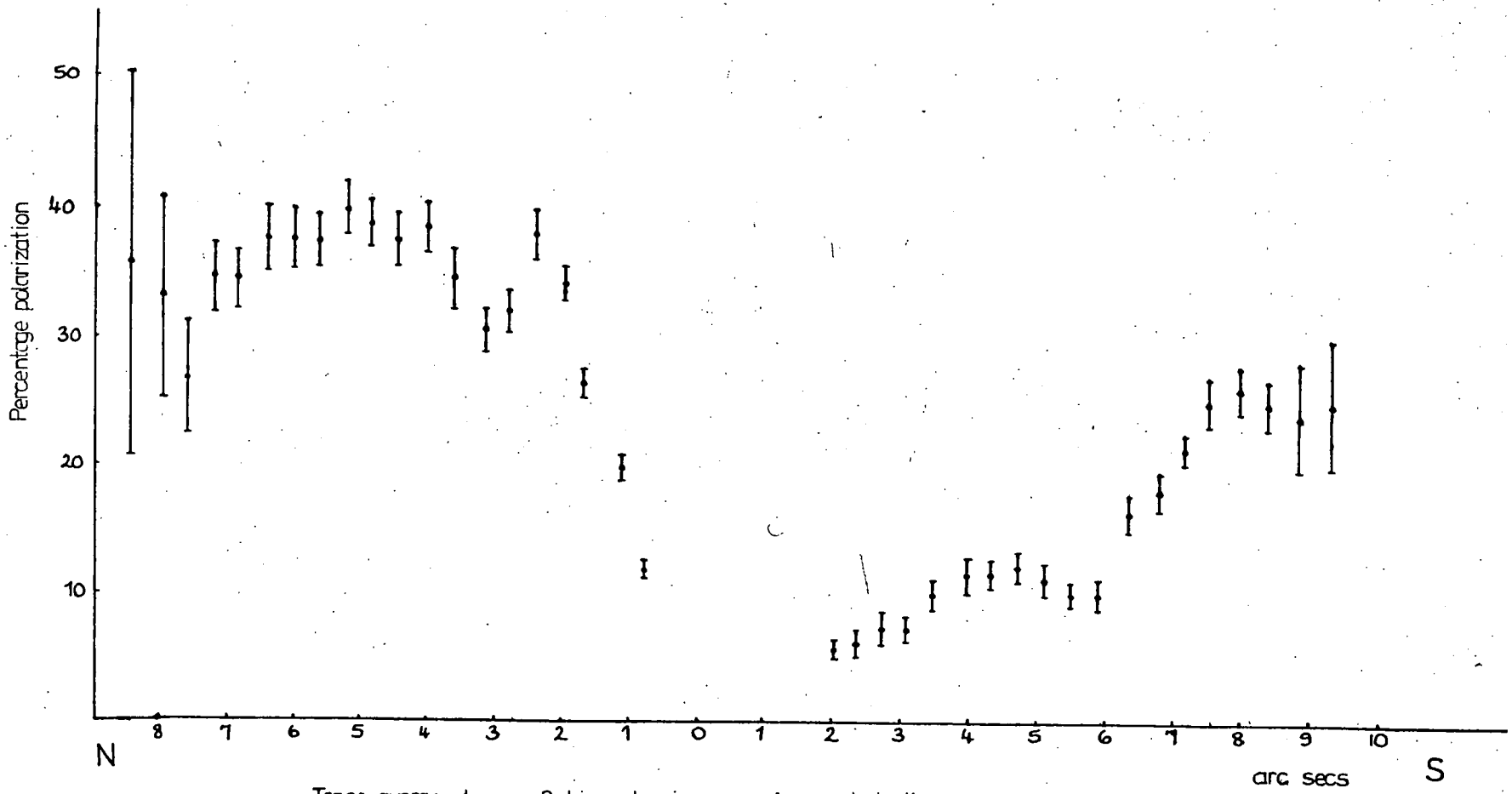

Trace averaged over 3 bins showing percentage polarisation

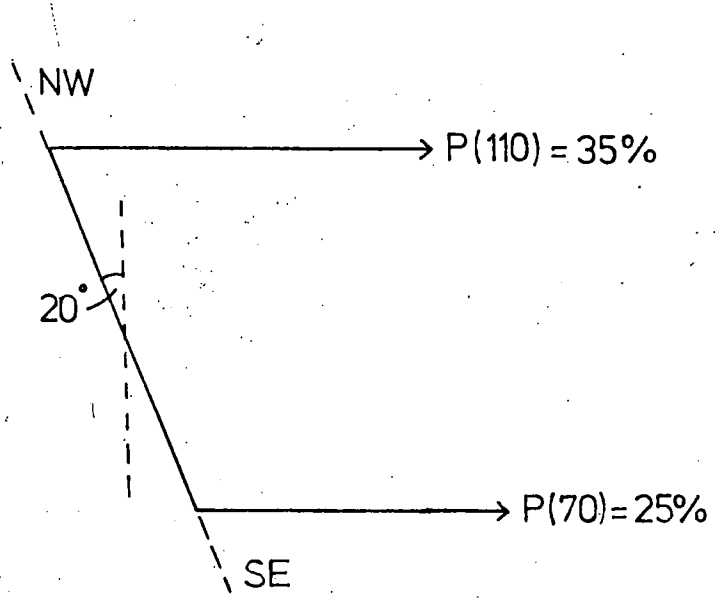

Figure 5.32. Definition of scattering angles.

conductivity of the particle material, and size parameter

$$x = 2\pi\, a/\lambda \tag{5.2}$$

where a is the radius of the (spherical) grain and λ the wavelength of the light.

The normalized scattering functions, following Hanner (1971) are

$$F_i(\theta,\lambda) = \frac{\int_0^\infty /S_i(x,\theta,\lambda)/^2\, n(x)\, dx}{\int_0^\infty n(x)\, dx} \tag{5.3}$$

where $S_i(x,\theta,\lambda)$ are the amplitude functions defined by van der Hulst (1957) and the subscripts i = 1,2 represent the contributions perpendicular and parallel.

The percentage polarization is given by

$$P = \frac{F_1 - F_2}{F_1 + F_2} .100 \tag{5.4}$$

The accuracy of the integration routine (from the * NAG LIBRARY) has been checked by reproducing the curves from Hanner's paper, using her parameters. These curves are shown in figure 5.41.

5.4.1 Refractive Index

Silicate minerals typically have real refractive indices in the range 1.55-1.75. Inclusion of a small imaginary component in the refractive index will reduce the amount of negative polarization and increase the positive polarization compared with the corresponding curves for a pure real refractive index. The refractive index used by Hanner was chosen, i.e. $m_1 = 1.65 - 0.05i$ on her suggestion that the inclusion of a small imaginary component for silicate may be more representative for models of grains than a pure refractive index (Hanner, 1971).

Figure 5·41 HANNER'S CURVES

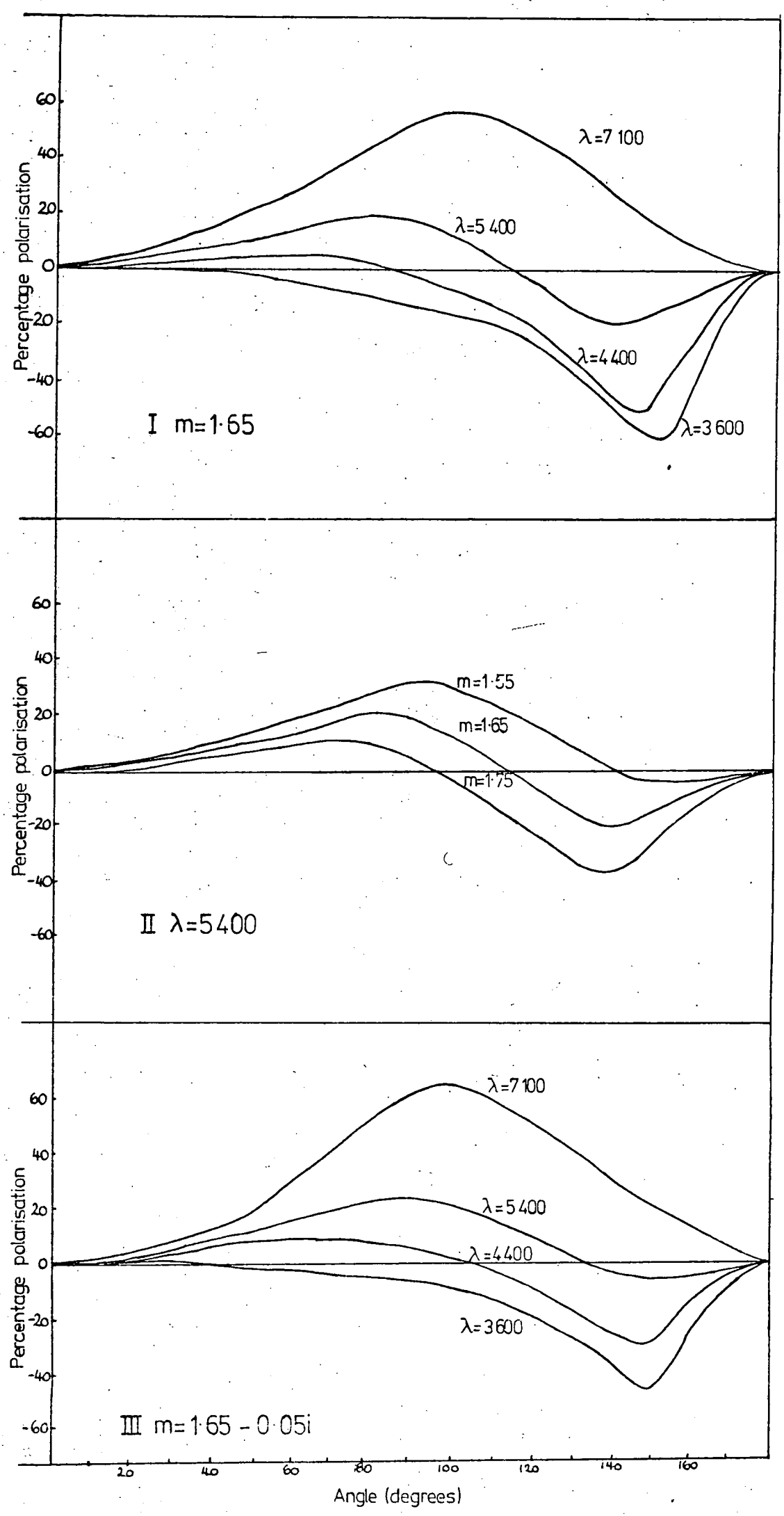

From calculations on interstellar circular polarization, Martin (1972) demonstrates that the wavelength of circular polarization is sensitive to the imaginary part of the complex refractive index of grain material. He suggests some possible grain materials including silicates, with $n \sim 1.7$ and k ranging from 0 to ~ 0.3. A refractive index, $m_2 = 1.7 - 0.3i$, was also chosen in order to contrast "dielectric" behaviour with that from more "metallic" grains.

5.4.2 Size distributions

It is highly improbable that any distribution of dust grains will consist of grains of a unique size only. A range of sizes is more likely to occur from say .01μ to greater than 1μ, in radius, with differing cross-section for scattering, and hence affecting the polarization differently. It is therefore necessary to incorporate a size distribution in any scattering model proposed. Various size distributions have been adopted by Wickramasinghe and Nandy (1973), in interstellar extinction studies, but here, the Greenberg distribution used by Hanner is initially considered, which is of the form

$$n(a) = \exp\left[-5\left(\frac{a}{a_o}\right)^3\right] \qquad (5.5)$$

with $a_o = 0.25$. Here $n(a)da$ represents the number of grains per unit volume with radii between a and a + da and the distribution is integrated between x = 0.01 and x = 20, convergence generally being reached after about seven or eight terms, where x is the size parameter, equal to $2\pi a/\lambda$, λ being the wavelength, with $x_o = 2\pi a_o/\lambda$. Hence an integral of the form

$$n(x) = \exp\left[-5\left(\frac{x}{x_o}\right)^3\right] \qquad (5.6)$$

is actually evaluated, since the Mie functions are calculated in terms of

x rather than a and since only a ratio is involved, the same results are obtained.

Rather poor agreement was obtained using this distribution and so a_o (or x_o) was varied to find an optimum value for the constant. The improvement was only marginal.

A greater degree of freedom could be obtained by varying the power and so a new distribution of the form

$$n(x) = \exp\left[-\left(\frac{x}{x_o}\right)^{\alpha}\right] \tag{5.7}$$

was investigated.

The effect of varying the power α, for both refractive indices is shown in figure 5.42, and it is clear that the percentage polarization is extremely sensitive to α. The main difficulty is that of obtaining the correct spacing between $P(110^o)$ and $P(70^o)$ at the right order of polarization. For m_1, the best fits were obtained with $0.24 < x_o < 0.27$ and $0.84 < \alpha < 0.87$. For m_2 there was a unique best fit at $x_o = 0.24, \alpha = 0.69$.

It can be seen that the refractive index has a greater effect on α than on x_o. The two size distributions

$$n(x) = \exp\left[-\left(\frac{x}{0.25}\right)^{.85}\right]$$

and

$$n(x) = \exp\left[-\left(\frac{x}{0.24}\right)^{0.69}\right]$$

are shown in figure 5.43a to be compared with the distributions obtained using the standard Greenberg distribution ($a_o = 0.25$) and this distribution optimized ($a_o = 0.22$ for m_1 and $a_o = 0.26$ for m_2) in figure 5.43b. All curves are normalized to an area of 1.

Although the Greenberg distributions are somewhat different from

Figure 5.42a

VARIATION OF $x\phi$ WITH α

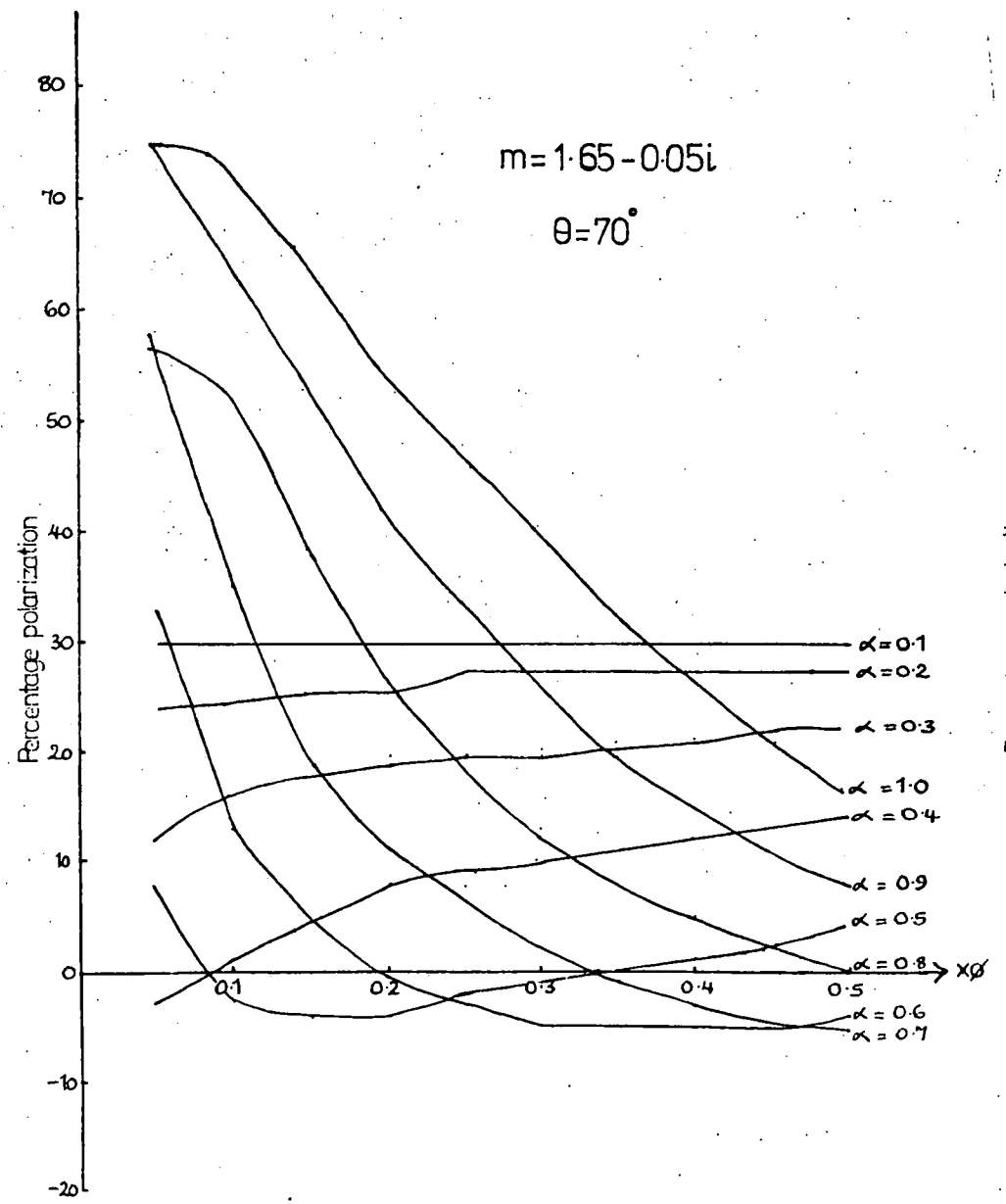

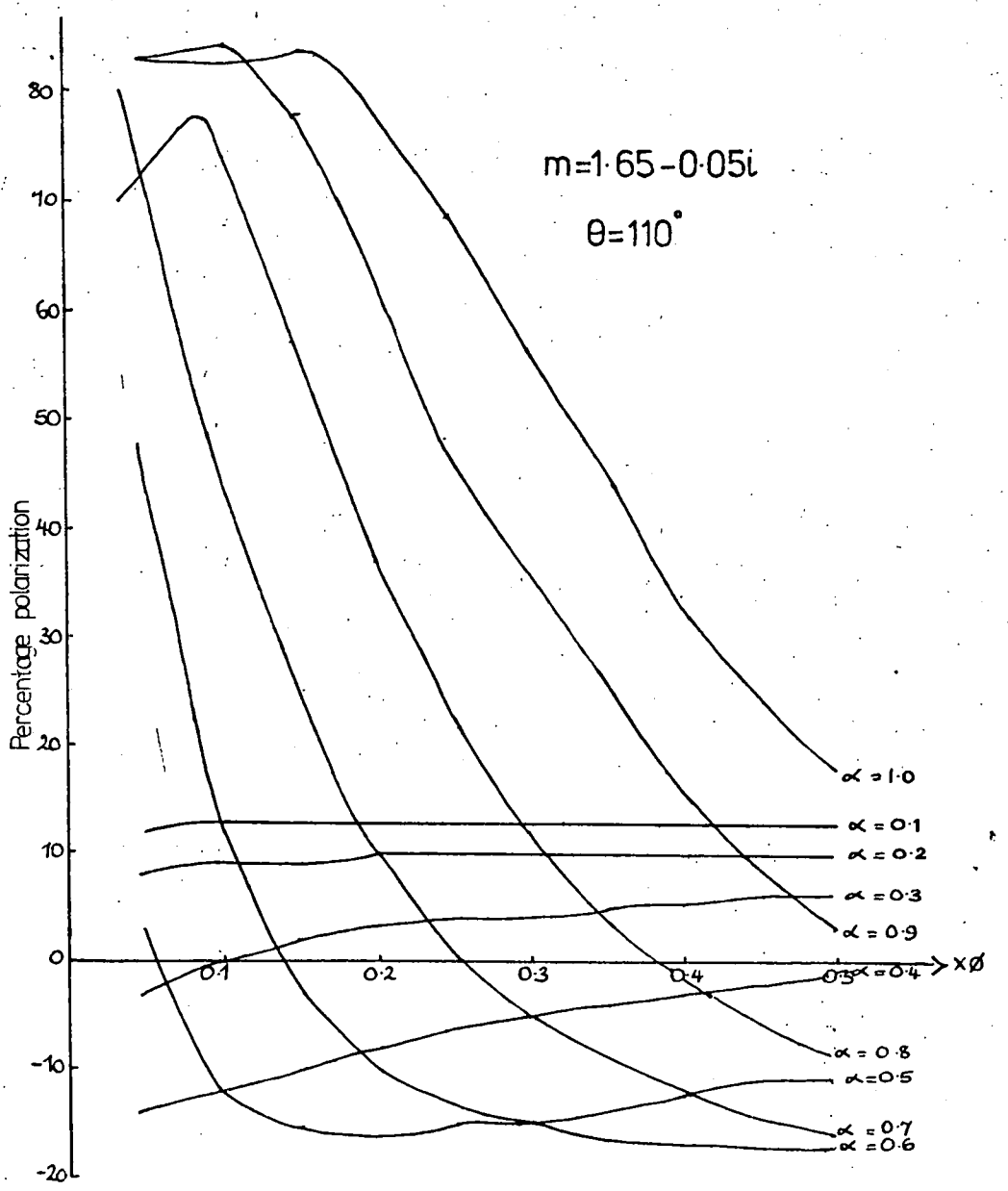

Figure 5.42b

VARIATION OF xø WITH α

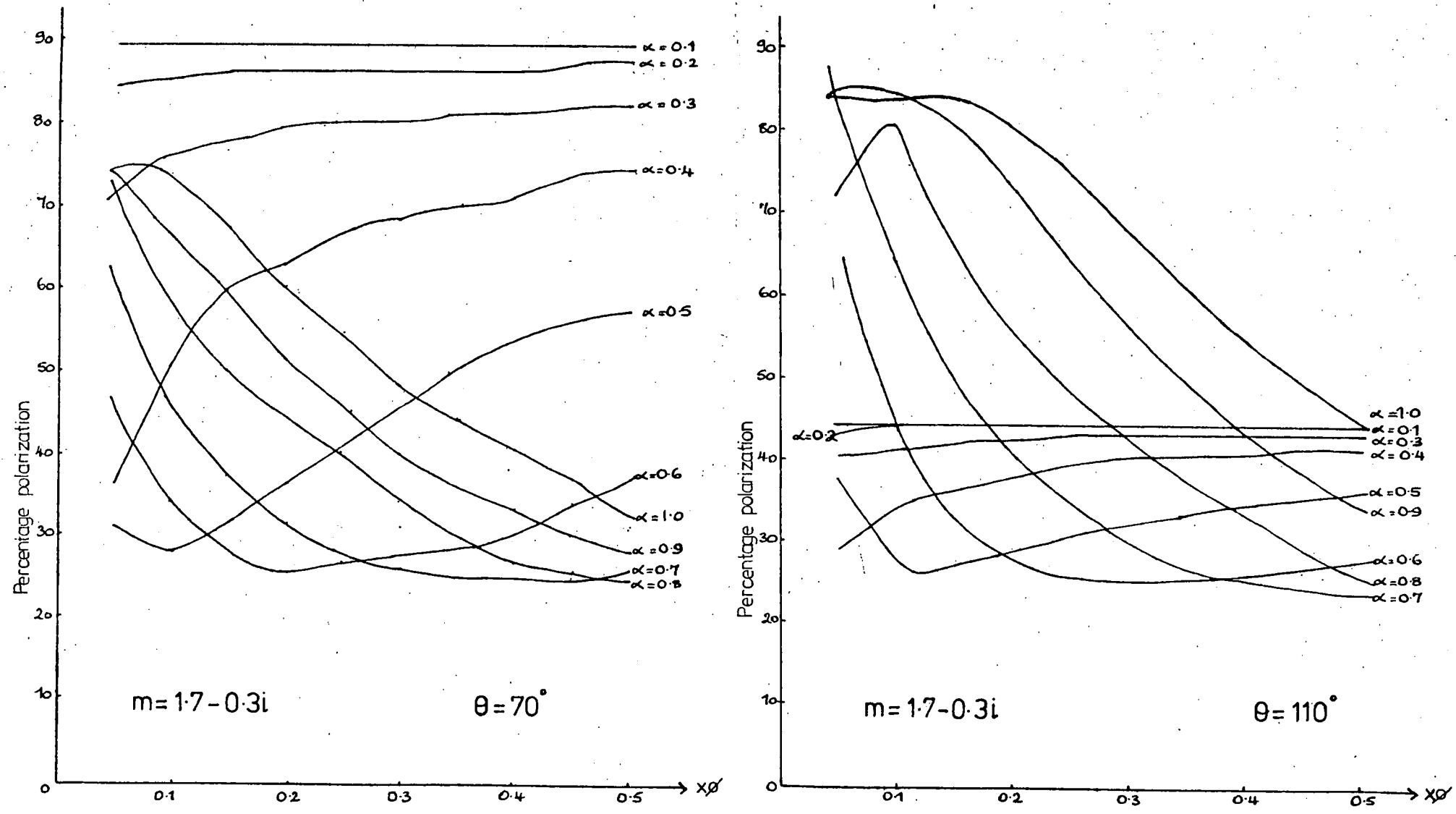

Figure 5.43a NEW SIZE DISTRIBUTIONS

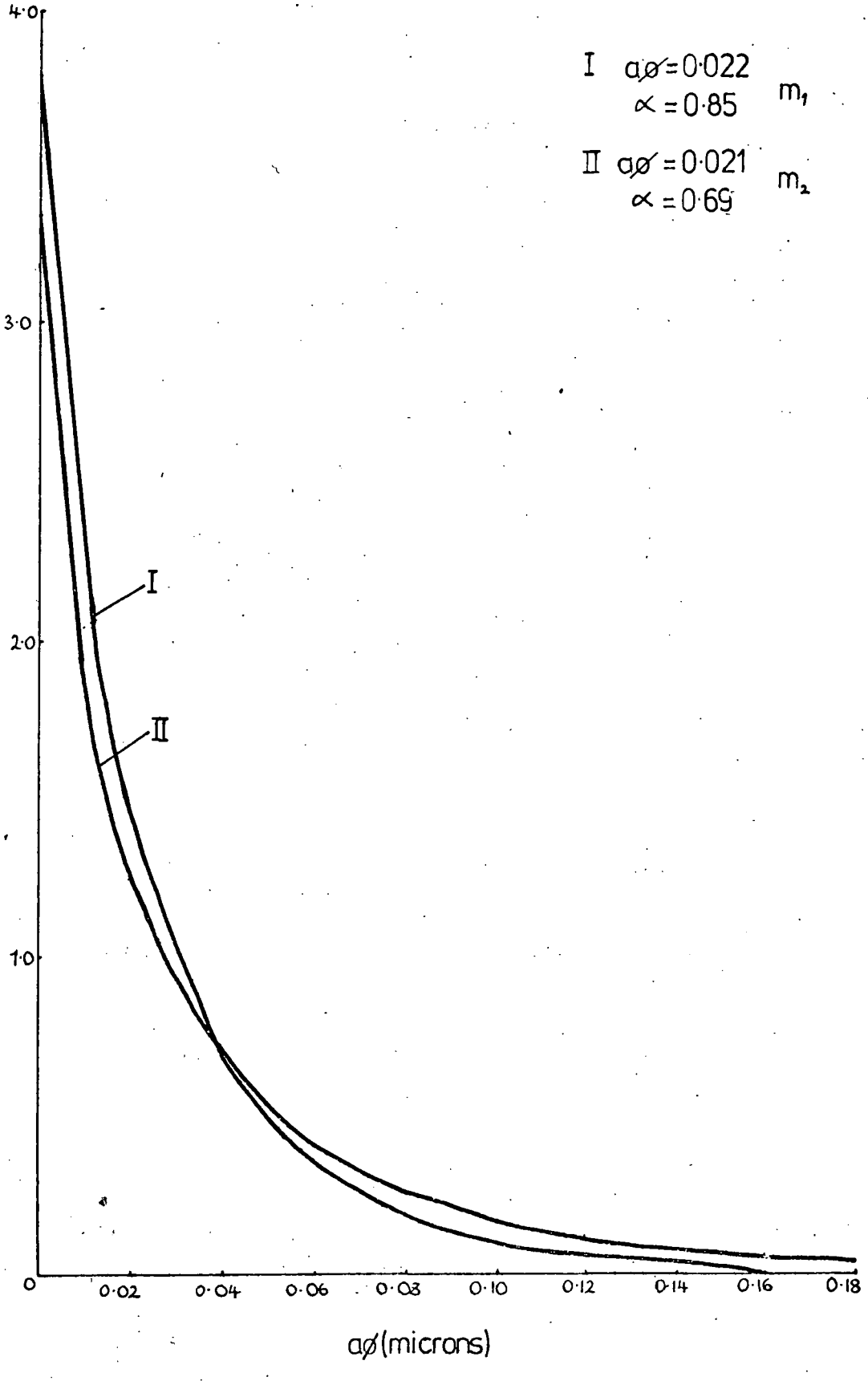

Figure 5.43b GREENBERG SIZE DISTRIBUTIONS

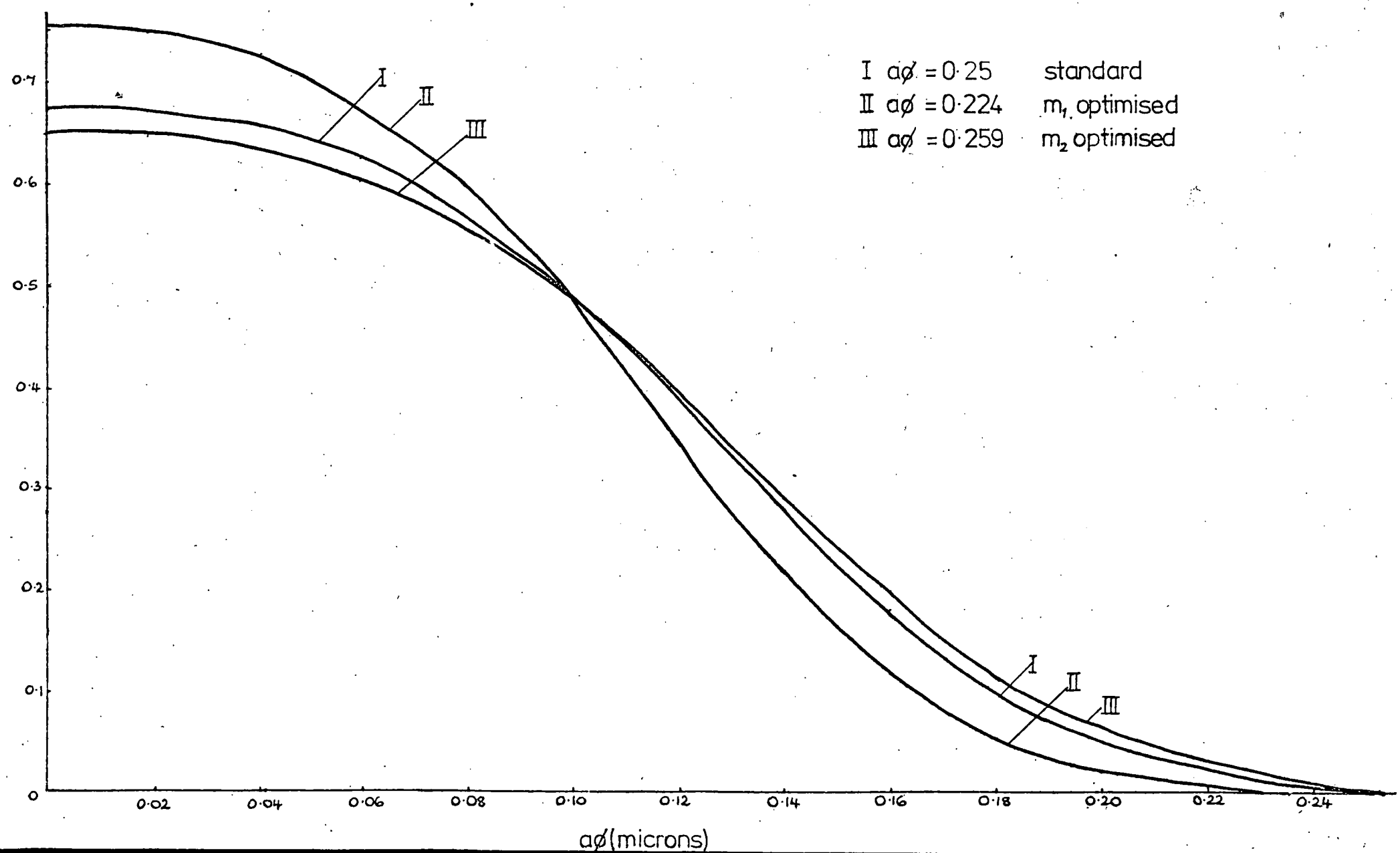

the new distributions, they are all very similar in the 0.1μ size region. The new distributions tend to include a greater number of both smaller and larger grains than the Greenberg distributions.

5.5 RESULTS

The results of the computations using various size distributions are summarized in Table 5.5A.

TABLE 5.5A

Percentage Polarizations obtained using various size distributions

Distribution	m = 1.65 - 0.05i		m = 1.7 - 0.3i	
	$P(70^\circ)$	$P(110^\circ)$	$P(70^\circ)$	$P(110^\circ)$
Greenberg-standard	23%	16%	36%	38%
Greenberg-optimized	31%	35%	34%	35%
New distribution	25%	36%	28%	34%
OBSERVATIONS	$P(70^\circ)$ = 25%		$P(110^\circ)$ = 35%	

Using the new distributions, it is possible to predict the variation of polarization with wavelength. This will be the most important factor determining the characteristics of the grain material since, as can be seen in Table 5.5B, the two refractive indices used predict very different polarizations at 70° and 110°.

TABLE 5.5B

Variation of Polarization with wavelength

Refractive Index	$\lambda = .4\ \mu$		$\lambda = .7\ \mu$	
	$P(70^\circ)$	$P(110^\circ)$	$P(70^\circ)$	$P(110^\circ)$
$m = 1.65-0.05i$	14%	14%	36%	52%
$m = 1.70-0.30i$	25%	27%	32%	41%

5.5.1 Efficiency Factors

The efficiency factors for scattering (Q_{sca}), absorption (Q_{abs}) and extinction ($Q_{ext} = Q_{abs} + Q_{sca}$) have been calculated, using the formalism of Wickramasinghe (1973). They are displayed in figures 5.51a and 5.51b as a function of grain size. The larger imaginary component in the refractive index (figure 5.51b) has the effect of smoothing the curves, otherwise, apart from the greater absorbing efficiency of m_2 over m_1, the two graphs are very similar.

5.5.2 Cross-sections

The total cross-sections for scattering (C_{sca}), absorption (C_{abs}) and extinction (C_{ext}) are shown in figures 5.52a, 5.52b, as a function of grain size. The cross-sections are equal to the relevant efficiency factor, multiplied by the geometrical cross-section, πa^2 (van der Hulst, 1957). Thus

$$Q_{sca} = C_{sca}/\pi a^2 \qquad (5.8)$$

$$Q_{abs} = C_{abs}/\pi a^2 \qquad (5.9)$$

$$Q_{ext} = C_{ext}/\pi a^2 \qquad (5.10)$$

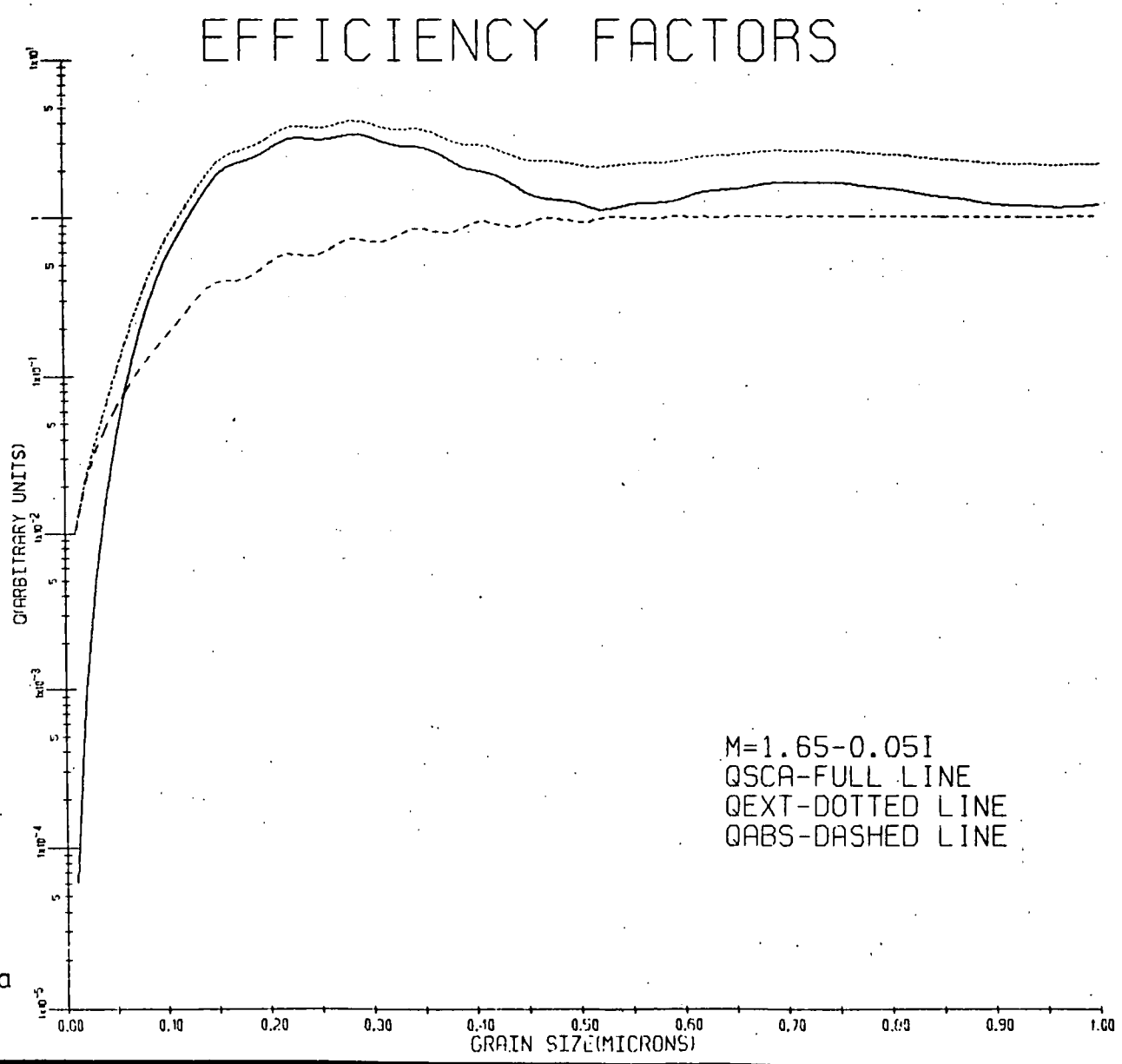
EFFICIENCY FACTORS
QARBITRARY UNITS)
GRAIN SIZE(MICRONS)
0.00
0.10
0.20
0.30
0.40
0.50
0.60
0.70
0.80
0.90
1.00
M=1.65-0.05I
QSCA-FULL LINE
QEXT-DOTTED LINE
QABS-DASHED LINE

Figure 5.51a

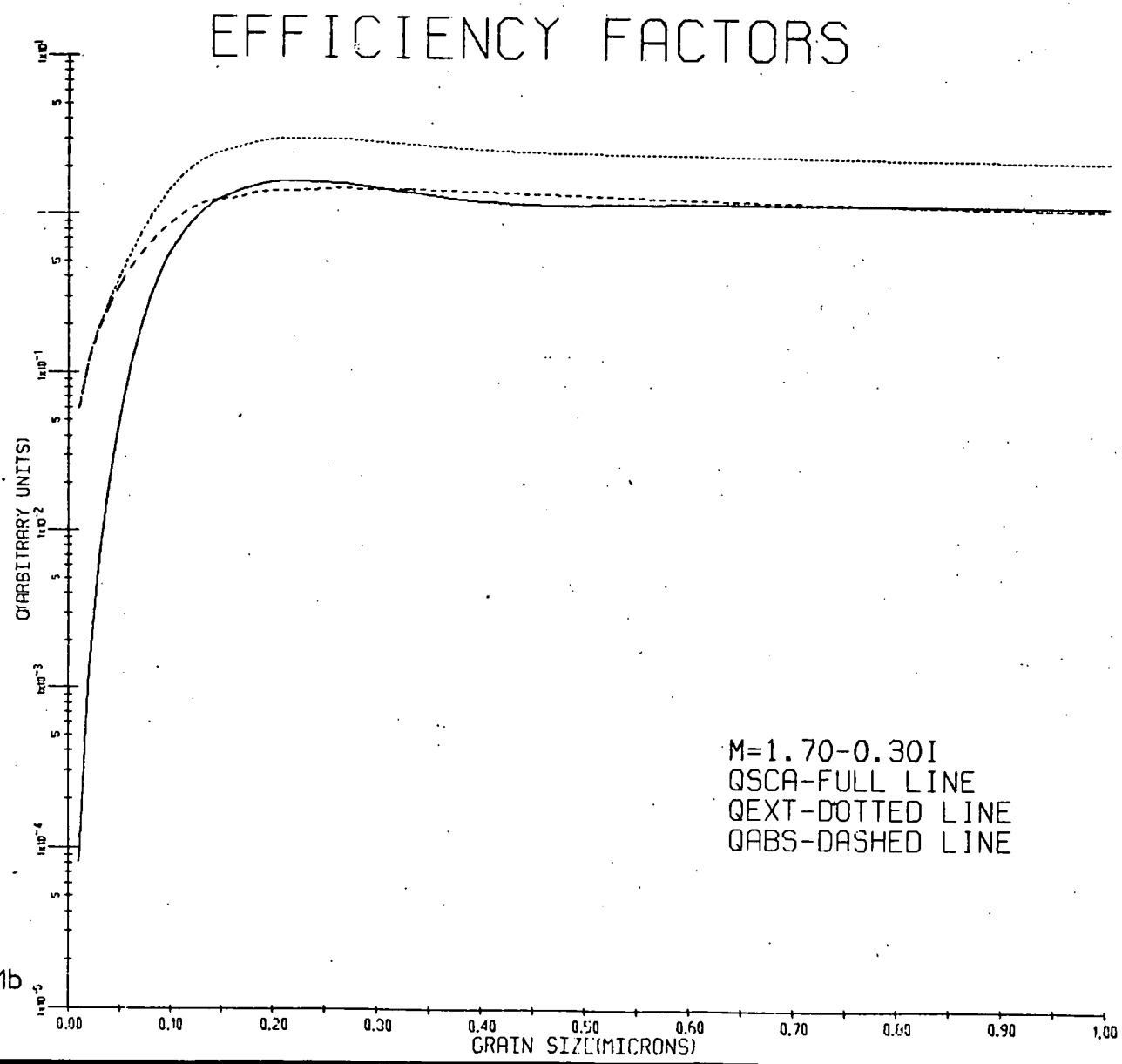
EFFICIENCY FACTORS
QARBITRARY UNITS)
GRAIN SIZE(MICRONS)
0.00
0.10
0.20
0.30
0.40
0.50
0.60
0.70
0.80
0.90
1.00
M=1.70-0.30I
QSCA-FULL LINE
QEXT-DOTTED LINE
QABS-DASHED LINE

Figure 5.51b

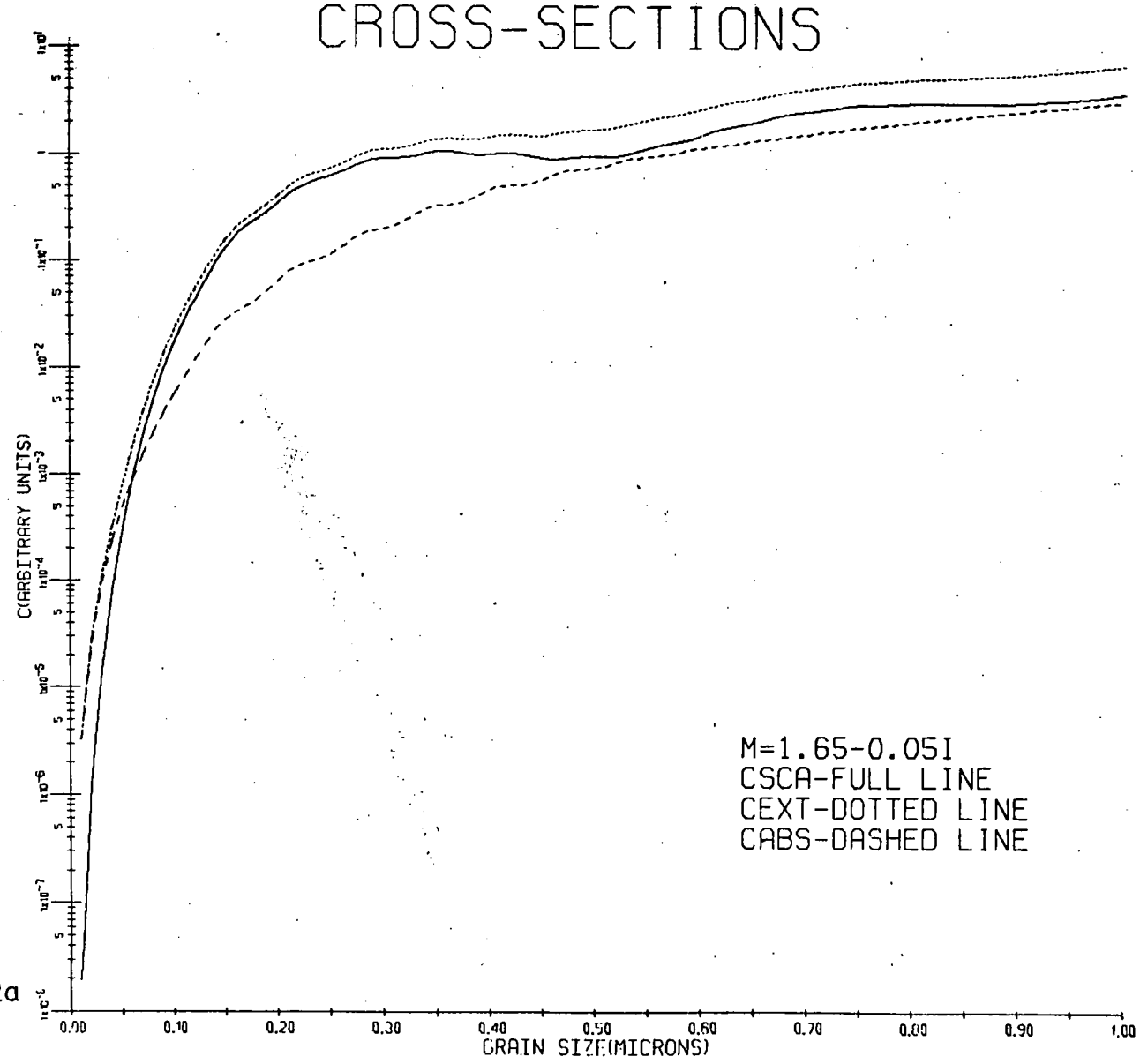
CROSS-SECTIONS
(ARBITRARY UNITS)
GRAIN SIZE(MICRONS)
0.00
0.10
0.20
0.30
0.40
0.50
0.60
0.70
0.80
0.90
1.00
M=1.65-0.05I
CSCA-FULL LINE
CEXT-DOTTED LINE
CABS-DASHED LINE

Figure 5.52a

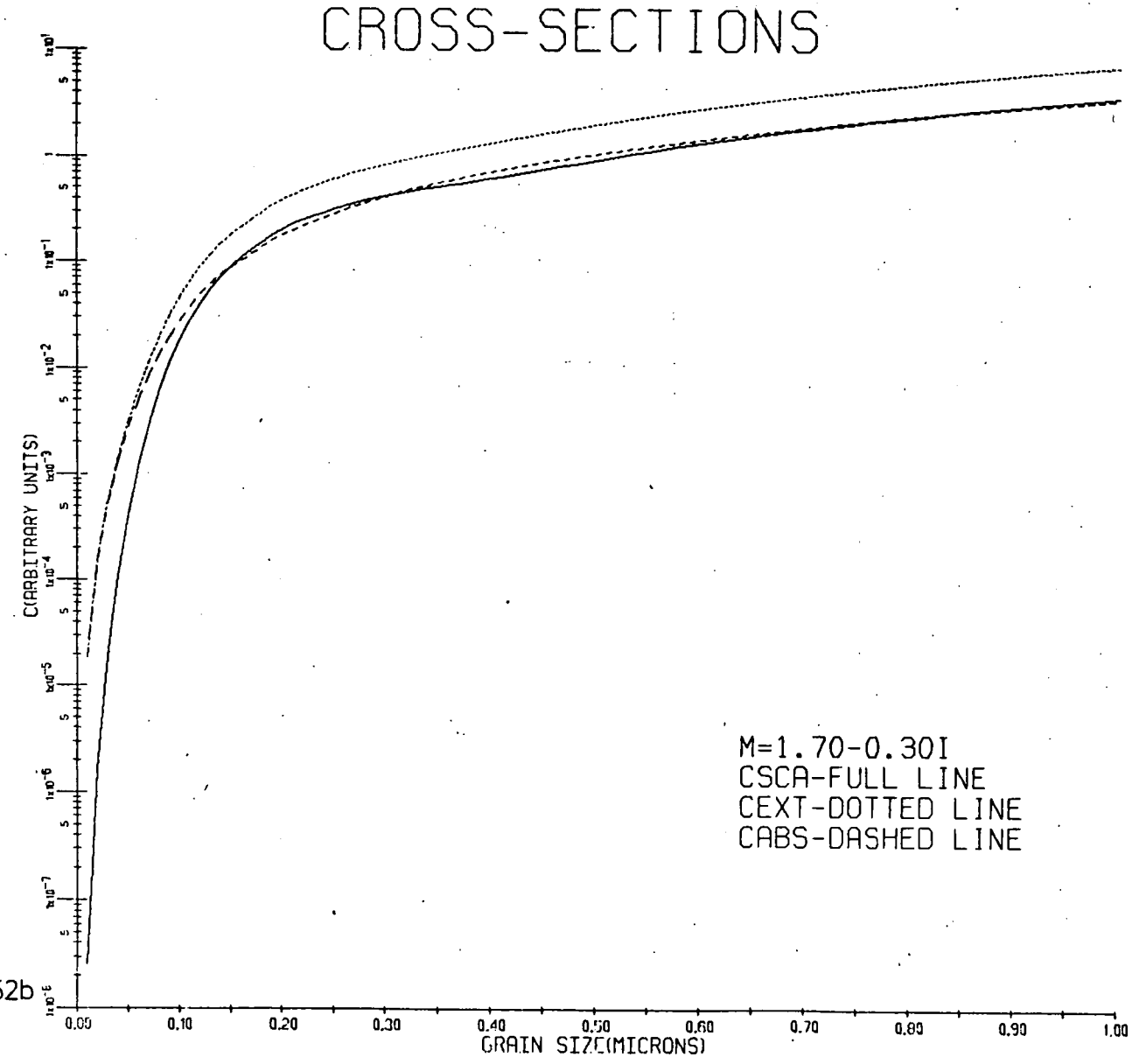
CROSS-SECTIONS
(ARBITRARY UNITS)
GRAIN SIZE(MICRONS)
0.00
0.10
0.20
0.30
0.40
0.50
0.60
0.70
0.80
0.90
1.00
M=1.70-0.30I
CSCA-FULL LINE
CEXT-DOTTED LINE
CABS-DASHED LINE

Figure 5.52b

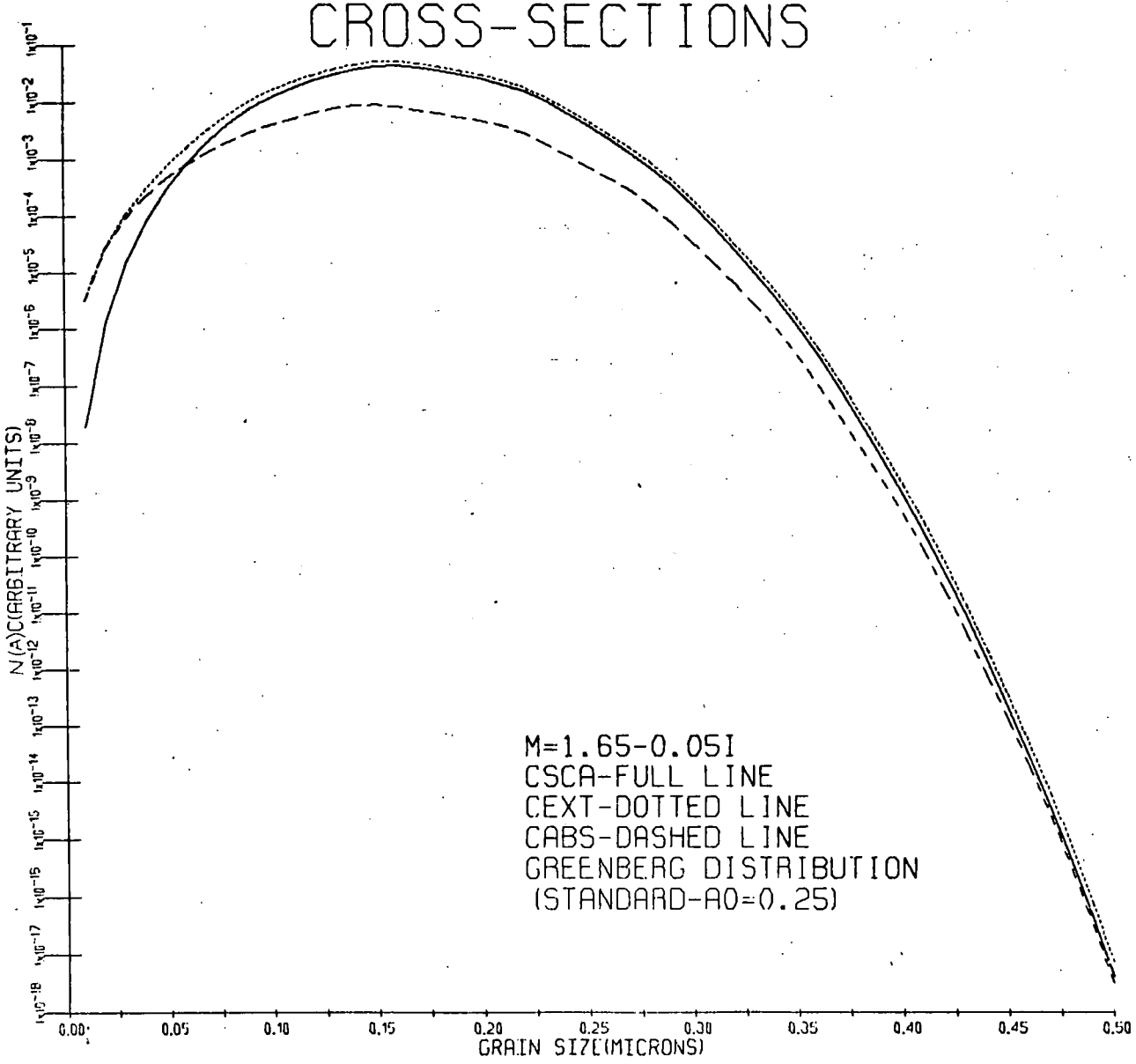
CROSS-SECTIONS
N(A)C(ARBITRARY UNITS)
GRAIN SIZE(MICRONS)
M=1.65-0.05I
CSCA-FULL LINE
CEXT-DOTTED LINE
CABS-DASHED LINE
GREENBERG DISTRIBUTION
(STANDARD-A0=0.25)

Figure 5.53a

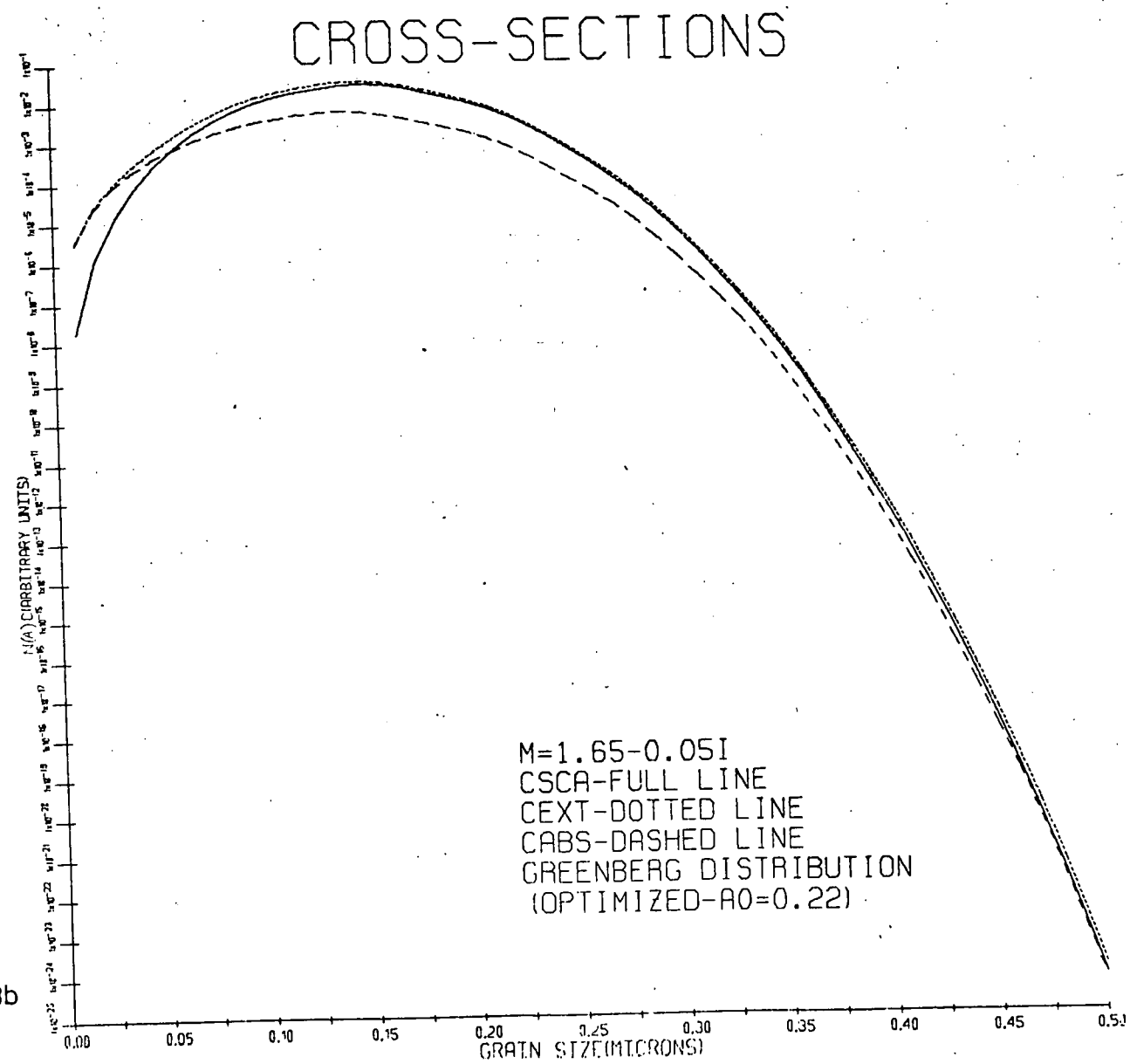
CROSS-SECTIONS
N(A)(ARBITRARY UNITS)
M=1.65-0.05I
CSCA-FULL LINE
CEXT-DOTTED LINE
CABS-DASHED LINE
GREENBERG DISTRIBUTION
(OPTIMIZED-A0=0.22)
0.00
0.05
0.10
0.15
0.20
0.25
0.30
0.35
0.40
0.45
GRAIN SIZE(MICRONS)

Figure 5.53b

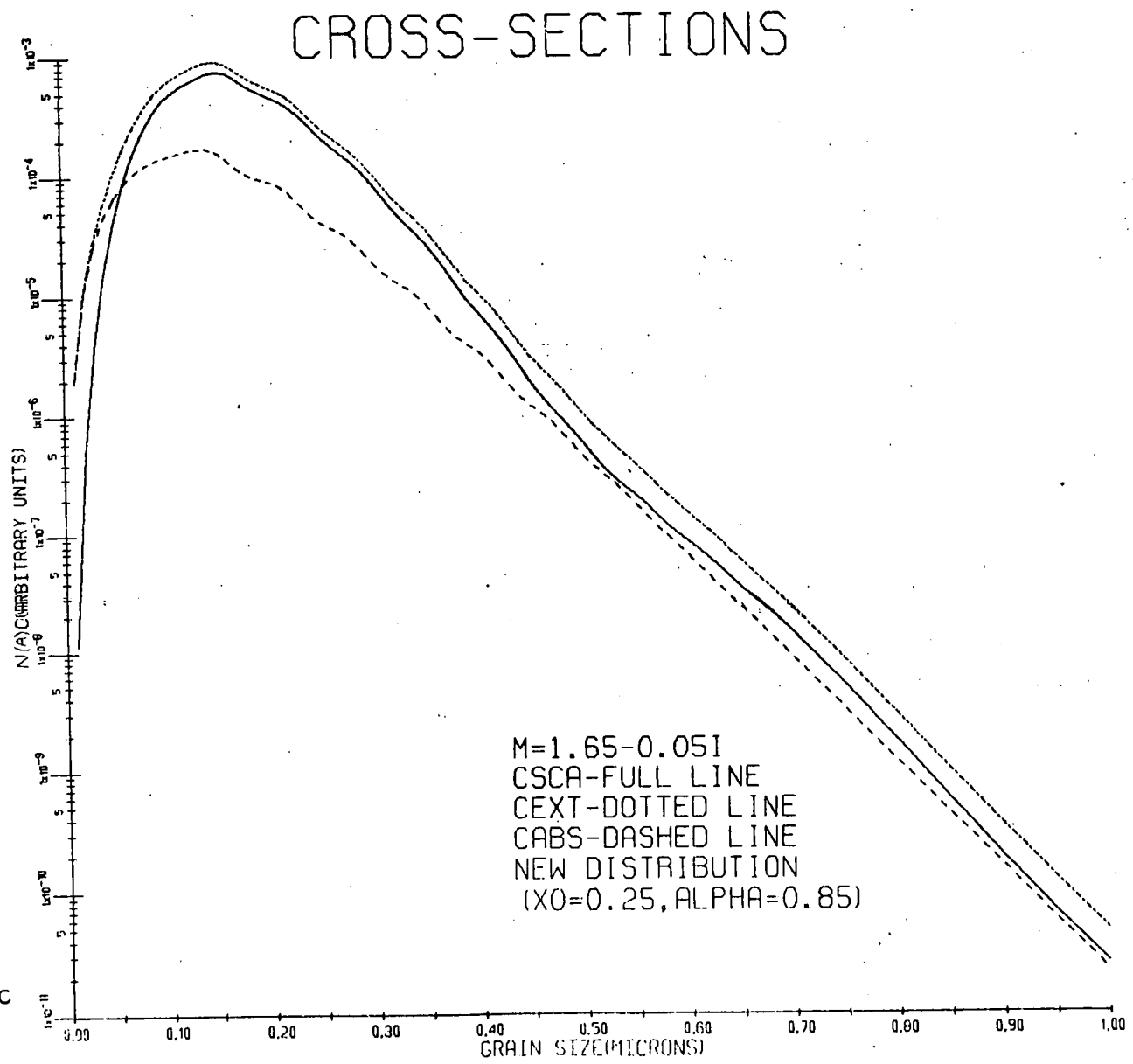
CROSS-SECTIONS
N(A)(ARBITRARY UNITS)
GRAIN SIZE(MICRONS)
0.00
0.10
0.20
0.30
0.40
0.50
0.60
0.70
0.80
0.90
1.00
M=1.65-0.05I
CSCA-FULL LINE
CEXT-DOTTED LINE
CABS-DASHED LINE
NEW DISTRIBUTION
(XO=0.25,ALPHA=0.85)

Figure 5.53c

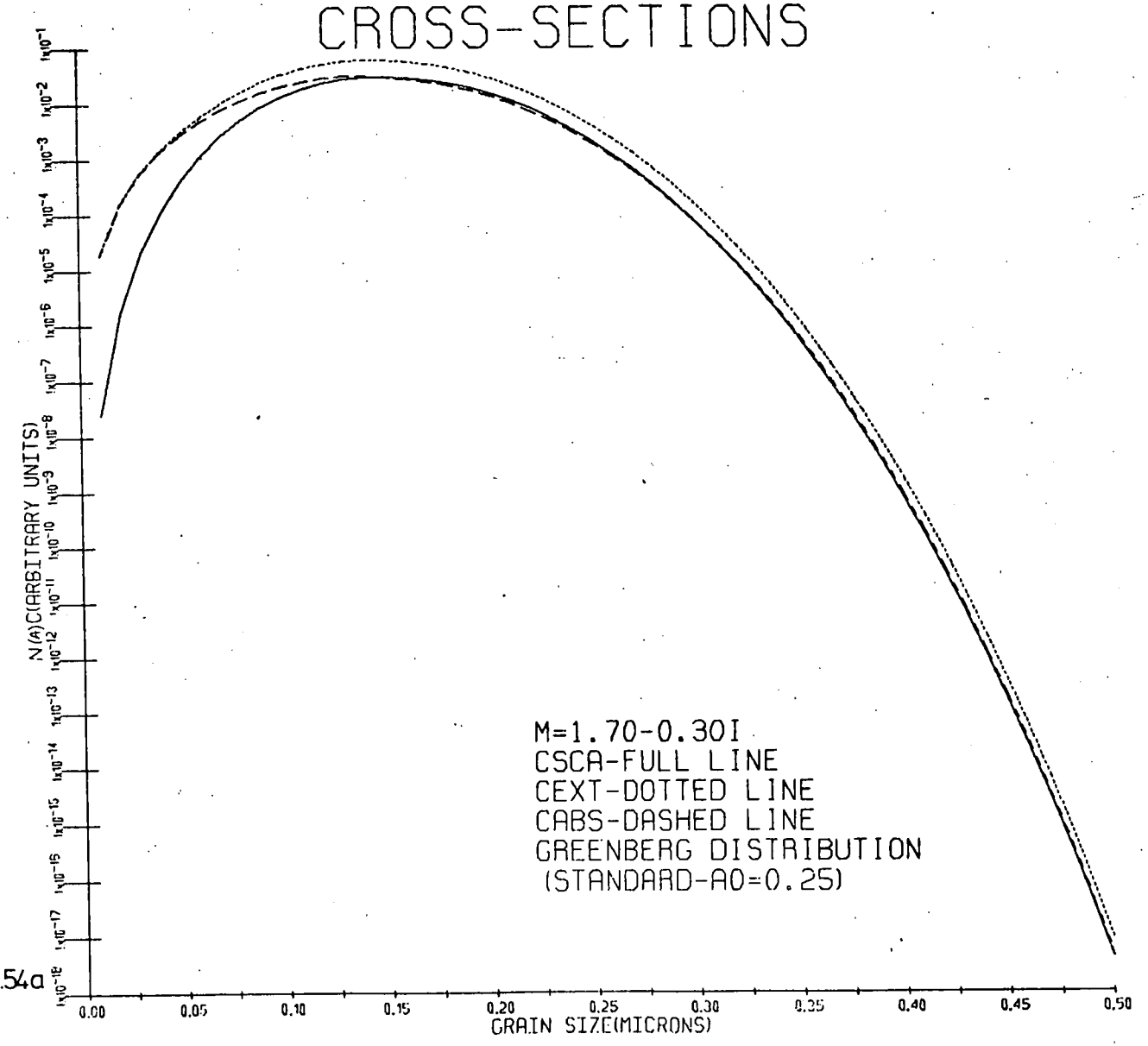
CROSS-SECTIONS
N(A)(ARBITRARY UNITS)
GRAIN SIZE(MICRONS)
M=1.70-0.30I
CSCA-FULL LINE
CEXT-DOTTED LINE
CABS-DASHED LINE
GREENBERG DISTRIBUTION
(STANDARD-A0=0.25)

Figure 5.54a

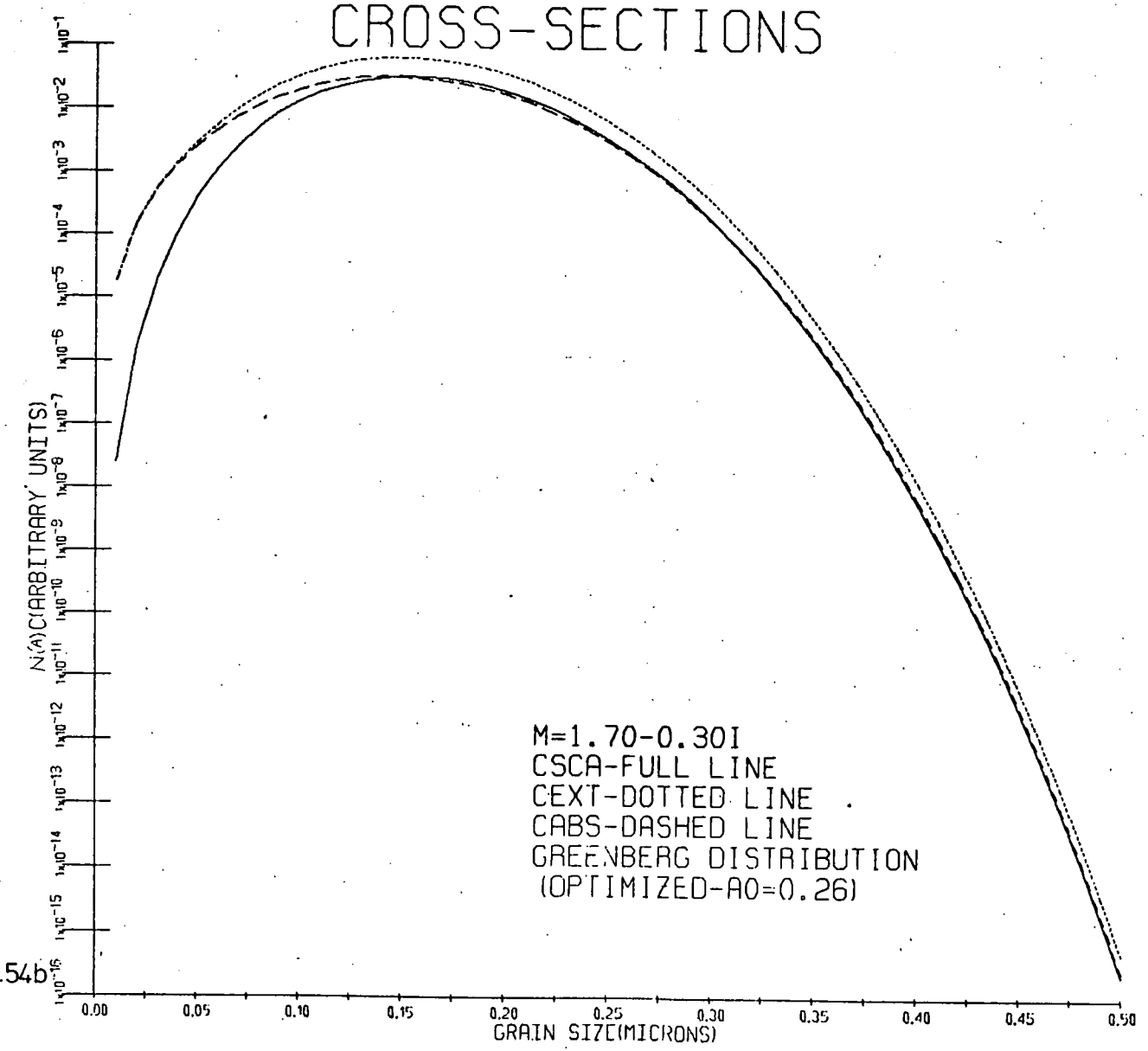
CROSS-SECTIONS
N(A)C(ARBITRARY UNITS)
GRAIN SIZE(MICRONS)
M=1.70-0.30I
CSCA-FULL LINE
CEXT-DOTTED LINE
CABS-DASHED LINE
GREENBERG DISTRIBUTION
(OPTIMIZED-A0=0.26)

Figure 5.54b

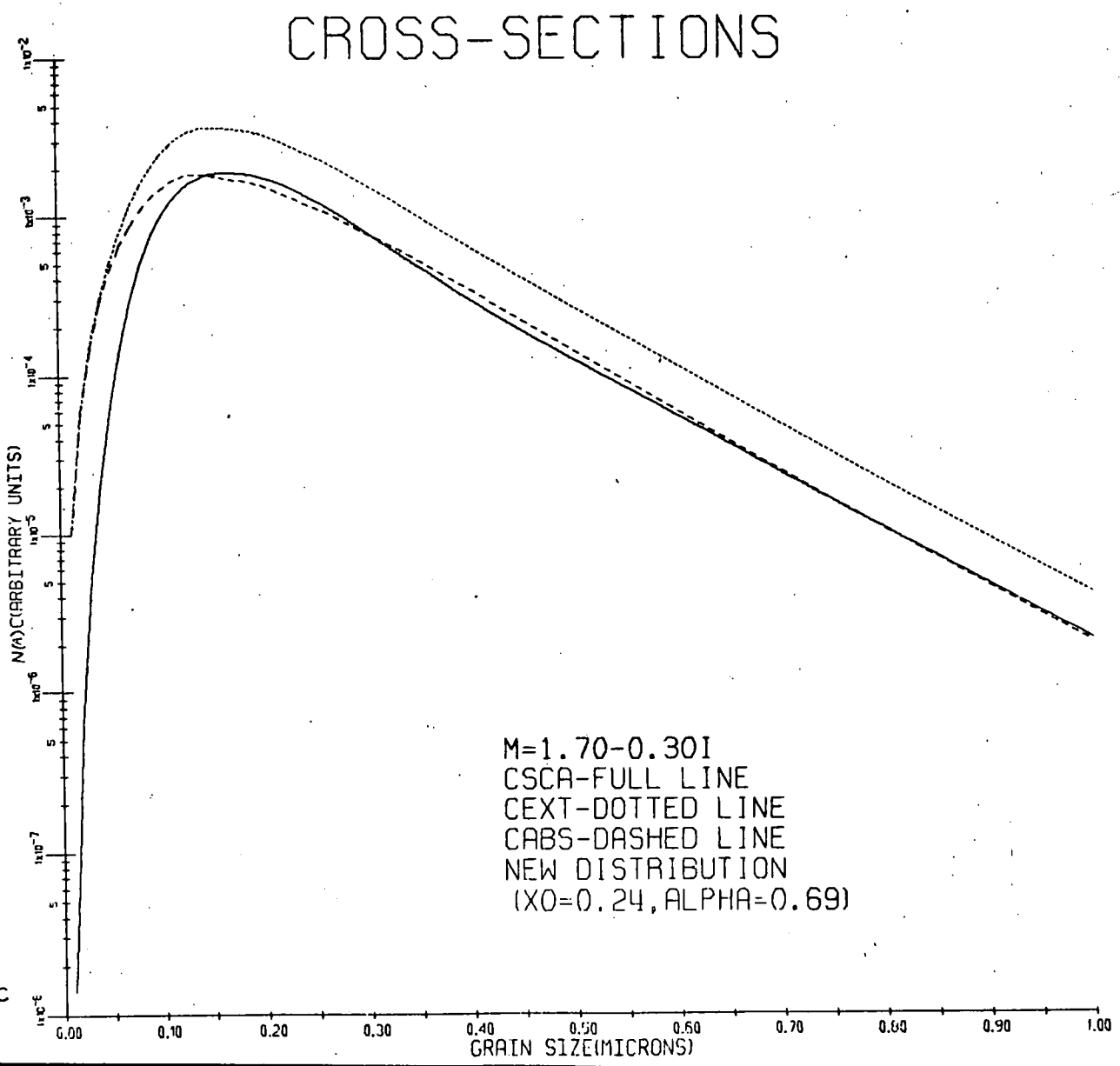
CROSS-SECTIONS
N(A)C(ARBITRARY UNITS)
GRAIN SIZE(MICRONS)
0.00
0.10
0.20
0.30
0.40
0.50
0.60
0.70
0.80
0.90
1.00
M=1.70-0.30I
CSCA-FULL LINE
CEXT-DOTTED LINE
CABS-DASHED LINE
NEW DISTRIBUTION
(XO=0.24, ALPHA=0.69)

Figure 5.54c

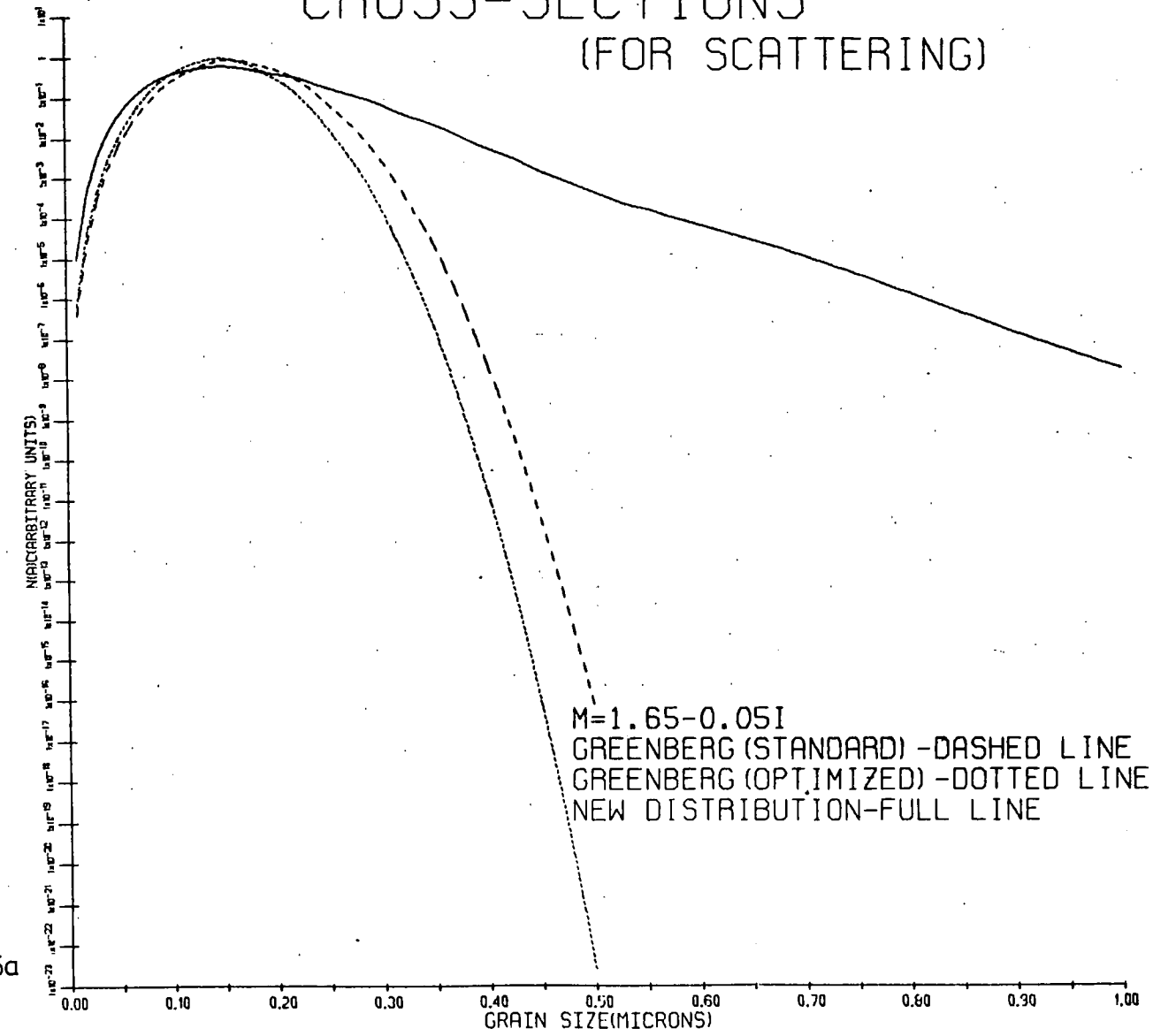
CROSS-SECTIONS
(FOR SCATTERING)
N(A)(CARBITRARY UNITS)
M=1.65-0.05I
GREENBERG (STANDARD) -DASHED LINE
GREENBERG (OPTIMIZED) -DOTTED LINE
NEW DISTRIBUTION-FULL LINE
0.00
0.10
0.20
0.30
0.40
0.50
0.60
0.70
0.80
0.90
1.00
GRAIN SIZE(MICRONS)

Figure 5.55a

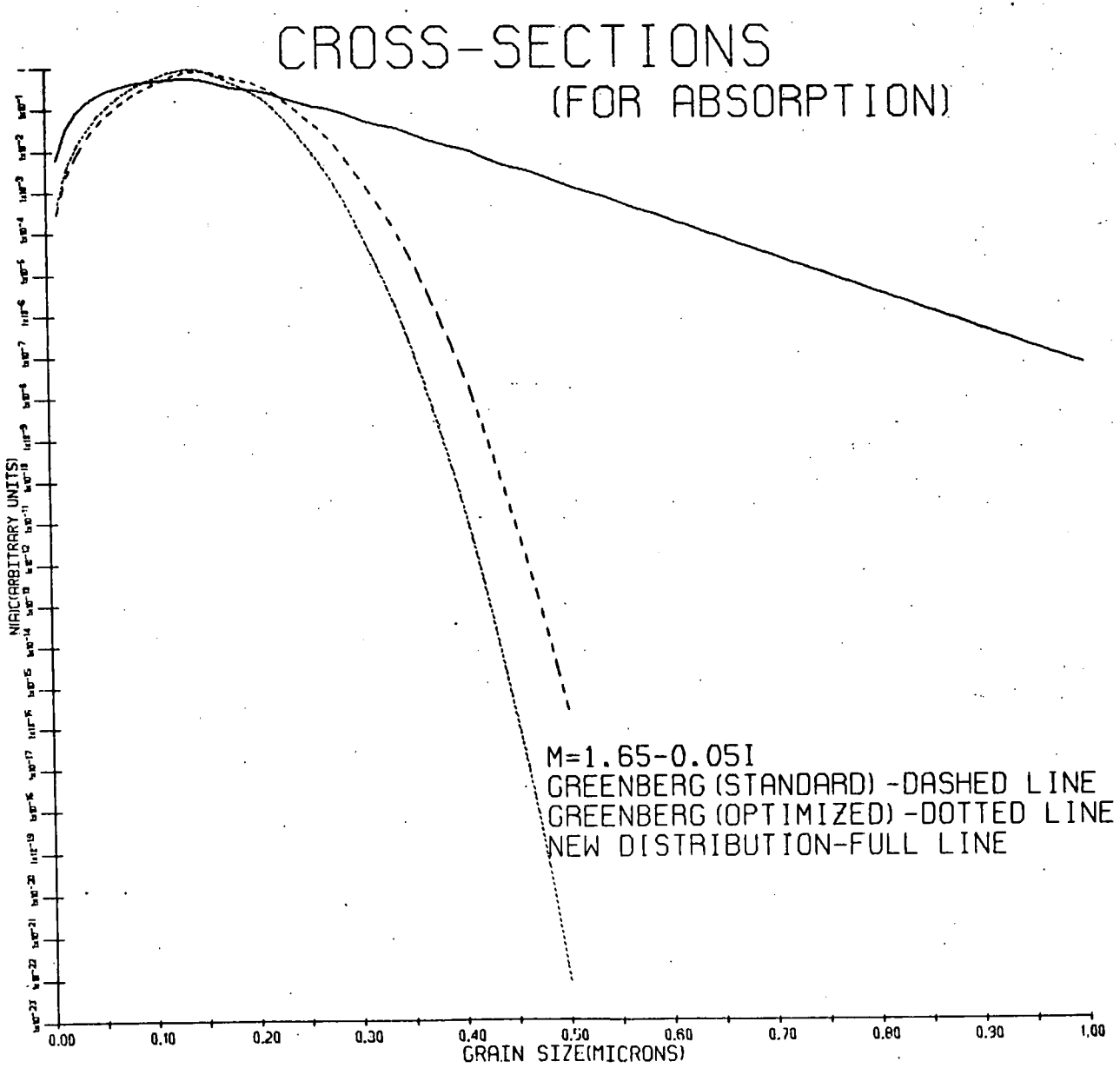
CROSS-SECTIONS
(FOR ABSORPTION)
NIAC(ARBITRARY UNITS)
M=1.65-0.05I
GREENBERG (STANDARD) -DASHED LINE
GREENBERG (OPTIMIZED) -DOTTED LINE
NEW DISTRIBUTION-FULL LINE
0.00
0.10
0.20
0.30
0.40
0.50
0.60
0.70
0.80
0.90
1.00
GRAIN SIZE(MICRONS)

Figure 5.55b

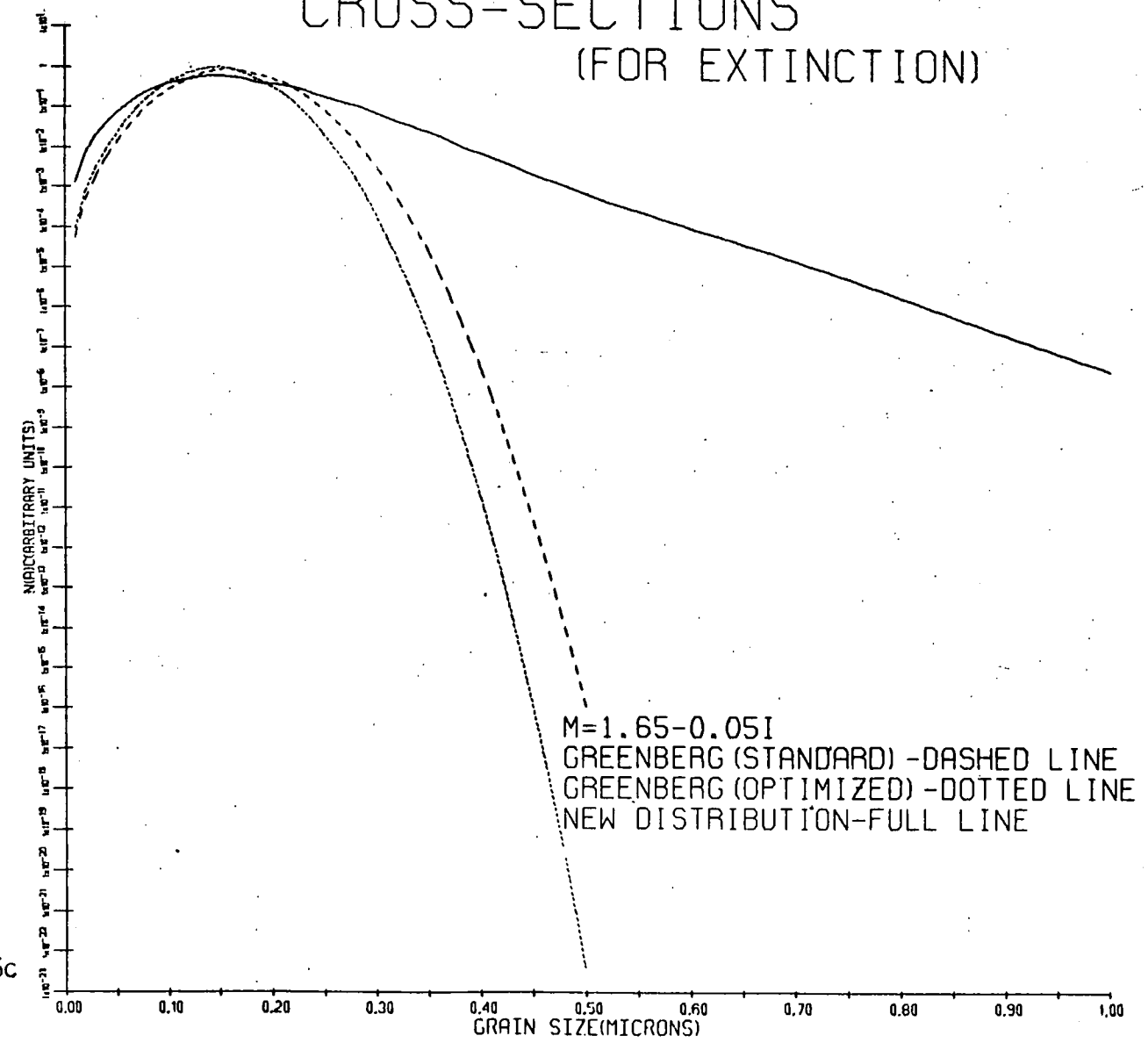
CROSS-SECTIONS
(FOR EXTINCTION)
NIAICARBITRARY UNITS)
M=1.65-0.05I
GREENBERG (STANDARD) -DASHED LINE
GREENBERG (OPTIMIZED) -DOTTED LINE
NEW DISTRIBUTION-FULL LINE
0.00
0.10
0.20
0.30
0.40
0.50
0.60
0.70
0.80
0.90
1.00
GRAIN SIZE(MICRONS)

Figure 5.55c

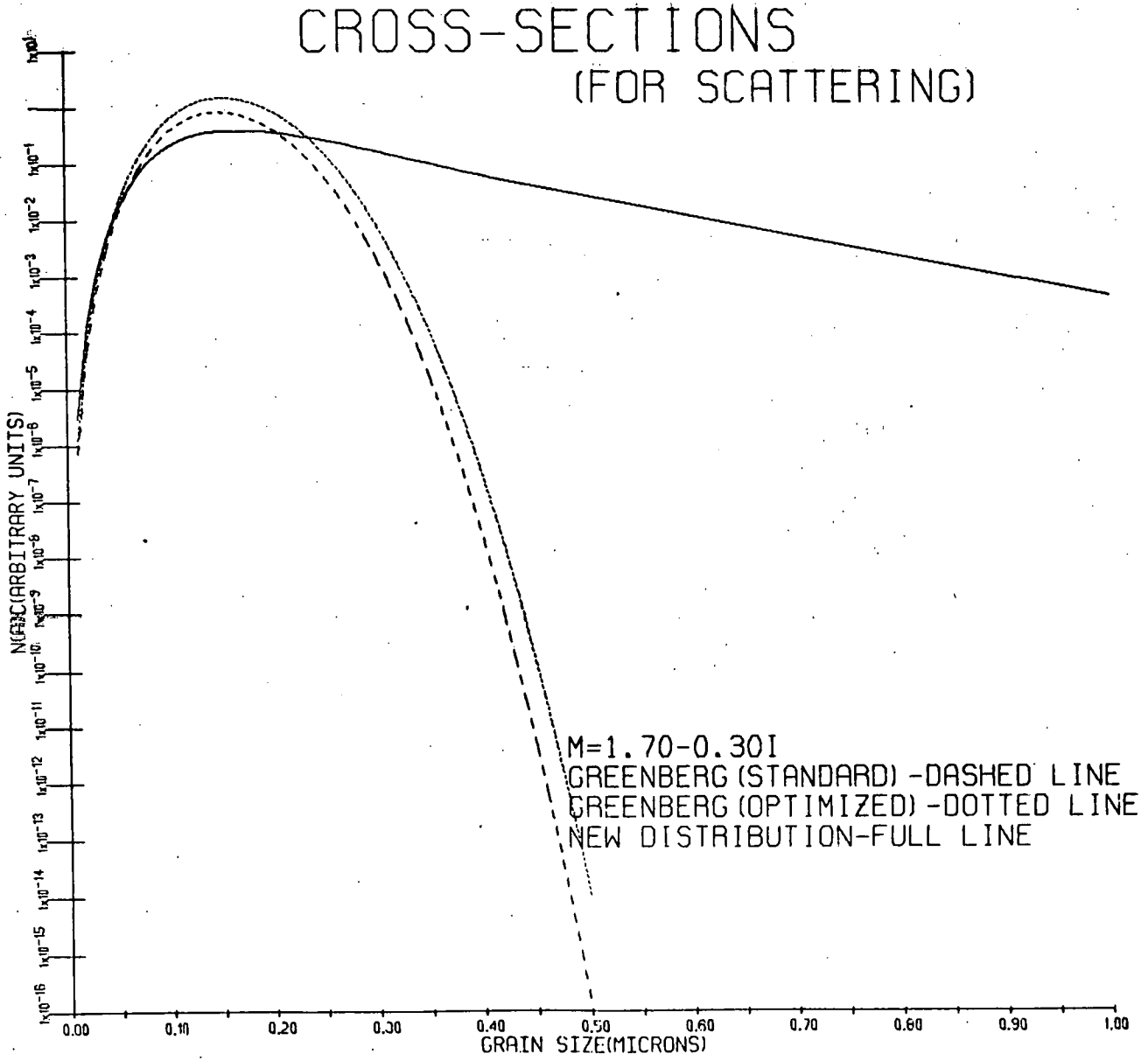
CROSS-SECTIONS
(FOR SCATTERING)
N(GRAIN)(ARBITRARY UNITS)
GRAIN SIZE(MICRONS)
0.00
0.10
0.20
0.30
0.40
0.50
0.60
0.70
0.80
0.90
1.00
M=1.70-0.30I
GREENBERG (STANDARD) -DASHED LINE
GREENBERG (OPTIMIZED) -DOTTED LINE
NEW DISTRIBUTION-FULL LINE

Figure 5.56a

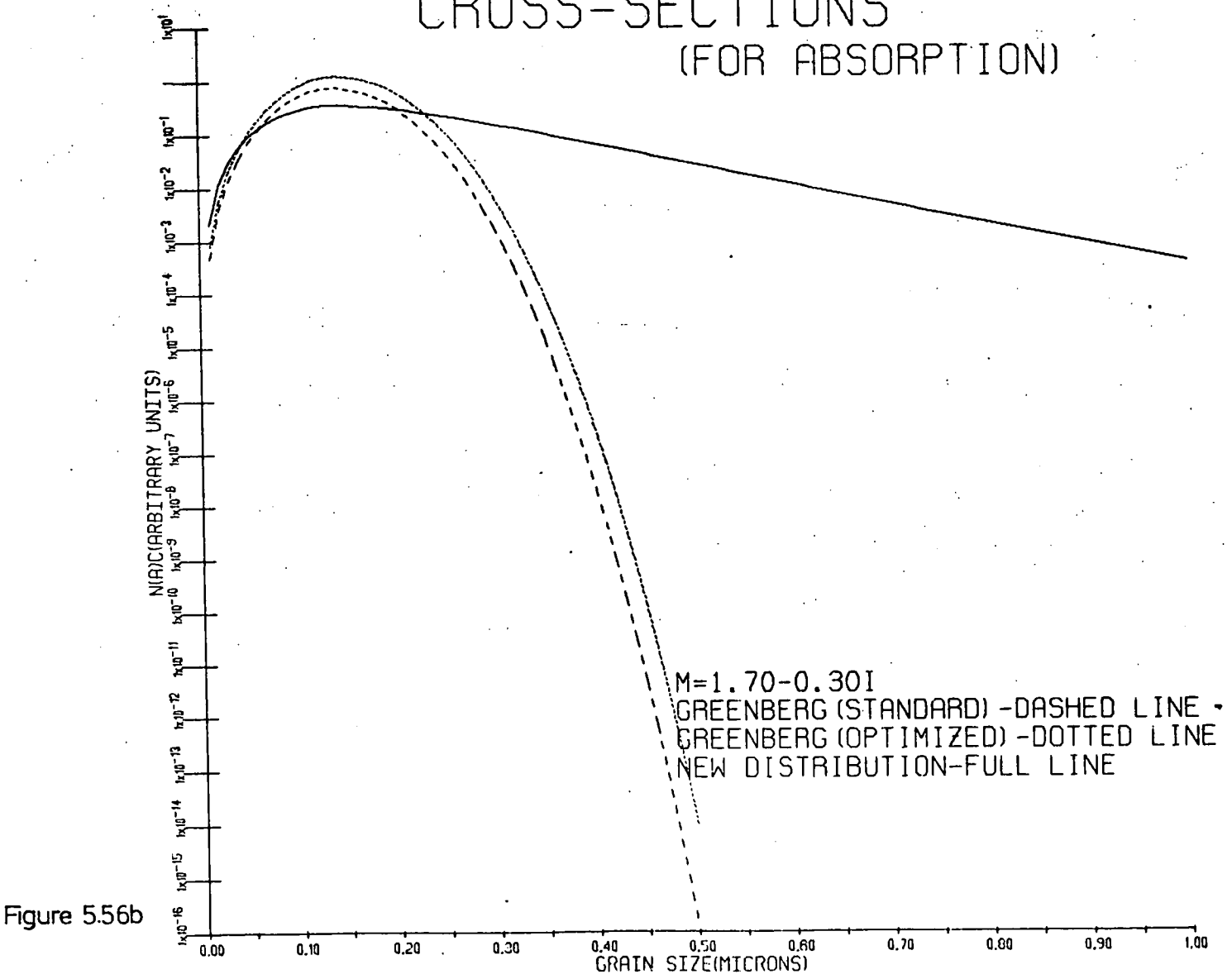
CROSS-SECTIONS
(FOR ABSORPTION)
N(A)(ARBITRARY UNITS)
GRAIN SIZE(MICRONS)
M=1.70-0.30I
GREENBERG (STANDARD) -DASHED LINE
GREENBERG (OPTIMIZED) -DOTTED LINE
NEW DISTRIBUTION-FULL LINE

Figure 5.56b

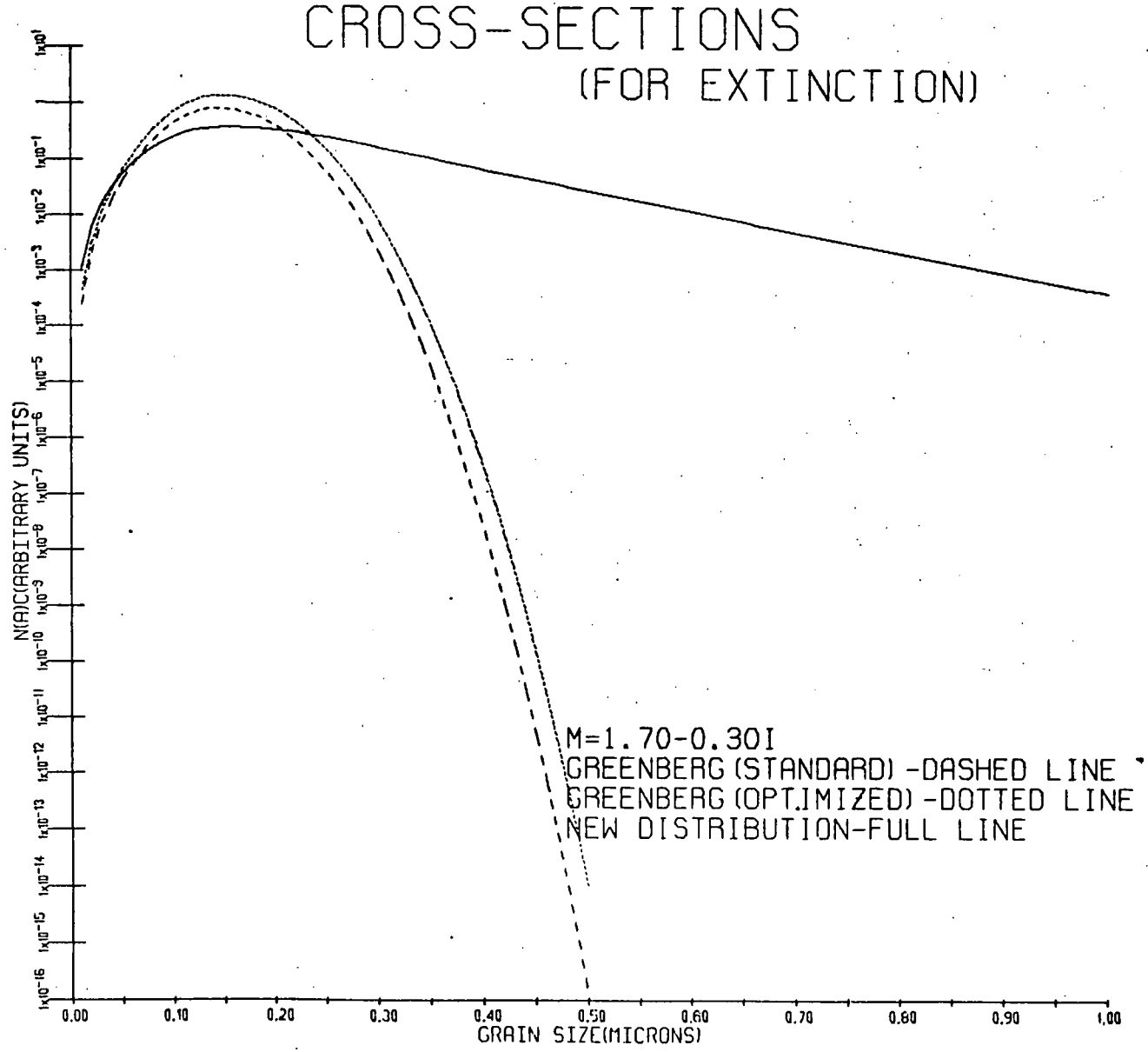
CROSS-SECTIONS
(FOR EXTINCTION)
N(A)C(ARBITRARY UNITS)
GRAIN SIZE(MICRONS)
0.00
0.10
0.20
0.30
0.40
0.50
0.60
0.70
0.80
0.90
1.00
M=1.70-0.30I
GREENBERG (STANDARD) -DASHED LINE
GREENBERG (OPTIMIZED) -DOTTED LINE
NEW DISTRIBUTION-FULL LINE

Figure 5.56c

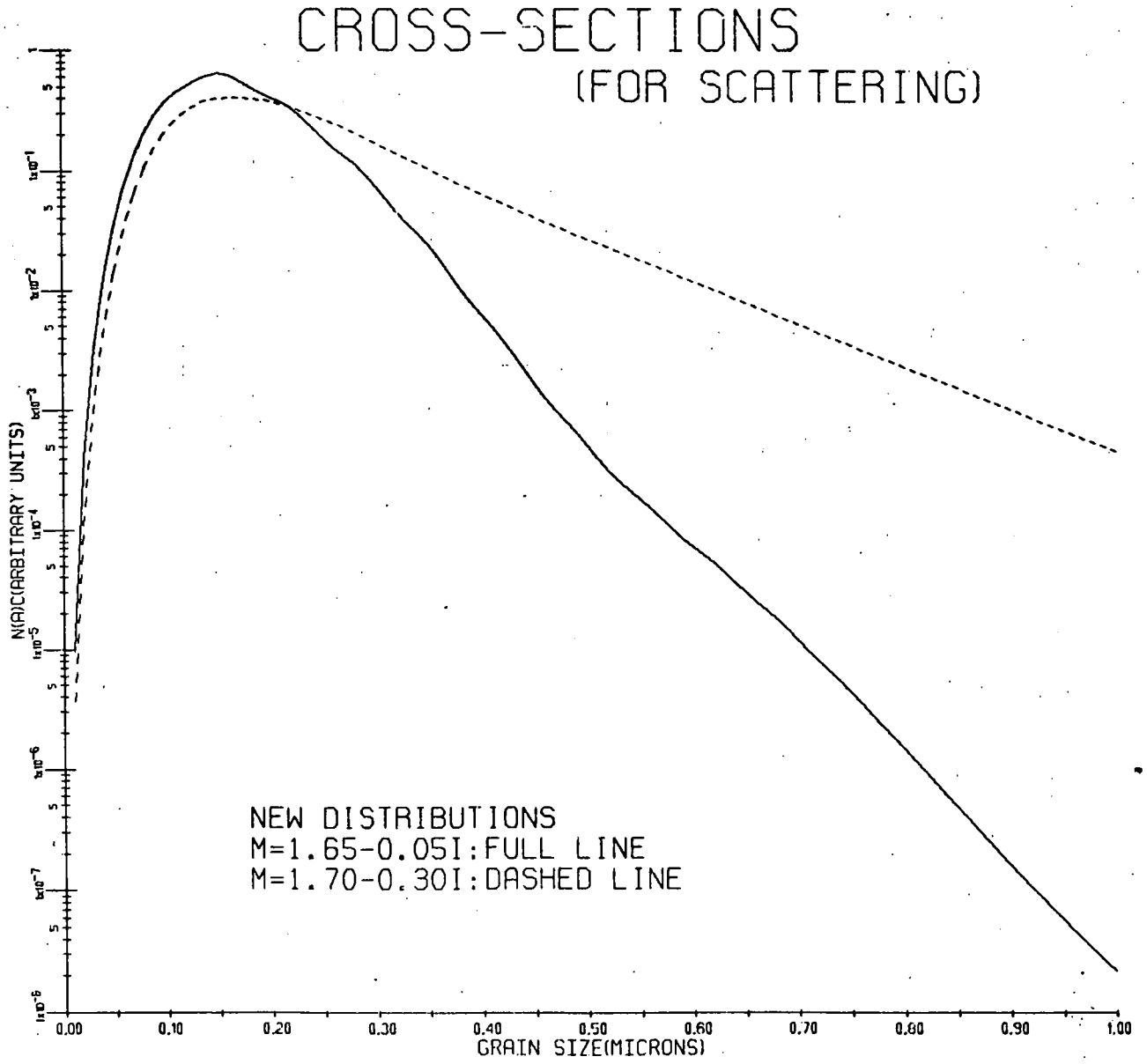
CROSS-SECTIONS
(FOR SCATTERING)
N(A)C(ARBITRARY UNITS)
GRAIN SIZE(MICRONS)
0.00
0.10
0.20
0.30
0.40
0.50
0.60
0.70
0.80
0.90
1.00
NEW DISTRIBUTIONS
M=1.65-0.05I:FULL LINE
M=1.70-0.30I:DASHED LINE

Figure 5.57a

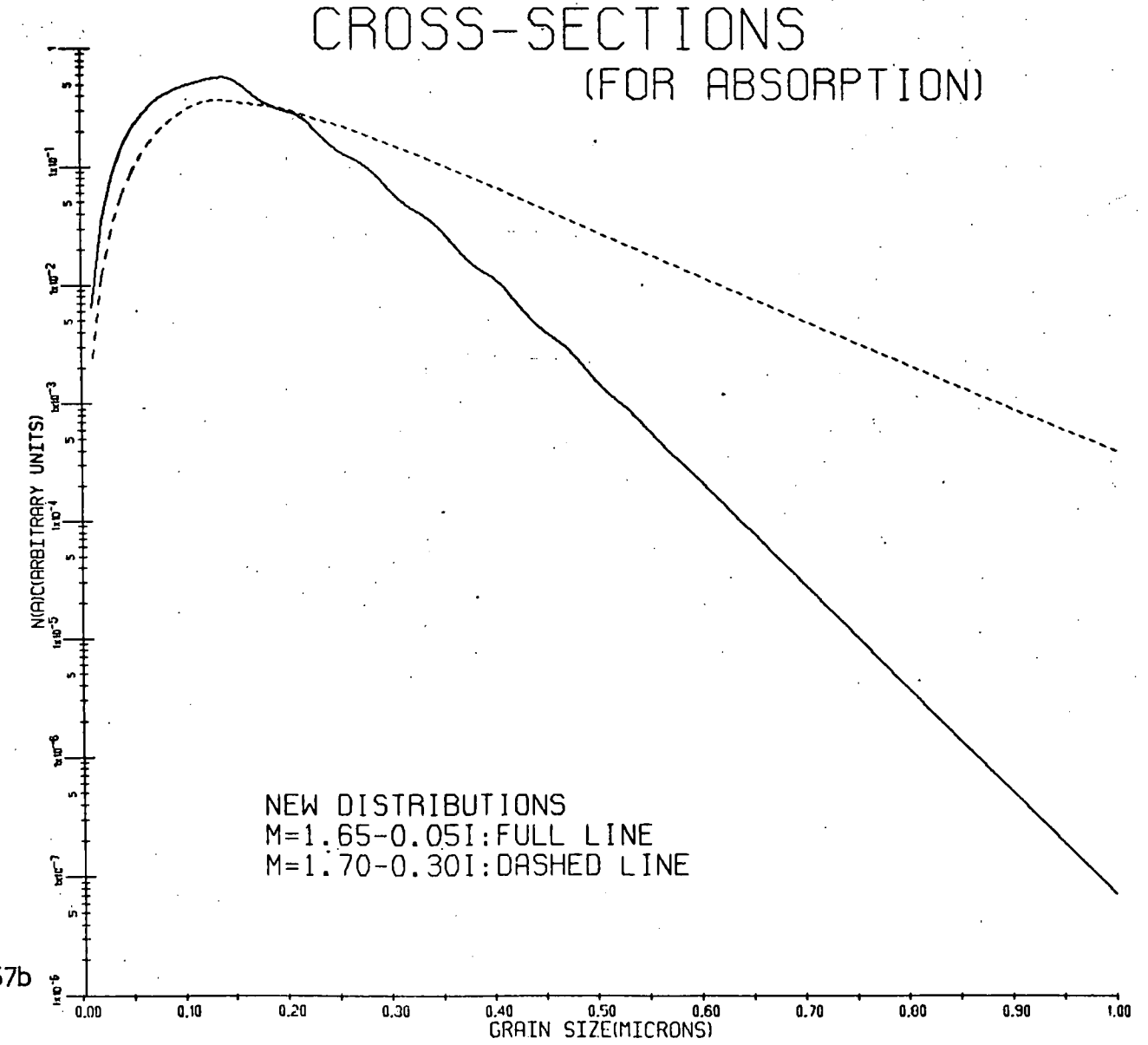
CROSS-SECTIONS
(FOR ABSORPTION)
N(A)(ARBITRARY UNITS)
GRAIN SIZE(MICRONS)
0.00
0.10
0.20
0.30
0.40
0.50
0.60
0.70
0.80
0.90
1.00
NEW DISTRIBUTIONS
M=1.65-0.05I:FULL LINE
M=1.70-0.30I:DASHED LINE

Figure 5.57b

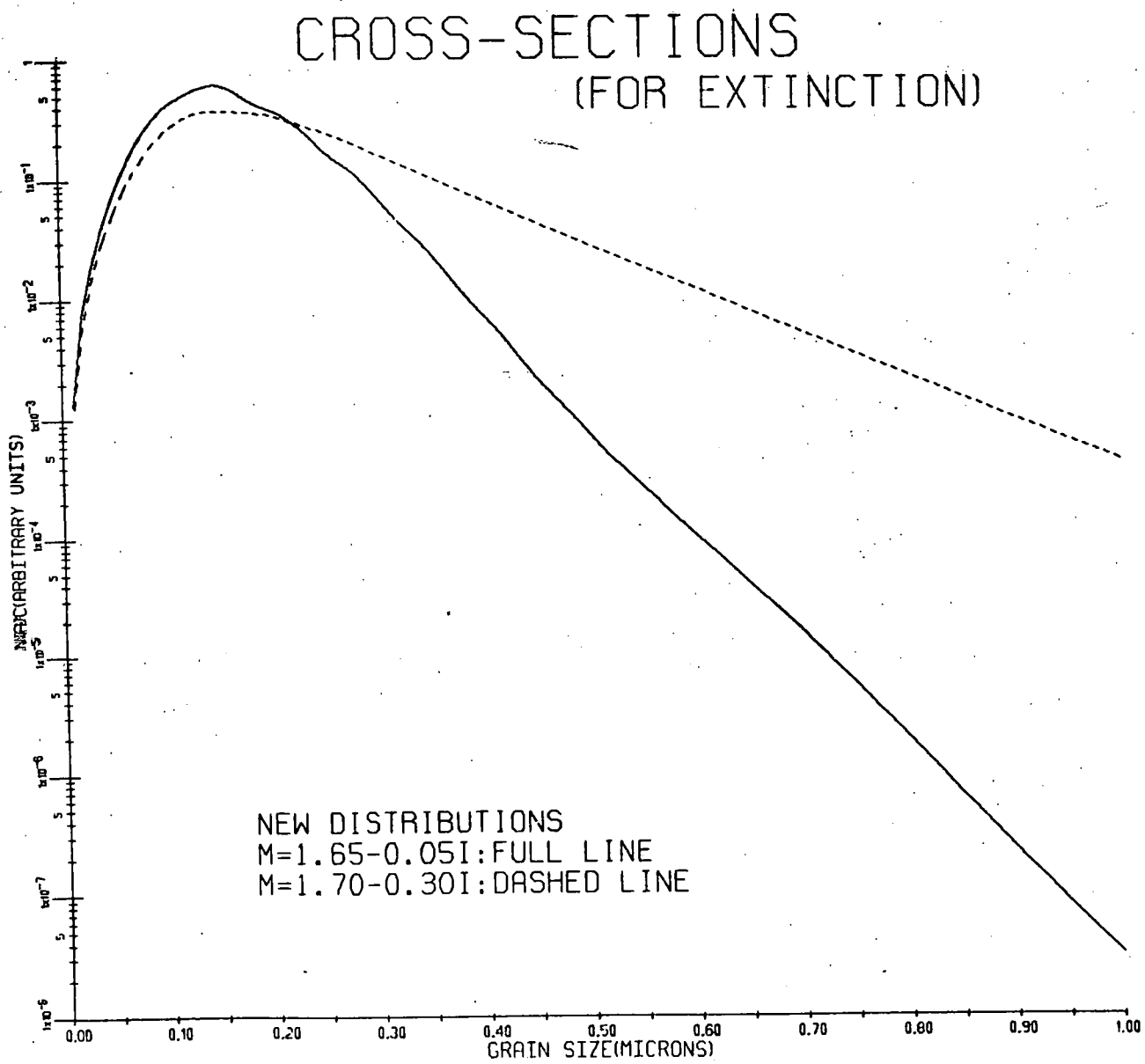
CROSS-SECTIONS
(FOR EXTINCTION)
NEW DISTRIBUTIONS
M=1.65-0.05I:FULL LINE
M=1.70-0.30I:DASHED LINE
GRAIN SIZE(MICRONS)
0.00
0.10
0.20
0.30
0.40
0.50
0.60
0.70
0.80
0.90
1.00

Figure 5.57c

Yet again, a large imaginary component in the refractive index has the effect of smoothing the curves (figure 5.52b) and naturally all cross-sections increase with larger grain size.

If the cross-sections are multiplied by the size distribution, the maximum of the curve will indicate those grains giving the greatest contribution to the scattering and absorption of the light, i.e. the most efficient polarizers. These results are shown in figures 5.53 for m_1, and figure 5.54 for m_2, for the two Greenberg distributions and the new distributions.

Without doubt, it is grains of $\sim$.15μ which are mainly responsible for both scattering and absorption.

In figures 5.55 and 5.56, the three distributions are compared for scattering, absorption and extinction, with the area under each curve normalized to 1. The new distributions involve a greater population of larger grains than the Greenberg distributions, contributing to the cross-sections.

The graphs in figure 5.57, where the new distributions are compared for scattering and absorption indicate that a larger imaginary component in the refractive index demands a greater population of larger grains for extinction.

However, the size of grain giving the greatest contribution to scattering and absorption is independent of the size distribution and the refractive index ; these only affect the details of percentage polarization in that they determine the range of particle sizes and relative numbers. The graphs show,without doubt, the grains of .15μ are chiefly responsible for the scattering in the Homunculus, irrespective of size distribution.

5.6 EMISSION AT 10μ

Since good absorbers are good emitters, those grains with maximum absorption at 10μ will be the most efficient emitters at 10μ . Andriesse (1978) and Apruzese (1975) suggest that grains of size 1μ are responsible for

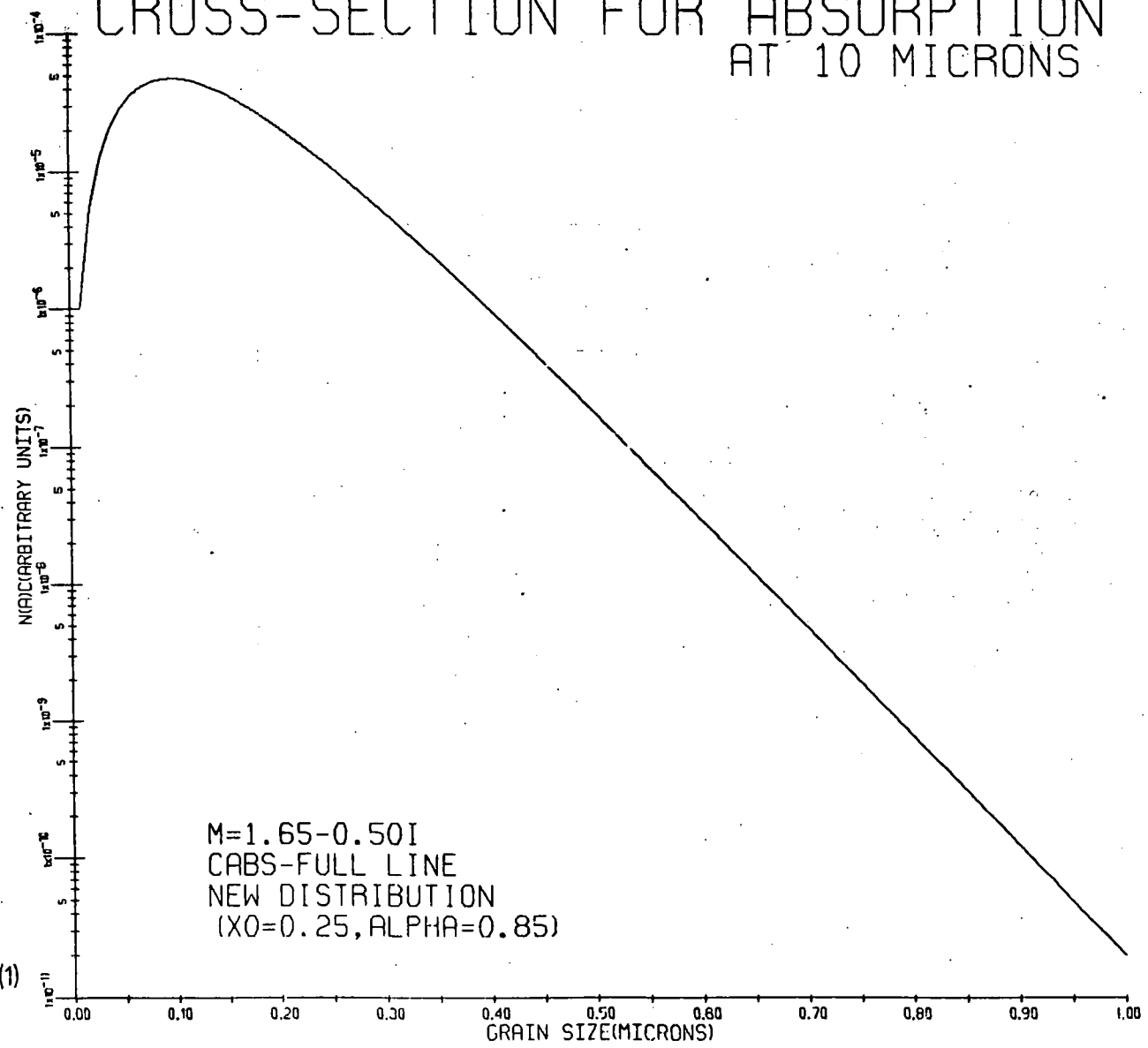
CROSS-SECTION FOR ABSORPTION
AT 10 MICRONS
N(A)(ARBITRARY UNITS)
M=1.65-0.50I
CABS-FULL LINE
NEW DISTRIBUTION
(XO=0.25,ALPHA=0.85)
0.00
0.10
0.20
0.30
0.40
0.50
0.60
0.70
0.80
0.90
1.00
GRAIN SIZE(MICRONS)

Figure 5.6(1)

the 10μ emission. Using a realistic imaginary component in the refractive index (Gaustad, 1963) for radiation at 10μ, the absorption cross-section, multiplied by the new size distribution (α = 0.85) is shown as a function of grain size in figure 5.6. As proved earlier, the maximum of $n(a) \times C_{abs}$ will be independent of size distribution in any case. The curve is shown to peak at $\sim$.1 grains, and in fact the contribution of 1μ grains to the absorption cross-section is negligible.

5.7 CALCULATION OF R

Using the new size distributions, R may be calculated as follows:-

$$A_V = 2.5 \log_{10} e \ \tau_V \qquad (5.11)$$

where A_V is the extinction and τ_V the optical depth at visual wavelengths.

$$\text{Since } \tau_V = no \int C_{ext}^{V} \ n(a) \ da \qquad (5.12)$$

where no is the total number of particles

$$A_V = k \int C_{ext}^{V} \ n(a) \ da \qquad (5.13)$$

where k is a constant

Now,

$$E_{B-V} = 2.5 \log_{10} e \ (\tau_B - \tau_V) \qquad (5.14)$$

where the B,V subscripts correspond to the UBV system of colours,

$$\therefore \quad E_{B-V} = k \left[\int C_{ext}^{B} \ n(a) \ da - \int C_{ext}^{V} \ n(a) \ da \right] \qquad (5.15)$$

$$\therefore \quad R = \frac{\int C_{ext}^{V} \ n(a) \ da}{\int C_{ext}^{B} \ n(a) \, da - \int C_{ext}^{V} \ n(a) \ da} \qquad (5.16)$$

Using the calculated value of R, and Pagel's (1969) estimate of

$E_{B-V} = 1.^{m}2$, estimates of A_V may be obtained and hence of M_V, the absolute visual magnitude of η Carinae, since $M_V = -12.7 - A_V$ (Paper 1). The results are summarized in Table 5.7A. Clearly the larger refractive index gives a totally unrealistic result.

TABLE 5.7A

Results of Calculation of R

m	R	A_V	M_V
1.65-0.05i	2.42	2.9	-15.6
1.70-0.30i	10.95	13.14	-25.8

5.8 DISCUSSION

The new distribution of silicate grains, characterized by a refractive index of m = 1.65-0.05i used in conjunction with the Mie formulae for light scattering by small particles gives excellent agreement with the polarimetric measurements of Warren-Smith et al (Paper 1). This distribution is very similar to those used in interstellar extinction studies, the main difference lying in the fact that it incorporates a larger number of smaller particles. Since contributions by smaller particles in a given size distribution are relatively more important to the polarization than to the extinction (Hong and Greenberg, 1978), it is reasonable that the mean of the new size distribution should be 0.03μ as opposed to 0.07μ for the Greenberg distribution.

Calculations of scattering and absorption cross-sections show that grains of size .15μ are the most effective at visual wavelengths, while at 10μ, grains of size .1μ are the most highly emitting. These results are independent of size distribution. Mitchell and Robinson (1978), from infrared studies have also obtained a size of .1μ for the silicate grains in η Carinae and hence the new size distribution characterizes one component of the grains in η Carinae.

The Greenberg distribution is a solution to the differential equation for grain growth and destruction. Since η Carinae is a region of grain growth (see Davidson, 1971) a different distribution may indeed be expected. This leads to a value of R, the ratio of total-to-selective absorption, which is slightly less than that of the interstellar medium.

Determinations of R have ruled out grains characterized by a large imaginary component in their refractive index since R ≈ 10.95 is totally outside the range delimited by Hong and Greenberg (1978). R = 2.4 however, agrees well with their value when using an exponential distribution which is nearly the form of the new distribution. Therefore it seems that the grains in η Carinae are distinctly "dielectric" as opposed to "metallic", the imaginary component in the refractive index being necessary, but small.

5.9 CONCLUSIONS

The polarimetric measurements of the Homunculus may be explained in terms of the geometry discussed in Section 5.2.1 by scattering from a distribution of silicate grains characterized by a refractive index of $m = 1.65-0.05i$.

The most effective scatterers seem to be grains of size .15μ at visual wavelengths, whilst at 10μ maximum infrared emission will come from grains of size .1μ . These sizes are similar to those resulting from recent observations of the interstellar medium (see Chapter 3) and it is likely that the grains originating in η Carinae will ultimately form one component

of the interstellar grain mixture.

Calculations of R have led to a value of M_V = -15.6 mag. for η Carinae at maximum, which is intermediate between those of novae and supernovae. Therefore, it does indeed seem that η Carinae, an ejection variable that has attained high luminosity, may be classed as a Hubble-Sandage Variable, these being the brightest irregular variables in other galaxies (Paper I).

References

Aitken D K, Jones B, Bregman J D, Lester D F, Rank D M, 1977 Astrophys Journ 217 103.

Allen C W, 1973 Astrophysical Quantities (U.London, Athlone Press).

Andriesse C D, Donne B D, Viotti R, 1978 Mon.Not. R.Astr.Soc (in press).

Apruzese J P, 1975 Astrophys Journ. 196 753.

Craine E R, 1974 Astrophys Journ. 191 105.

Davidson K, 1971 Mon.Not. R. Astr.Soc. 154 415.

Gehrz R D, Ney E P, 1972 Sky and Telescope 44 4.

Hanner M S, 1971 Astrophys Journ. 164 425.

Hubble E, Sandage A, 1953 Astrophys. Journ. 118 353.

Martin P G, 1972 Mon. Not. R. Astr. Soc. 159 179.

Mitchell R M, Robinson G, 1978 Astrophys Journ. 220 841.

Neugebauer G, Westphal J A, 1968 Astrophys Journ. 152 L89.

Pagel B E J, 1969 Nature 221 325.

Robinson G, Hyland A R, Thomas J A, 1973 Mon.Not.R.Astr. Soc., 161 281.

Schmidt G D, Angel J R P, Beaver E A, 1978 Astrophys Journ. 219 477.

Thackeray A D, 1961 Observatory 81 99.

Warren-Smith R F, Scarrott S M, Murden P, Bingham R G, 1978 preprint.

Westphal J A, Neugebauer G, 1969 Astrophys Journ. 156 L45.

Van der Hulst H C, 1957 Light Scattering by Small Particles (New York, John Wiley & Sons).

Wickramasinghe N C, 1973 Light Scattering Functions for Small Particles (Adam Hilger, London).

Wickramasinghe N C, Nandy K, 1972 Rep.Prog. Phys. 35 157.

Hong S S, Greenberg J M, 1978, Astron. & Astrophys, 70 695.

CHAPTER 6

A POLARIMETRIC INVESTIGATION OF THE CARINA NEBULA NEAR η CARINAE

"It would manifestly be impossible by verbal description to give any just idea of the capricious forms and irregular gradations of light affected by the different branches and appendages of this nebula ..... nor is it easy for language to convey a full impression of the beauty and sublimity of the spectacle it offers when viewed in a sweep, ushered in as it is by so glorious and innumerable a procession of stars, to which it forms a sort of climax...."

Sir John Herschel (1848)

6.1 INTRODUCTION

With an apparent diameter of about 2 degrees, the great Carina Nebula forms one of the most powerful laboratories available for investigating the early evolution of very massive stars (Walborn, 1973). This region, the most brilliant spot in the southern Milky Way is the most prominent feature of what is generally believed to be a spiral arm or segment, stretching along the line of sight to great distances. Several young clusters are associated with the nebula which in fact contains the strongest concentration of extremely early O stars known in the galaxy (Herbst, 1976). Also associated with the nebula are the radio continuum peaks known as Carina I and Carina II.

Walborn (1973) has shown that of the clusters associated with the nebula viz. Trumpler 14, Trumpler 16 and Collinder 228, Trumper 14 is the most distant at 3500 pc and is an exceedingly young cluster whose brightest

member is a possible pre-or post - Wolf-Rayet star ; and that Trumpler 16 and Collinder 228, both at distances of 2600 pc in fact may belong to the same complex, the apparent separation being due to the dense obscuring lane superimposed on the HII region.

In general, the stars are the brighter stars of spectral type O, several of them being amongst the hottest known, i.e. O3 stars with spectra showing lines of ionized Helium, but not neutral Helium. Most of them appear to be Main Sequence objects and may be the most massive stars known (Walborn and Ingerson, 1977).

The positions of the radio peaks suggests some possible association of the radio with the optical structure. The centre of Carina I coincides with the centre of a semi-circular rim on the edge of the very abrupt absorption lane to the north-west of the nebula (Gardner et al, 1970). Carina II seems to be situated near the centre of a ring of nebulosity about 3' arc in diameter (2.4 pc) with a band of enhanced emission along its southern edge. Near their junction is a well-defined patch of absorption about 1 pc wide which extends into the ring. Several rays are visible outside the ring starting at about 3' arc from the centre (Gardner et al, 1970). The optical ring may be the result of chance superpositions of bright and dark material, but the existence of Carina II at its centre strongly suggests a physical structure (Walborn 1973).

The brightest nebulosity does not seem to be associated with any of the visually brightest stars and occurs in a region where no O-stars are yet known. Although the stars of Trumpler 16 may be contributing to the general excitation of the nebula, it is possible that the exciting stars are hidden behind dust cocoons, which obscure the visible light without greatly affecting the ionization, (Gardner et al, 1970).

The positions of the various features in the nebula are indicated in Figure 6.11 which superimposes on a photograph of Walborn's (1975) plate,

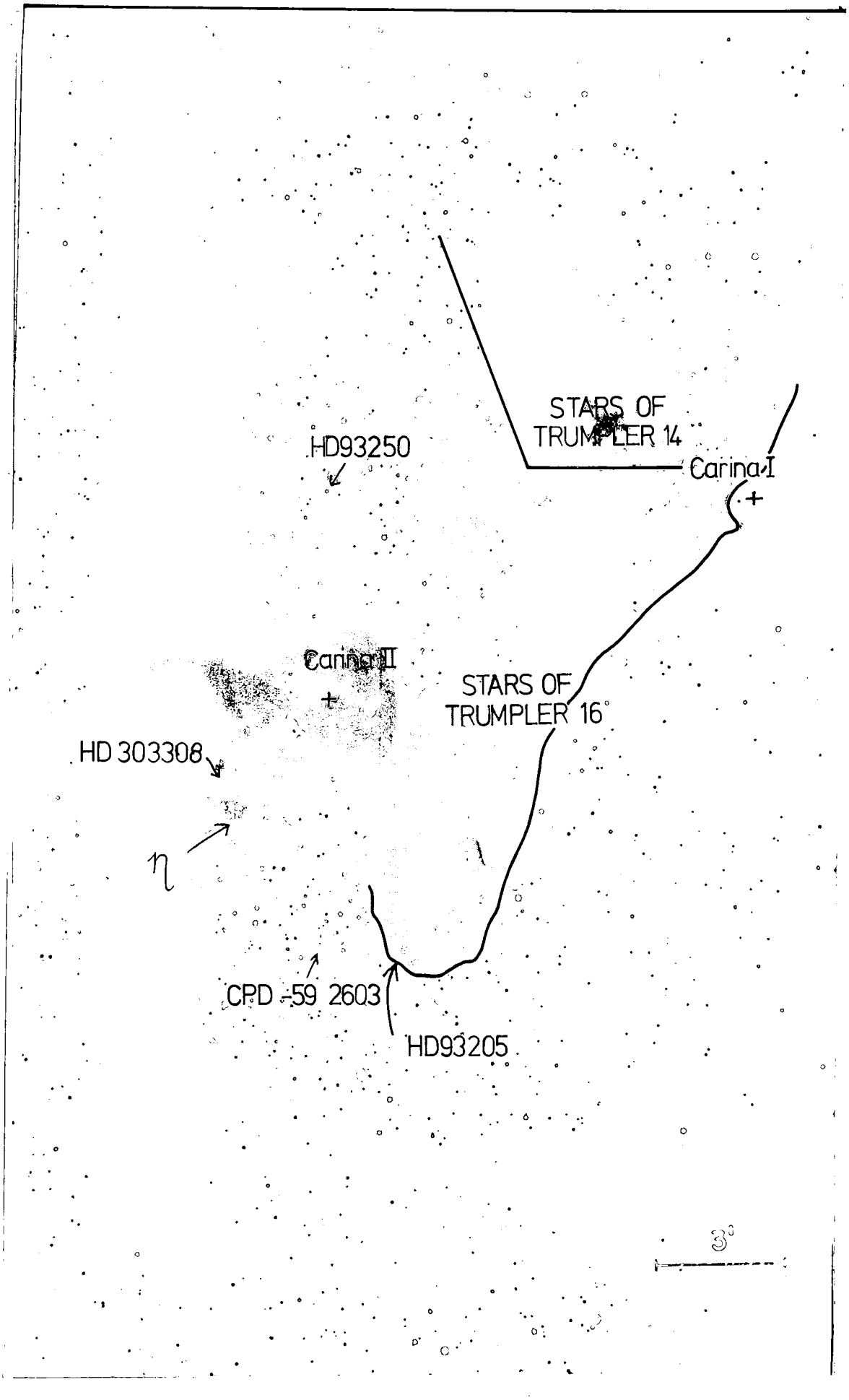

Figure 6.11 The main features of the Carina Nebula, superimposed on [SII] photograph of Walborn (1975)
North is upwards, East to the left

in the light of [SII] .

6.2 OBSERVATIONS OF THE CARINA NEBULA

6.2.1 Optical Studies

The regions around the radio peaks Carina I and II are regions of high excitation, (strong in [O III] radiation) whilst the surrounding nebulosity is of low (strong in [O II] radiation) excitation (Faulkner, 1963). Monochromatic photographs of regions centred on Carina I and II reveal a similar appearance in [N II] and [S II], and in Hα, Hβ and [O III] . This is due to the ionization structure since [N II] and [S II] are emitted by low excitation regions and [O III] by high excitation ones. As a whole, this part of the nebula is of high excitation hence there are many O^{++} and few O^{+} ions so the appearance is the same in Hα, Hβ and [O III], (Deharveng and Mancherat, 1975). [N II] and [S II] enhance the rims, globules and ring of nebulosity around Carina II, revealing them to be regions of lower excitation than the surrounding nebulosity.

Walborn's (1975) [S II] and [O III] interference-filter photographs of the northern part of the nebula reveal striking differences between the features enhanced in the light of each filter. The most prominent feature in [S II] is the ring structure associated with Carina II, but of the several outer rays, only ridge E (see figures 6.1 and 6.36), seems to be structurally associated, the others being prominent in [O III] . Walborn makes the following remarks about individual features identifiable in the copy of his photograph (figure 6.36) :-

Arc A - the gas seems to be twisted or helical about a north-south axis ;

Arc B - the two branches at its northern end are of quite different excitation , the outer one being brighter in [O III] ,

the inner brighter in [S II] and [N II] and both being similar in Hα ;

Cloud C – similar to A, B and E in that it is enhanced in [S II] and [N II], while suppressed in [O III] and Hα but it is relatively more prominent in [O I] and the red continuum and hence bearing some resemblance to Cloud D ;

Cloud D – different from the other features near the ring being relatively suppressed in [S II] and [N II] and not particularly prominent in Hα or [O III]. Progressing through the Balmer series from Hα to Hγ, it gradually brightens and in [O I] and narrow-band red and blue continuum photographs appears as the brightest feature. It is also bright in [O II]; hence it may be of very low excitation and possibly in part a reflection nebula which may be less heavily reddened than the rest of the ring ;

Clouds 1, 2 and 3 – conspicuous in [S II] but only associated dust seen in projection in [O III]. Cloud 1 has a billowy structure, Cloud 2 is more amorphous and Cloud 3 has a spiral or looped form. They appear distinctly different from classical bright rimmed globules.

Splitting of the Hα and [N II] λ6584 lines has been observed by Deharveng and Mancherat (1975) and Louise (1972) using interference techniques with high angular and spectral resolution. This occurs over a region equivalent to 11 p c with the strongest splitting occurring near η Carinae (with radial velocity differences of more than 50 km s^{-1}). Slightly weaker splitting occurs both in the obscured regions and in the bright nebulosity but is not observed in the northern region or in the north-west absorbing lane.

The only possible correlation between splitting and optical structure

exists in the region of the ring where strong splitting (more than 40 km s^{-1}) is observed at the centre and to the south-east of the ring on each side of the absorption patch. On the western edge of the ring, where no splitting occurs, the velocity is the mean between each component. Within the ring, radial velocity differences between the two components of Hα and [N II] are in good agreement, but outside, in some places, only one component is observed for [N II] whilst two are observed for Hα , the [N II] velocity corresponding to the velocity or one or other of the Hα components.

Deharveng and Mancherat interpret these results in terms of two clouds emitting Hα , and only one, receding or approaching emitting [N II]. The clouds must be in different states of ionization (low excitation emitting Hα and [N II] , high excitation emitting Hα and [O III]) and this interpretation is confirmed by the occurrence of this phenomenon in a region where the structure appears quite different in [N II] and [O III] The presence of these clouds reinforces the idea of Dickel (1974) of an expanding shell model and Deharveng and Mancherat find the centre of the expansion, which is non-spherical, to be the peculiar object, η Carinae with an expansion velocity of $\geq$ 25 km s^{-1}.

Complex structure has also been found in the interstellar Calcium II (H (λ3958) and K (λ3933)) lines by Walborn and Hesser (1975) on 9 Å mm^{-1} wide spectrograms of stars in the Carina Nebula. The profiles show large variations over small angular distances with as many as six components in a single spectrum. A total velocity range of 330 km s^{-1} has been measured. Most of the stars observed are members of Trumpler 16 and Collinder 228. Since stars associated with the outer parts of the nebula show only line-of-sight calcium components, the additional high velocity components in the inner region are very probably formed there, or in its immediate foreground.

Walborn and Hesser postulate that these complex, high-velocity

interstellar line profiles represent a new kind of structure connected with either, one or more of the outbursts of η Carinae, with the ultra-violet radiation and stellar winds caused by the energy input to the surrounding medium of the O3 stars, or with the bright optical ring structure, where it seems that some energetic event has occurred or is occurring.

Double nebular emission lines (e.g. [O II] λλ3726, 3729) were also observed (Walborn and Hesser, 1975) but the nebular absorption feature, He I λ3889, observed in the spectra of all stars in the brighter regions of the Carina Nebula was found to be only single corresponding to the negative velocity of the doublets. Hence Walborn and Hesser conclude that the positive-velocity ionized material must lie predominantly beyond the stars, and thus cannot give rise to an absorption feature in their spectra.

Relationships are unclear between the Ca II and the nebular line phenomena but the complex nebular line profiles appear to extend to much larger distances from the centre of the nebula than the calcium profiles.

6.2.2 Radio Observations

The Carina Nebula has been observed at 85.5 MHz (Mills, Little and Sheridan, 1956), 1400 MHz (Hindman and Wade, 1959), 1410 and 2650 MHz (Beard and Kerr, 1966), 5 GHz (Gardner and Morimoto, 1968), 6 m (Gardner, Milne, Mezger, and Wilson, 1970), 408 MHz (Shaver and Goss, 1970), 30 MHz in absorption (Jones 1973) and at 3.4m and 6 cm (Huchtmeier and Day, 1975).

The early observations did little more than to verify the hypothesis that ordinary emission nebulae emit radio waves as a result of their high electron temperatures by the process of free-free transitions (Mills et al 1956) and to invoke the existence of several O-stars in order to maintain the ionization of the nebula (Wade, 1959). The half-power beamwidths at 85.5 and 1400 MHz were of the order of 1°, that is, approximately the diameter of the visible nebula and hence appreciable aerial smoothing

obliterated any possible structure in the continuum maps.

Beard and Kerr (1966) observed the nebula at 1410 and 2650 MHz in order to try to detect synchrotron radiation from η Carinae. They found, however, no evidence for any non-thermal radiation. Their results did produce a radio-contour map consisting of a maximum peak, due to emission from a part of the nebula obscured by overlapping dust, and several subsidiary peaks, the secondary maximum being near the bright ring structure and the others corresponding to areas of high excitation on a photograph taken in Hα. The 2650 MHz observations also indicate that the southern side of the bright northern part of the nebula is due to overlying absorption because the radio contours carry right across whereas the dark areas further south are due to low excitation, because here the contours show troughs.

The primary and secondary maxima of Beard and Kerr (1966) were found by Gardner and Morimoto (1968), using higher resolution at 5 GHz to be of similar peak intensity and angular size and separated by some 10' arc. Carina I is on the edge of the very abrupt absorption lane to the north-west of the nebula and Carina II is in the centre of the optical ring structure (Gardner et al, 1970).

Comparison by Gardner et al (1970) of the 5 GHz radio emission with the optical emission reveals that for the outer regions there is good general agreement. To the north-west, near Carina I, because the radio contours come in along the lane, it seems that the absorbing matter is connected with the ionization and that the sharp ionization boundary to the west of Carina I (where the intensity falls by half in 1' arc) is due to the absorption of the ultraviolet radiation by dense matter in the nebula, even though the ionization boundary as revealed by the radio contours is more nearly north-south than the absorption edge on the plate. The other principal region of

obscuration in the nebula shows no evidence of any connection between the radio contours and the absorption in agreement with the results of Beard and Kerr.

The results of Gardner et al (1970) and of Shaver and Goss (1970) also confirm that the radio spectrum of the Carina Nebula is thermal and that the nebula is optically thin down to 400 MHz.

Recombination line observations have been made by McGee and Gardner (1968) at 126α and 127α, McGee, Batchelor, Brooks and Sinclair (1969) at 158α and 199β, Gardner, Milne, Mezger and Wilson (1970) at 137β and 109α and by Huchtmeier and Day (1975) at 109α and 90α .

The lines have been observed at both continuum peaks but around Carina II, the profiles have been found to be double (Gardner et al (1970), Huchtmeier and Day, 1975). Around Carina II, the wide profiles are all very similar as regards the intensity of the two peaks and the velocity separation ; the narrower profiles have smaller component separations and as Carina I is approached, the profiles become single peaked and gradually narrow until those around Carina I are typical of the lines found in other HII regions. The mean radial velocities for the regions with complex line structure are found to be equal to the radial velocities of the remainder.

Huchtmeier and Day interpret the clear separation of the line components in terms of an expanding "shell" or of different clouds being expelled into different directions, the approaching and receding parts forming two distinct line components. The distribution of mean radial velocities shows a difference of about 6 to 8 km s^{-1} between Carina I and Carina II (-16 and -24 km s^{-1} respectively). Since the velocities in the molecular cloud in front of the nebula are near the mean velocity of the Carina II complex, it appears that the molecular cloud may be associated with this source. However, the region of greater line separation around the cluster Trumper 14 seems to be associated with Carina I.

By obtaining the distributions for radial velocities greater than or equal to +10 km s^{-1}, and less than or equal to -50 km s^{-1} (maximum line separation being 44 km s^{-1}), Huchtmeier and Day find two very similar distributions, both centred to the same position, southward of the continuum peak Carina II, approximately on Trumpler 16. Hence the extreme velocities represent the expelled clouds of the "expanding sphere" which are furthest away from and closest to us. Chance coincidence of two clouds along the line of sight would not necessarily give coincident distributions for extreme velocities.

η Carinae, if situated within the nebula could be responsible for the expanding sphere but since the expansion velocities seem to be highest away from the maximum density of ionized hydrogen (Carina I and Carina II) and away from the regions of maximum dust and molecule concentrations, the dust may have been dispersed by stellar wind and radiation pressure, (Huchtmeier and Day (1975)) from Trumpler 14 and 16 which may well be responsible for the observed phenomena as they are located in areas of large line separations.

Observations of H_2CO absorption at 4829 MHz (Gardner et al 1973) and OH absorption at 1665 and 1667 MHz (Dickel and Wall, 1973) give absorption positions which form very similar distributions at the two frequencies. Both H_2CO and OH molecules form two concentrations, both peaking near each other in the two dust lanes. The peak optical depths for the OH concentrations are the same whilst for the H_2CO absorption, the optical depth for the higher longitude component is more than twice that of the lower longitude component. Both distributions have similar central velocities, widths and profile shapes and these, together with the association of the molecules with the dust, suggest that the molecules are physically associated in the dust clouds producing the optical absorption lanes across the nebula (Dickel and Wall, 1974).

Comparison of the OH optical depths with a map of visual absorption (Dickel, 1974) shows excellent agreement between the Av (visual absorption) contours and the OH optical depths, thus supporting the hypothesis of Dickel and Wall (1974) that the OH and H_2CO molecules are physically associated with the dust. Subtraction of possible foreground absorption clearly leaves much absorption near the nebula remaining, and since this absorption has the same position, shape, and extent as for the molecules, it seems likely that the dust and molecules are actually associated within the nebula (Dickel, 1974).

Dickel (1974) interprets the results of the observations of H_2CO and OH absorption in terms of an expanding shell containing concentrations of dust, neutral hydrogen and molecules, surrounding the ionized hydrogen, with a centre of expansion mid-way between Carina I and Carina II and an expansion velocity of 7 km s^{-1}.

The differing expansion velocities of Dickel, and Dehaveng and Maucherat are not incompatible because each set of observations refers to a different region ; that is, the molecular observations refer to the outer, approaching, neutral regions) and the HII observations refer to the inner ionized gas, (Deharveng and Maucherat, 1975). However, the expansion centres are different and Deharveng and Maucherat favour an expansion with non-spherical symmetry in contrast to Dickel's model invoking spherical symmetry.

30 MHz observations of the Carina Nebula (Jones 1973) reveal the presence of a strong non-thermal source in front of the nebula. This is presumably a supernova remnant which has escaped detection at higher frequencies due to increasing contrast at low frequencies between the non-thermal source and the thermal emission of the nebula. The 30 MHz position is 14' arc to the east of η Carinae.

The results of the Aerial V sky survey (Seward et al, 1976) have

identified an X-ray source in the same region as SNR 287.8 - 0.5 and it is possible that the X-ray source may be associated with the radio supernova remnant since their positional errors both overlap. η Carinae lies within the error box of the X-ray source which also includes the ring of optical filaments. Kinematic measurements of the optical emission from within the ring reveals that the Hα and Hβ lines are composed of two components due to high-velocity and low-velocity gas, the high velocities being consistent with the supernova remnant hypothesis (Elliott, 1979). Therefore, according to Elliott, it seems likely that the X-ray and radio features refer to the same object which displays the high velocity gas, and hence that the ring is the optical counterpart of the radio and X-ray remnants.

The splitting of the [N II] and Hα lines, the complex interstellar Ca II lines and the double radio line profiles all indicate that the Carina Nebula is undergoing some sort of internal activity. This activity is interpreted in terms of an expansion which, in the case of Deharveng and Maucherat has η Carinae as the centre with an expansion velocity of ≥ 25 km s^{-1} assuming non-spherical symmetry, and in the case of Dickel has a centre midway between the radio continuum peaks Carina I and Carina II and an expansion velocity of 7 km s^{-1} assuming spherical symmetry. In general, all phenomena seem to be associated with either the ring structure with Carina II at its centre, η Carinae or the stars of Trumpler 16. The fact that a radio supernova remnant and an X-ray source which may or may not be associated with each other have also been located in this part of the nebula poses many intriguing questions and makes further investigation of this region a necessity.

6.3 ANALYSIS OF THE DATA

An area 8' x 8' arc of the Carina Nebula around η Carinae was

observed at the f/15 focus of the 1.0m SAAO telescope during June and July 1978 by Scarrott and Warren-Smith, using the Durham polarimeter and the 4 cm electronographic image tube. Eight plates were obtained (four each for "grids in" and "grids out") and these were analysed according to the procedure outlined in Chapter two. A brief description of the output and input data involved during each stage of the reduction follows.

6.3.1 Digitization

Digitization of the eight plates converts the recorded densities on the plates to intensities in the form of a 512 x 512 matrix, part of which is shown in figure 6.31. Here, the intensities have been integrated over 3 x 3 pixels and each intensity range is represented by a symbol. ' ' corresponds to the lowest intensity range, i.e. clear plate followed by '.', '1', '2', etc. up to '9', then through the alphabet, until '*' represents the brightest portions of the plate. Each symbol represents a contour interval of 25 intensity units. The fainter regions of the plate correspond to the dust lanes, and the brightest regions to the brightest stars on the plate.

5.3.2 Clear Plate Subtraction

The clear plate intensities on both sides of the plate (the digitized portion of the plate is larger than the exposed area) are averaged to give a single trace down either side of the plate. These are shown in figure 6.32 where '.' represents the average clear plate level on the left-hand side of the exposed region and '+' that on the right-hand side. These two traces are composed of "smoothed" intensities where certain points have been rejected as being inaccurate. The numbers give the values of these intensities and their errors. A linear interpolation of these two numbers is subtracted across the plate. The asterisk '*' represents the mean of the average intensity of the left and right-hand sides of the plate before the data has been smoothed.

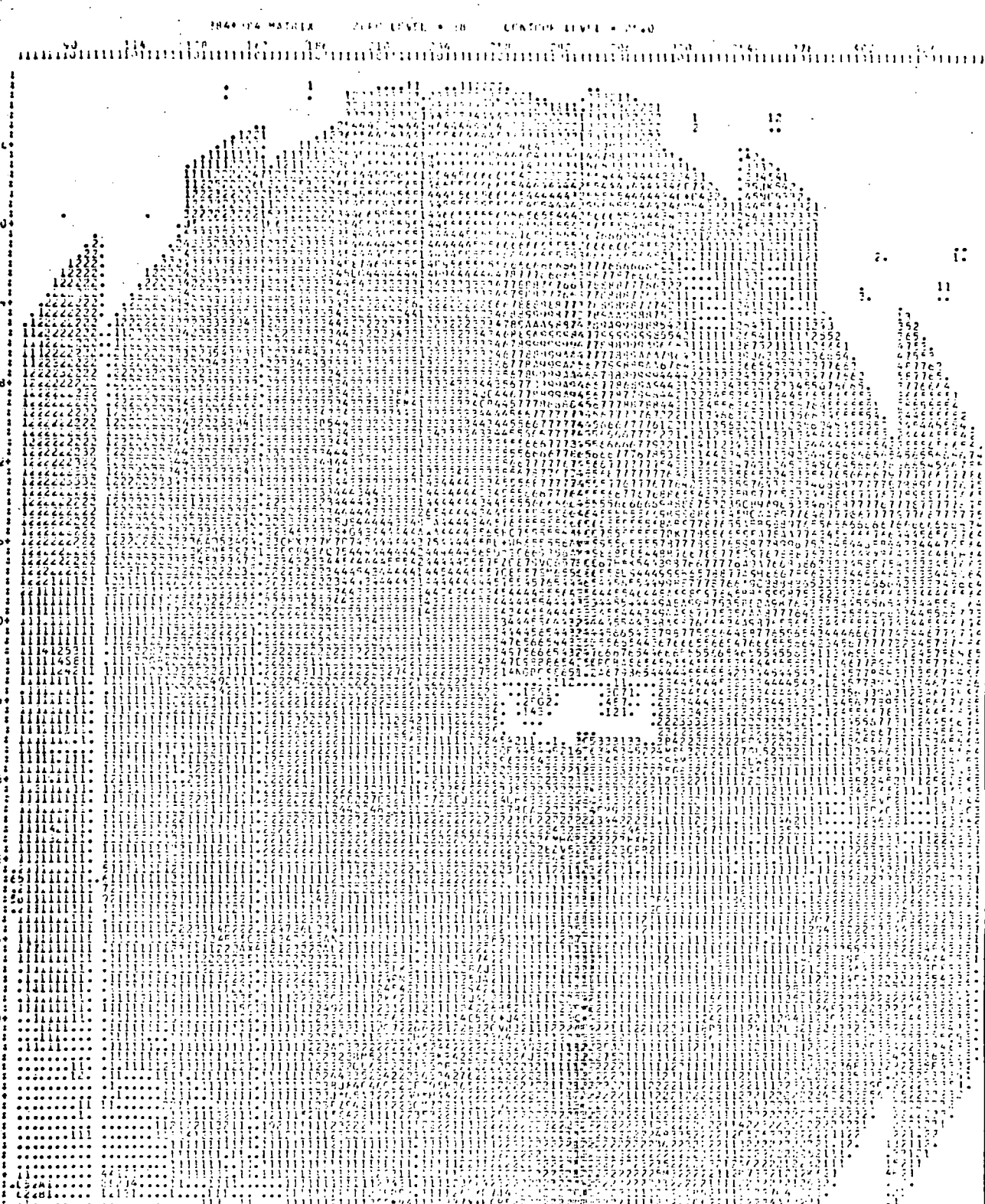

Figure 6.31 The digitized Plate

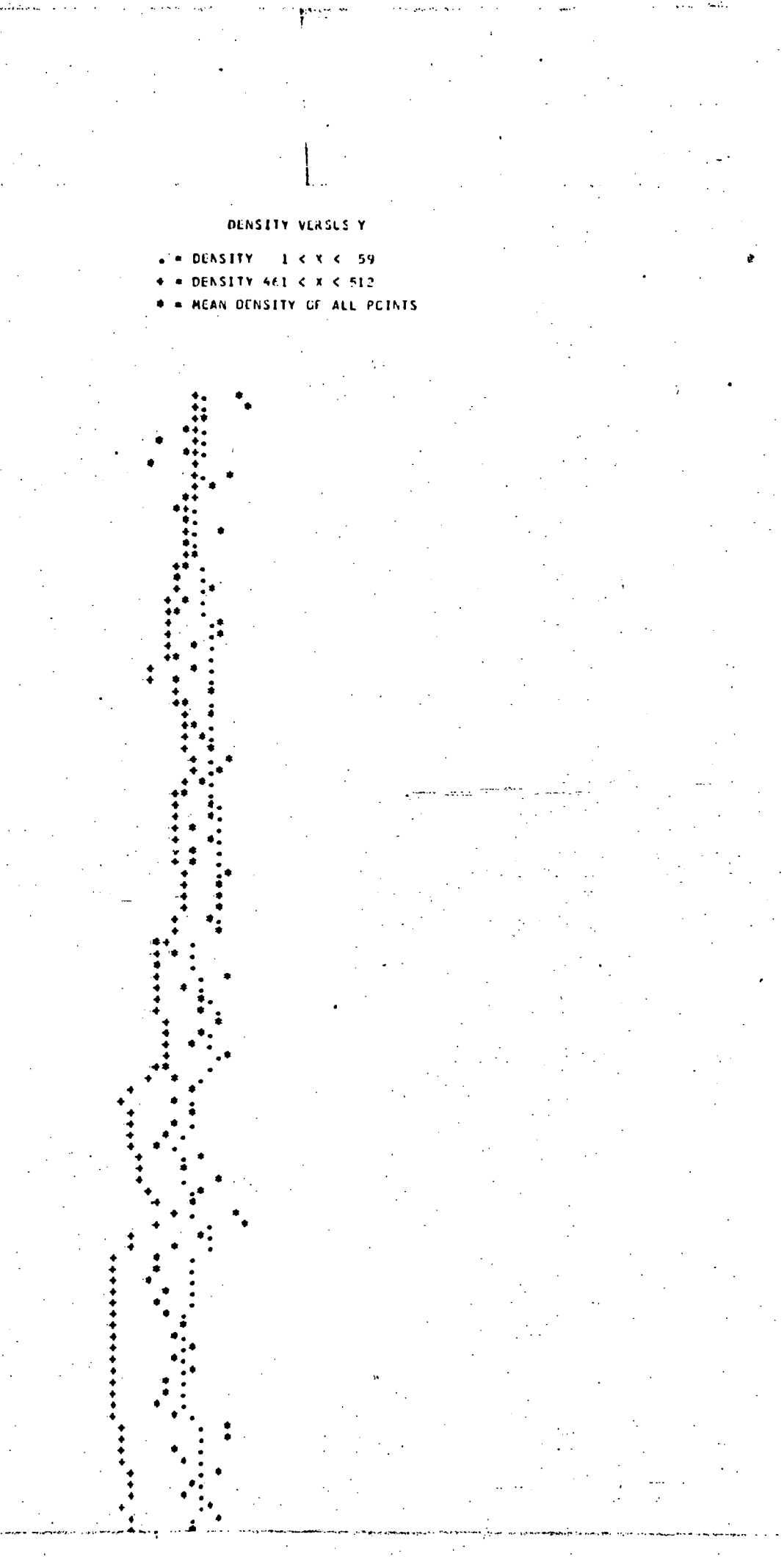

"."		"+"	
40.89	0.09	40.86	0.08
40.89	0.09	40.86	0.08
40.89	0.09	40.86	0.08
40.89	0.09	40.86	0.08
40.89	0.09	40.86	0.08
40.89	0.09	40.86	0.08
40.86	0.09	40.86	0.08
40.91	0.10	40.88	0.09
40.88	0.09	40.88	0.09
40.87	0.08	40.85	0.08
40.87	0.08	40.82	0.08
40.87	0.08	40.82	0.07
40.88	0.08	40.80	0.07
40.85	0.08	40.79	0.07
40.89	0.08	40.77	0.07
40.90	0.07	40.73	0.07
40.91	0.07	40.73	0.07
40.91	0.07	40.72	0.07
40.91	0.07	40.71	0.07
40.91	0.07	40.68	0.07
40.99	0.08	40.69	0.07
41.00	0.08	40.68	0.07
40.97	0.08	40.68	0.07
40.95	0.09	40.68	0.07
40.99	0.09	40.59	0.08
40.98	0.06	40.59	0.08
40.98	0.08	40.72	0.09
40.97	0.07	40.75	0.09
40.97	0.07	40.79	0.08
40.95	0.08	40.75	0.08
40.95	0.06	40.79	0.08
41.00	0.08	40.80	0.08
41.00	0.09	40.86	0.08
40.96	0.08	40.86	0.08
40.96	0.09	40.81	0.08
40.95	0.08	40.73	0.08
41.01	0.07	40.73	0.08
41.02	0.07	40.73	0.08
41.02	0.06	40.73	0.08
41.02	0.06	40.75	0.09
41.03	0.06	40.74	0.08
41.04	0.06	40.75	0.08
41.05	0.06	40.81	0.07
41.04	0.06	40.80	0.07
41.03	0.07	40.80	0.07
41.03	0.07	40.79	0.07
41.04	0.07	40.76	0.07
41.04	0.08	40.77	0.07
40.98	0.09	40.67	0.08
40.88	0.09	40.64	0.07
40.87	0.10	40.63	0.07
40.92	0.11	40.63	0.08
40.90	0.10	40.63	0.08
40.97	0.10	40.62	0.09
41.01	0.09	40.61	0.08
41.01	0.08	40.60	0.09
41.00	0.08	40.69	0.08
41.00	0.08	40.69	0.09
41.01	0.09	40.68	0.09
40.97	0.09	40.64	0.09
40.92	0.09	40.55	0.08
40.89	0.09	40.46	0.08
40.87	0.08	40.40	0.08
40.86	0.08	40.43	0.08
40.84	0.08	40.44	0.08
40.82	0.08	40.44	0.08
40.75	0.08	40.47	0.08
40.81	0.08	40.51	0.09
40.80	0.08	40.53	0.09
40.82	0.08	40.53	0.09
40.85	0.08	40.56	0.09
40.88	0.08	40.65	0.09
40.87	0.09	40.74	0.09
41.00	0.10	40.60	0.08
40.98	0.10	40.47	0.08
40.97	0.10	40.46	0.08
40.84	0.08	40.36	0.08
40.83	0.08	40.35	0.08
40.64	0.07	40.35	0.09
40.83	0.07	40.31	0.08
40.84	0.07	40.31	0.08
40.83	0.07	40.32	0.07
40.81	0.07	40.33	0.07
40.81	0.07	40.33	0.06
40.81	0.07	40.32	0.06
40.81	0.07	40.33	0.06
40.81	0.08	40.34	0.06
40.80	0.08	40.34	0.06
40.79	0.08	40.34	0.07
40.78	0.09	40.33	0.07
40.84	0.07	40.32	0.07
40.94	0.08	40.36	0.09
40.96	0.08	40.40	0.09
40.91	0.08	40.39	0.09
40.90	0.08	40.42	0.09
40.90	0.08	40.43	0.08
40.89	0.07	40.43	0.08
40.89	0.08	40.43	0.07
[illegible]	[illegible]	[illegible]	[illegible]
40.89	0.08	40.42	0.07
40.88	0.08	40.42	0.07

Figure 6.32 Clear plate density

6.3.3 Photocathode Correction

By the construction of a "photocathode map" of intensities it is possible to obtain the relative sensitivity of each point on the photocathode. These sensitivity factors are used to correct the data, point by point, for any changes in the photocathode sensitivity.

6.3.4 Sky Subtraction

Since the whole field of the polarimeter was filled by the nebula, leaving no regions of sky on the plate, the intensity of the faintest part of the dust lane was assumed to give a reasonable estimate of the sky intensity. Histograms of these regions were obtained for each plate (those for plate 4, "grids out" being shown in figure 6.33), the mean value for each was subtracted off, as sky intensity, from the data.

6.3.5 E- and F-Factors

Since $I1 = (I6/F) \cdot E2$

$I2/F = I5 \cdot E2$

$I3 = (I8/F) \cdot (E3/E1)$

$I4/F = I7 \cdot \frac{E3}{E1}$ (see Figure 2.41)

graphs of I1 v I6, I2 v I5, I3 v I8 and I4 v I7 will give gradients G1, G2, G3, G4 where

$$F1 = \sqrt{G1/G2}$$

and $$F2 = \sqrt{G3/G4}$$

with $$F = \sqrt{F1 \times F2}$$

The relative sensitivity factor between left-hand and right-hand grids is calculated in this way.

Graphs of I1 + I2/F v I3 + I4/F, I1 + I2/F v I5 + I6/F and I1 + I2/F v I7 + I8/F will give the relative exposure between Plate 1, and

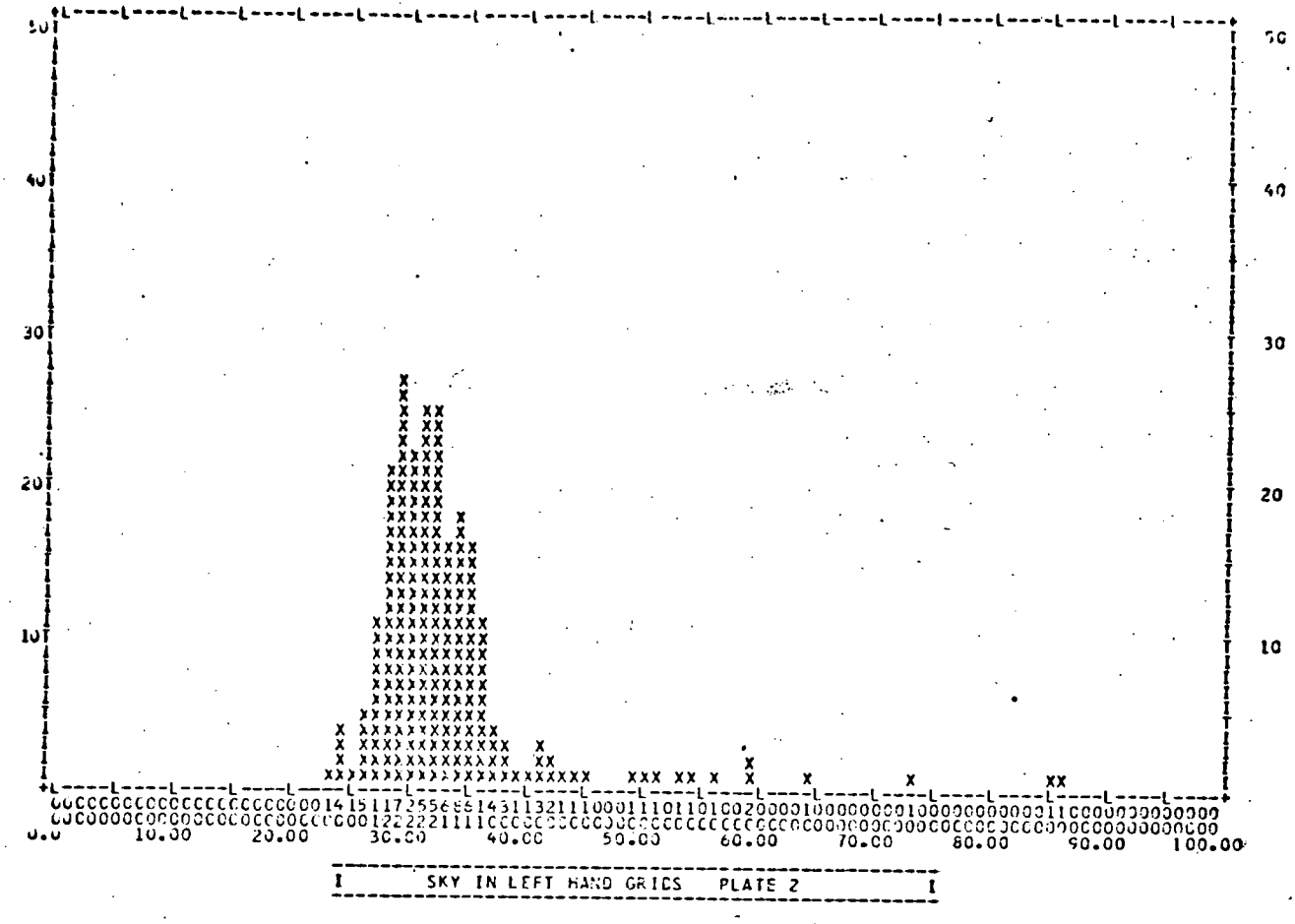

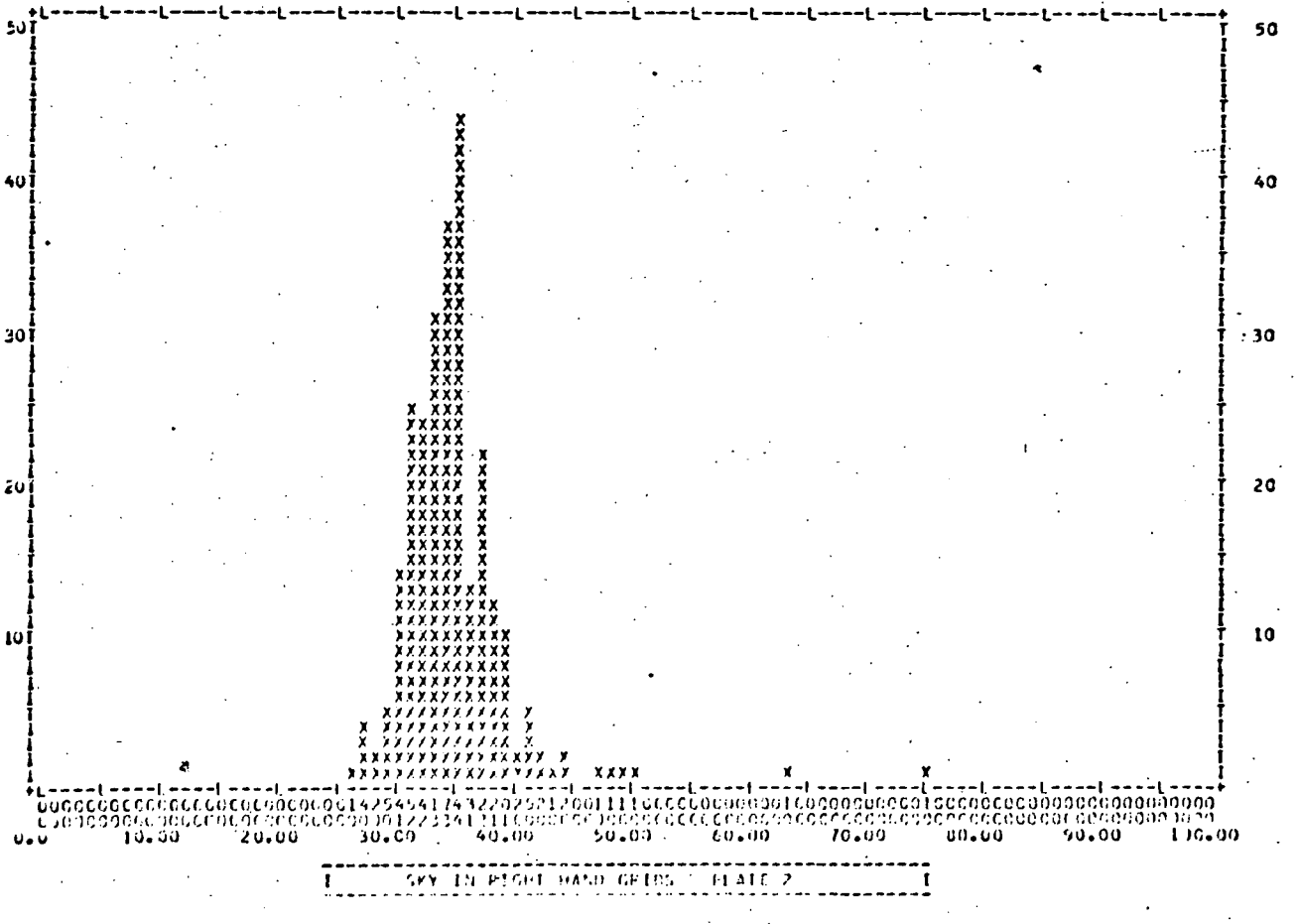

Figure 6.33

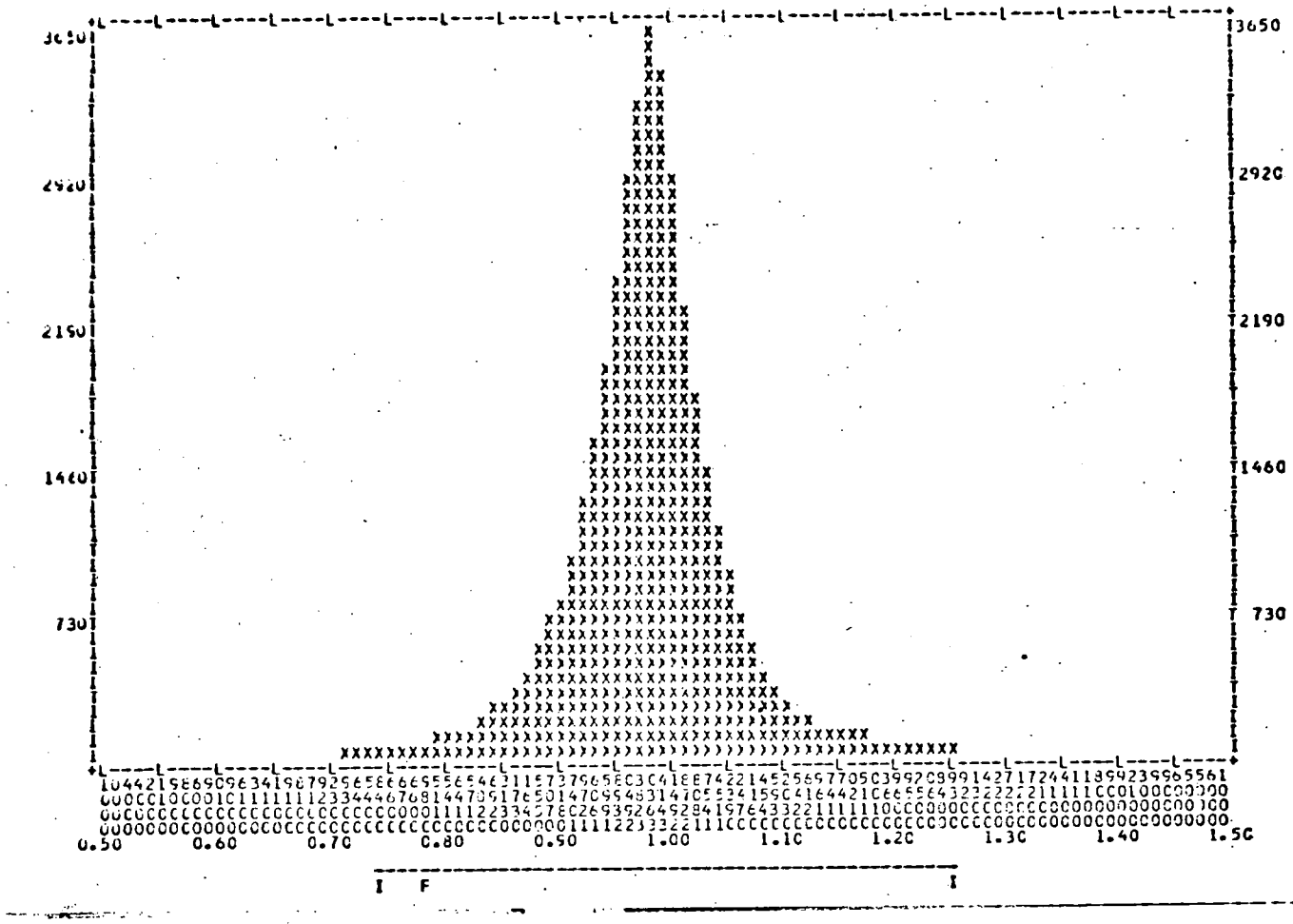
3650
2920
2190
1460
730
0.50
0.60
0.70
0.80
0.90
1.00
1.10
1.20
1.30
1.40
1.50
I F
I

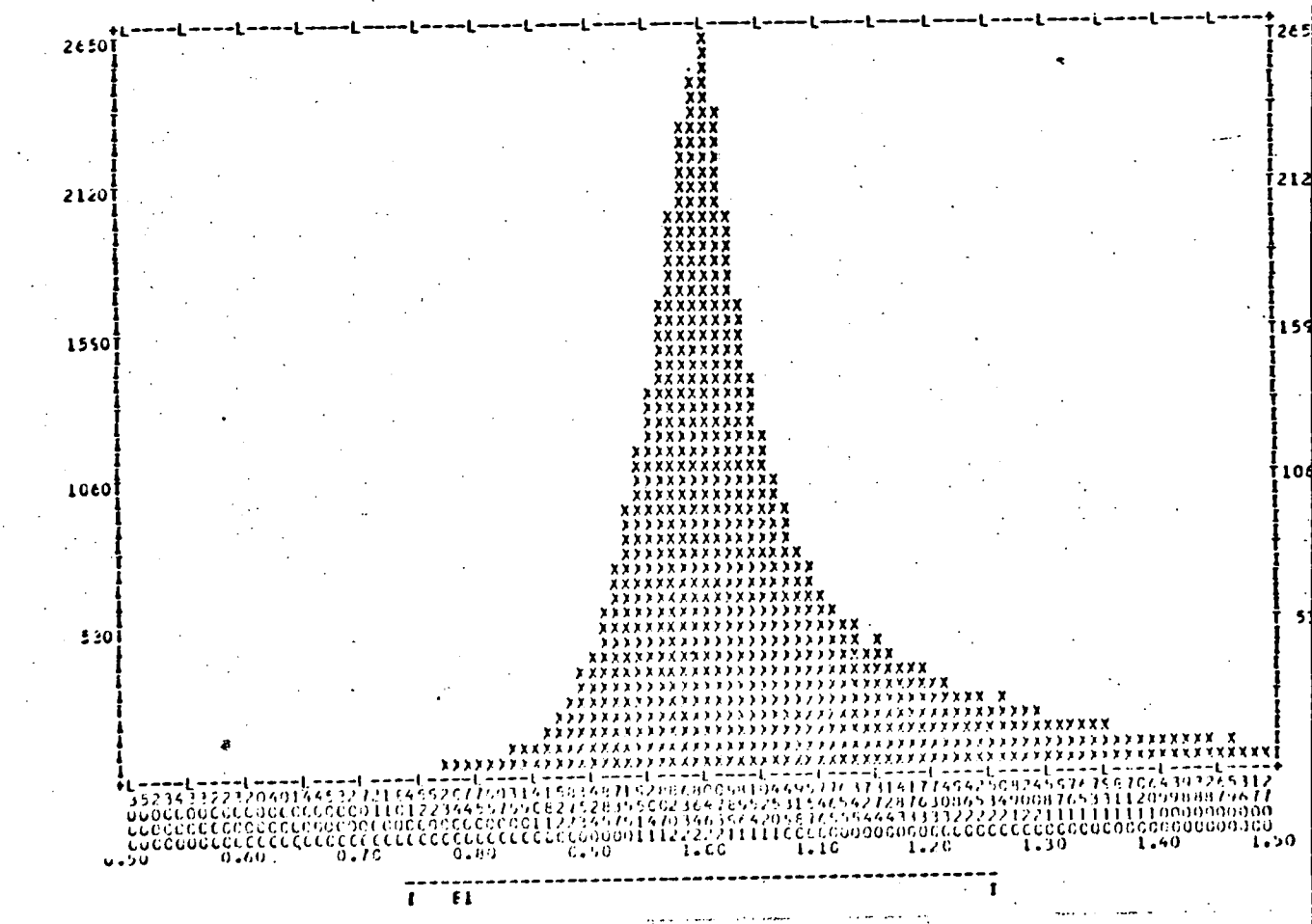
2650
2120
1590
1060
530
0.50
0.60
0.70
0.80
0.90
1.00
1.10
1.20
1.30
1.40
1.50
I E1
I

Figure 6.34a

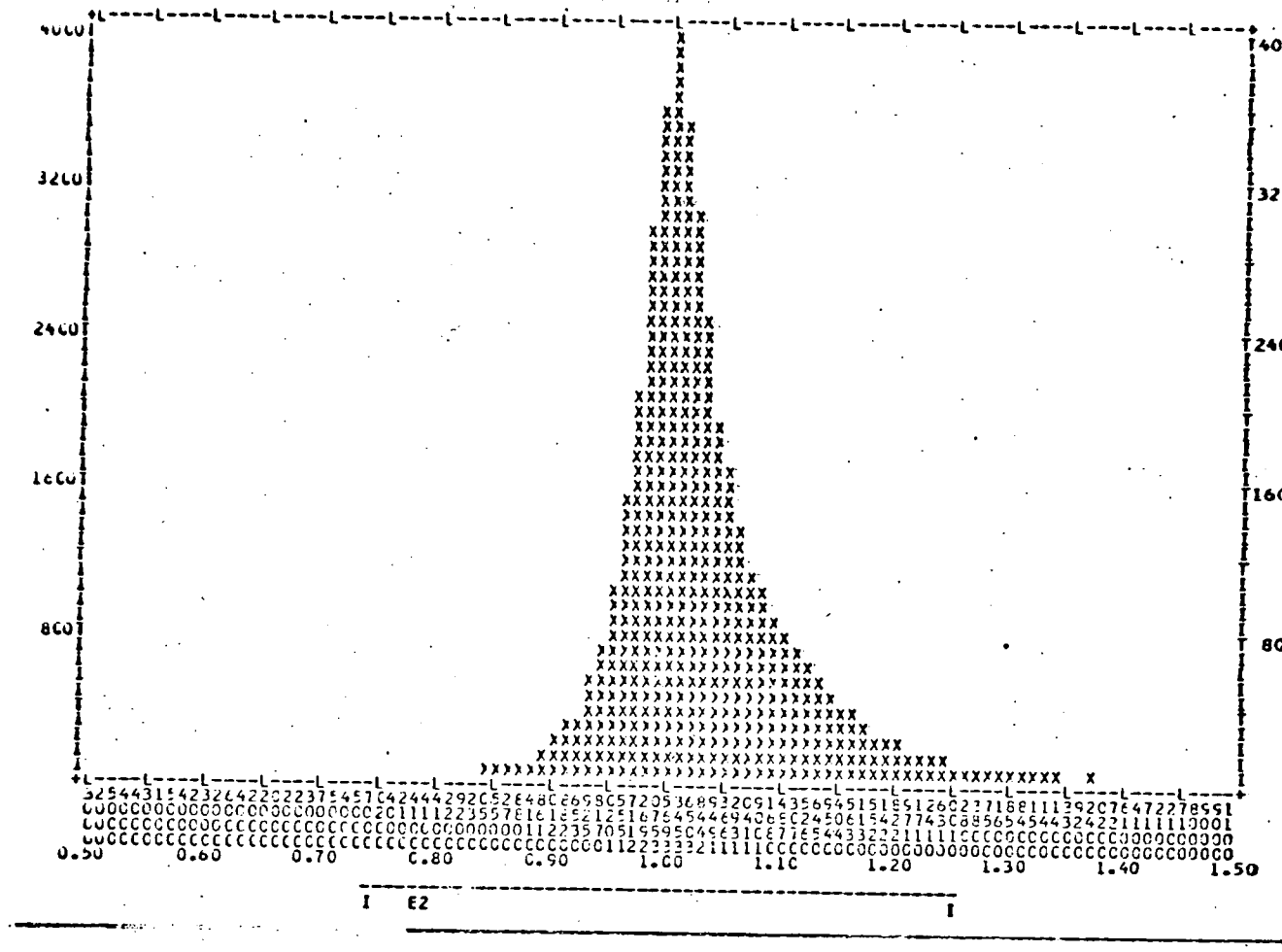
0.50
0.60
0.70
0.80
0.90
1.00
1.10
1.20
1.30
1.40
1.50
I E2 I

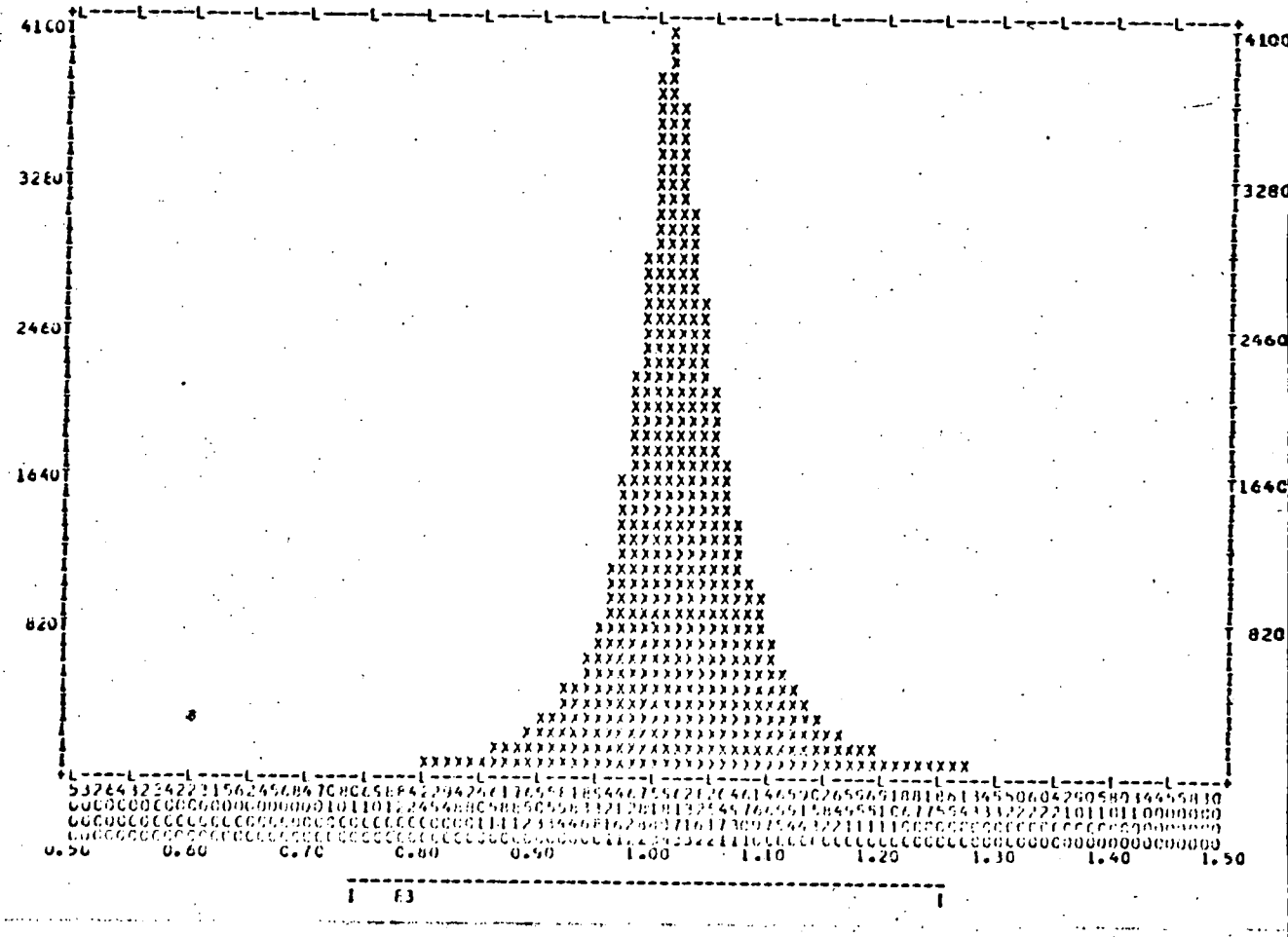
0.50
0.60
0.70
0.80
0.90
1.00
1.10
1.20
1.30
1.40
1.50
I E3 I

Figure 6.34b

Plates 2, 3 and 4 (i.e. E1, E2, E3).

E- and F-factors may also be calculated on a point-by-point basis and the width of the frequency distributions is a measure of the accuracy with which the clear plate and sky signals have been subtracted, since over a plate the E- and F-factor should be constant. Figure 6.34 shows typical distributions indicating that the sky and clear-plate signals have been subtracted with sufficient accuracy.

6.3.6 Calculation of the Stokes' Parameters

Unwanted components of the data having been removed, the data is now "filtered" as briefly outlined in Section 2.4.4. (full details given in Warren-Smith's thesis). On the calculation of the Stokes' Parameters, using a least squares fit to the sine curve each point is weighted with its error.

The intensities have been integrated over 5" arc x 5" arc with a spacing of 5" arc and the complete map is shown in figure 6.35 where each vector represents the degree and orientation of the polarization at that point.

Figure 6.36 shows part of the map superimposed on the [S II] photograph of Walborn (1975). The superposition is achieved by matching the reference stars on the plate with stars on the photograph.

6.3.7 Errors

Representative errors (those for polarizations in the region of clouds C and D) are shown in figures 6.37a and 6.37b where the fractional polarization error, and the error on the angle are plotted against the polarized intensity. Since the errors are inversely proportional to the $\sqrt{}$size of the signal, i.e. the $\sqrt{}$intensity, it is realistic that the errors should decrease with increasing polarized intensity.

6.4 THE POLARIZATION MAP

The main structure in the polarization pattern occurs within the

Figure 6.35 POLARIZATION MAP (North up; East to left)

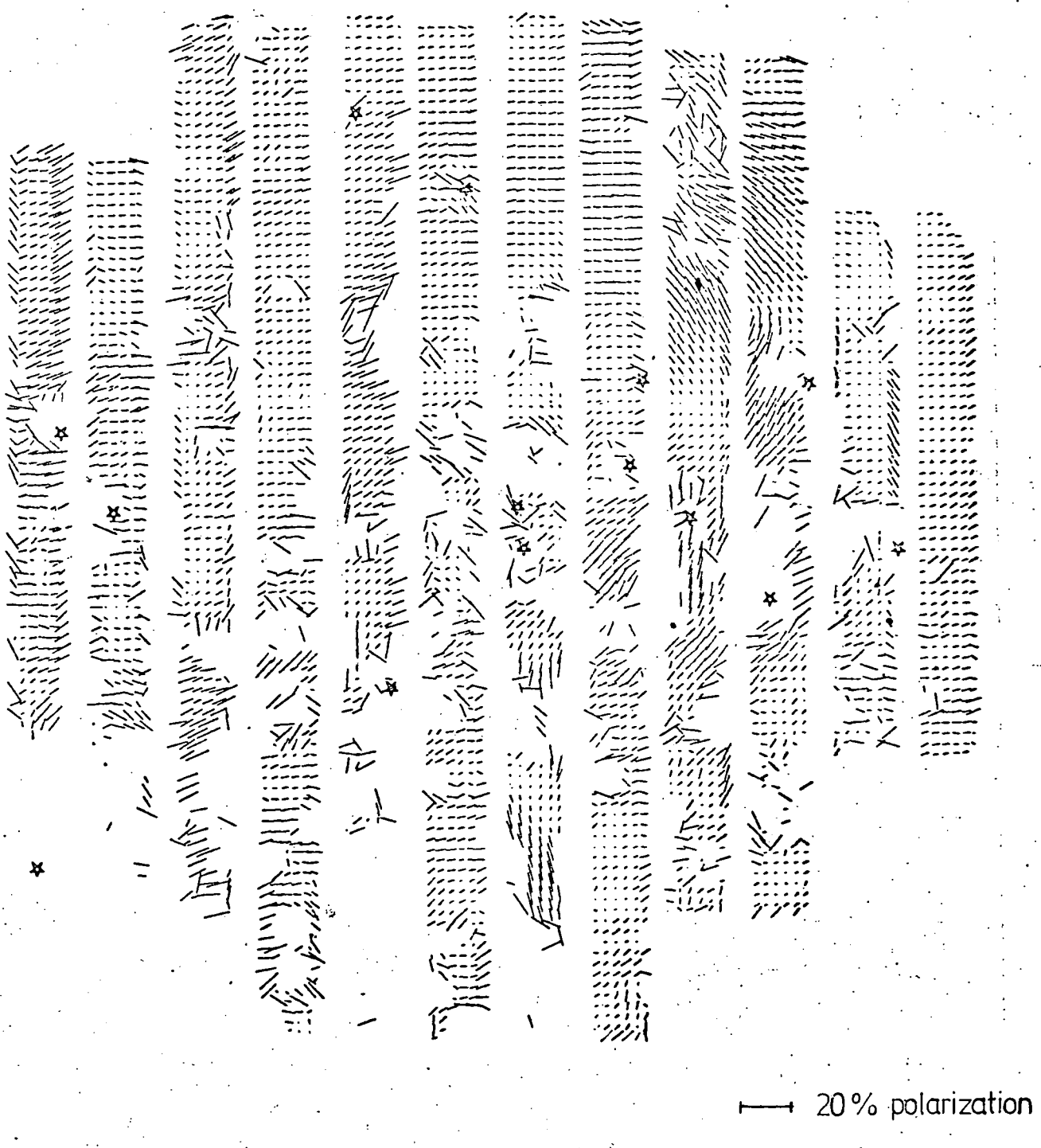

Figure 6.36 Polarization map of Carina Nebula superimposed on the [SII] photograph of Walborn (1975) North is up, East to the left

⟵⟶ 20% polarization

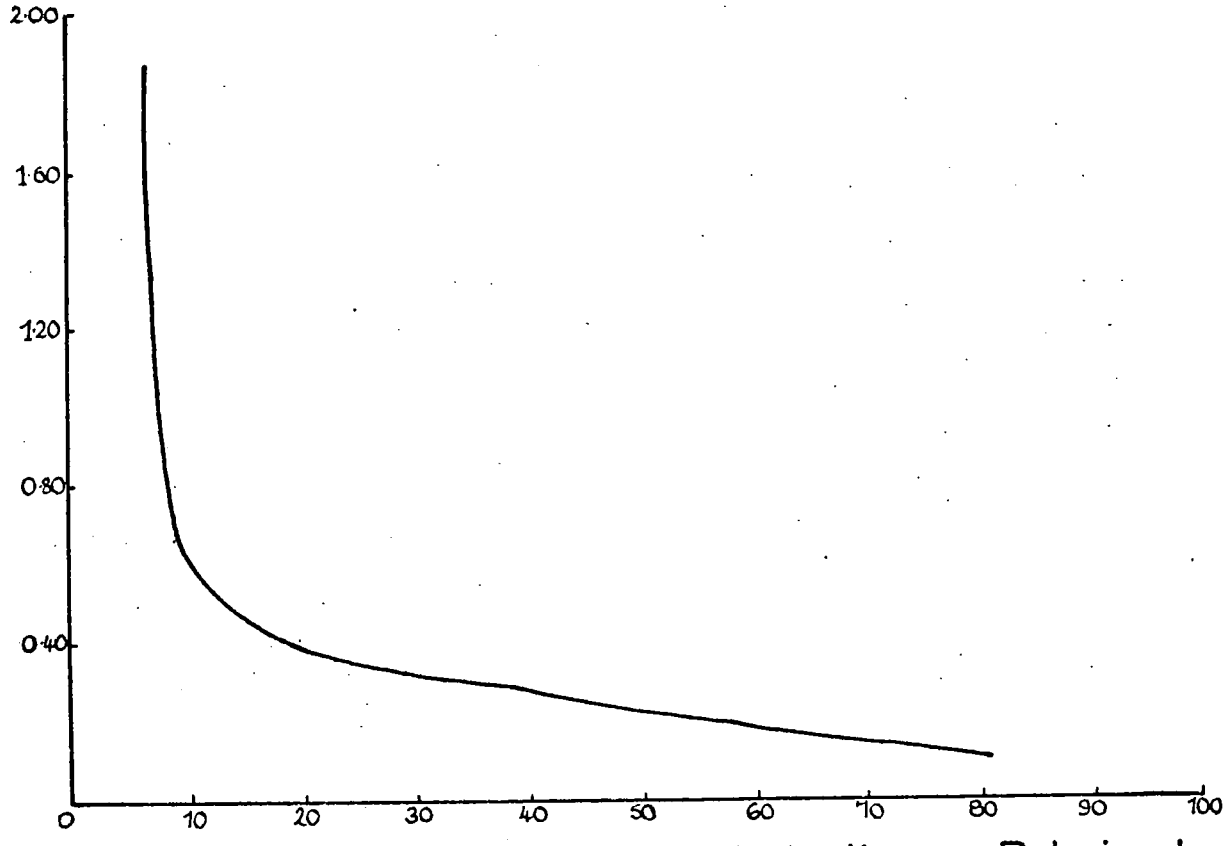

Figure 6.37a Fractional error on Polarization v. Polarized Intensity

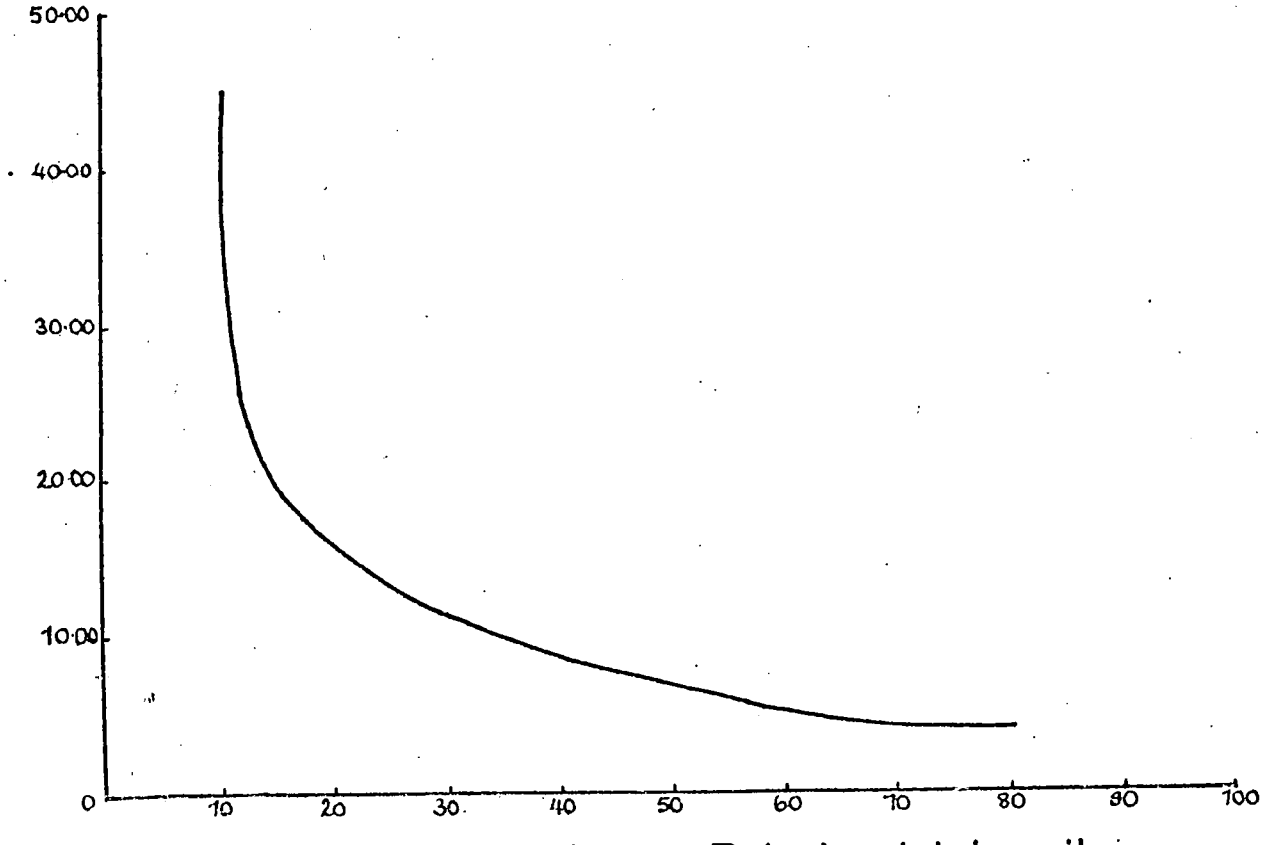

Figure 6.37b Error on angle v. Polarized Intensity

peculiar ring, where clouds C and D are about 8% (± 2%) polarized at position angle 45° (approximately).

A large area of the map consists of nearly horizontal vectors of about 2% polarization. The regularity of this feature, especially in the southern region of the map is much disturbed by the effect of the numerous stars in the field.

There is some small evidence for the existence of 45° vectors of about 6% polarization running along the edges of the dust lane to the south-west of η Carinae.

The presence of clouds 2 and 3, and of clouds A and E, do not seem to affect the polarization pattern. There are no measurements in the region of cloud 1 or cloud B, or in the centre of the peculiar ring structure.

6.5 DISCUSSION

The horizontal vectors represent polarization of interstellar origin ; subtraction of this component - 2.4% at position angle 108° (Visvanathan 1967) - yields very small polarizations over the map, except in the region of clouds C and D. However, a map of the polarized intensity, which is more meaningful than the polarization, since now only the polarized regions are registering, shows that significant amounts of polarized intensity are present in cloud E when the interstellar component has been subtracted (see figure 6.38). The polarized intensity along the edges of the dust lane is insignificant.

A general feature of the polarized intensity map is the existence of several distinct segments of independent centro-symmetric patterns. There seems to be no single source responsible for the polarization of this region of the Carina Nebula.

Clouds C and D seem to be reflecting the light from η Carinae. These are both low excitation clouds and the results confirm the sugges-

Figure 6.38 Polarized intensity map of Carina Nebula superimposed on the [SII] photograph of Walborn (1975) North is up, East to the left
The interstellar polarization has been removed
⟵ 20 PDS units Polarized Intensity

tion of Walborn (1975) that they are in part reflection nebulae, associated with η Carinae. It is possible that these clouds are also reflecting the light from stars nearby, and the vague existence of a semi-circular pattern of vectors associated with cloud C is suggestive of a source hidden somewhere behind cloud D.

No single source can be responsible for the polarization of cloud E. The western part of cloud E may well be reflecting the light from η Carinae. The polarization eastwards is suggestive of a source somewhere to the north of HD 303308. The vectors just north of cloud E suggest a source northwards of cloud E. Therefore multiple sources must be responsible for the polarization of cloud E.

The general lack of uniformity in the polarization pattern of the ring structure raises the question as to whether or not the ring is indeed a physical feature of simply the result of chance superpositions of cloud along the line of sight (Walborn 1975).

It is possible that cloud E is more deeply embedded in the nebula than clouds C and D, which may be at the forefront of a three-dimensional "rim" structure, and hence the contribution of light from η Carinae is negligible or small compared with that of stars in the immediate vicinity of cloud E.

The most westerly portion of the arc to the south of cloud E may be reflecting the light from η Carinae, but eastwards, the pattern centres on a source in the vicinity of HD 303308.

It is difficult to draw conclusions about clouds A and B, since there are only a few measurements in these regions but there is a suggestion that the vectors associated with the cloud between C and A are generally perpendicular to a radius vector drawn from η Carinae.

Over the rest of the field the polarized intensity is negligible and there are no particular features discernible in the polarized intensity map

Very few of the observations of the Carina Nebula specifically embrace the ring structure. Dickel's (1974) observations involve large regions of the nebula ; those of Walborn and Hesser (1974) do not include the ring structure. Both Gardner et al (1970) and Huchtmeier and Day (1975) observe double recombination line profiles being wide and very similar in intensity, but the resolution of the observations makes it impossible to associate a particular profile with a particular cloud.

Deharveng and Maucherat (1974) have observed the spectral splitting of the [N II] and Hα lines of part of the ring structure. They find that [N II] splitting occurs in cloud B, C and the westerly portion of cloud E, in addition to the central regions of the ring. Cloud D, being of low excitation is not observed in [N II]. The most easterly regions of cloud E and the arc below cloud E are interpreted in terms of a receding cloud, whilst the southern part of cloud A is interpreted in terms of an approaching cloud.

The only possible correlation between these and the polarization results is that the [N II] splitting occurs in regions where the polarization may be attributed to reflection of the light from η Carinae. Deharveng and Maucherat propose η Carinae as the centre of their "expanding sphere" and therefore it is not unreasonable that η Carinae is also responsible for the polarization of cloud C and part of cloud E. The results of Deharveng and Maucherat seem to suggest that cloud E is really a multiple cloud structure and in view of this, it is reasonable that more deeply embedded clouds should have a different source of illumination.

6.6 CONCLUSIONS

Clouds C and D are polarized by reflection of the light from η Carinae, and possibly that from stars in the vicinity. Multiple sources are necessary to explain the polarization of cloud E, but it

seems that cloud E is a multiple cloud structure, the most westerly clouds being associated with the η Carinae - cloud C and D complex.

There is no apparent central source in this region, and it is likely that η Carinae and the O-stars all contribute to the general excitation.

However, it must be noted that observations made with a broad band V-filter have been superposed on an [S II] photograph. Therefore, features enhanced in [S II] are not necessarily those enhanced in V and so a detailed correspondence between the polarization map and the photograph cannot be expected. Hence it is important to obtain further polarimetric measurements of this region of the Carina Nebula with very narrow-band filters in order to make some definite conclusions about the various relationships between η Carinae, the ring structure, and the O-stars of Trumpler 16.

References

Beard M, Kerr F J, 1966, Australian J. Phys. 19 825.

Deharveng L, Maucherat M, 1975, Astron. & Astrophys. 41 27.

Dickel H R, 1974, Astron. & Astrophys. 31 11.

Dickel H R, Wall J V, 1974, Astron. & Astrophys. 31 5.

Elliott K H, 1979, Mon. Not. R. Astr. Soc. 186 9P.

Faulkner D J, 1963, Publ. Astron. Soc. Pacific, 75 269.

Gardner F F, Dickel H R, Whiteoak J B, 1973, Astron. & Astrophys. 23, 51.

Gardner F F, Milne D K, Mezger P G, Wilson T L, 1970, Astron. & Astrophys. 7 349.

Gardner F F, Morimoto M, 1968, Australian J. Phys. 21 881.

Herbst W, 1976, Astrophys. Journ. 208, 923.

Hindman J V, Wade C M, 1959, Australian J. Phys. 12 258.

Huchtmeier W K, Day G A, 1975, Astron. & Astrophys. 41 153.

Jones B B, 1973, Australian J. Phys. 26 545.

Louise R, 1972, Astron. & Astrophys. 18 475.

McGee R X, Gardner F F, 1968, Australian J. Phys. 21 149.

McGee R X, Batchelor R A, Brooks J W, Sinclair M W, 1969, Australian J. Phys. 22 631.

Mills B Y, Little A G, Sheridan K V, 1956, Australian J. Phys. 9 218.

Seward F D, Page C S, Turner M J L, Pounds K A, 1976, Mon.Not.R.Astr.Soc. 177 13 P.

Shaver P A, Goss W M, 1970, Australian J. Phys. Astrophys. Suppl. 14.

Wade C M, 1959, Australian J. Phys. 12 418.

Walborn N R, 1973, Astrophys. Journ. 179 517.

Walborn N R, 1975, Astrophys. Journ. 202 L129.

Walborn N R, Hesser J E, 1975, Astrophys. Journ. 199 535.

Walborn N R, Ingerson T E, 1977, Sky and Telescope, 54 22.

Walborn N R, Liller M H, 1977, Astrophys. Journ. 211 181.

GENERAL CONCLUSIONS

From polarimetric measurements it has been possible to obtain information regarding the nature of the dust grains in η Carinae and the relationship between η Carinae and the Carina Nebula.

Assuming that η Carinae has a bipolar structure, one component of the dust has been found to consist of a size distribution of silicate grains of effective size $\sim$ 0.1μ and refractive index m = 1.65-0.05i.

Clouds in the Carina Nebula have been found to be reflecting the light from η Carinae, hence associating η Carinae with the Carina Nebula.

It is, however, important to make further investigations at different wavelengths. Although optical polarization is very sensitive to the size of grains giving rise to the scattered radiation, spectro-polarimetric data is necessary in order to consider grain mixtures and place further constraints on models.

As regards the observations of the Carina Nebula, in a region striking for its changing appearance in different wavebands it is extremely important to unite spectral and spatial polarimetric observations. The present results are mainly preliminary.

Spectro-polarimetry is therefore the next step in completely defining the nature of the dust grains in η Carinae and also the nature of the relationships between the various unusual features of the Carina Nebula, in the vicinity of η Carinae.

In η Carinae "we have a star fitfully variable to an astonishing extent and whose fluctuations are spread over centuries, apparently in no settled period and with no regularity of progression.... Its future career will be a subject of high physical interest" (Sir John Herschel).

APPENDIX

RESULTS OF THE ANALYSIS OF THE POLARIMETRIC DATA FOR THE HOMUNCULUS

X	Y	I	Q	U	IP	P	θ
214.50	169.50	374.61	83.29	-80.79	115.04	30.98	-22.07
216.50	169.50	291.46	54.01	-83.47	99.42	34.11	-28.55
218.50	169.50	207.70	30.66	-81.82	89.09	43.27	-31.74
196.50	171.50	46.00	-0.00	8.82	9.08	19.74	65.87
198.50	171.50	78.10	-5.80	8.58	10.36	13.25	62.05
200.50	171.50	113.53	3.19	13.54	13.91	12.28	38.37
202.50	171.50	150.61	11.32	18.89	22.03	14.63	29.53
204.50	171.50	282.41	13.07	43.31	45.24	17.24	36.60
206.50	171.50	647.04	122.16	78.29	145.10	22.42	16.33
208.50	171.50	1617.74	500.91	135.70	518.98	32.08	7.58
210.50	171.50	1695.71	745.46	3.78	745.47	39.37	0.15
212.50	171.50	977.70	288.72	-87.98	301.82	30.87	-8.47
214.50	171.50	622.93	126.21	-133.50	187.38	30.08	-23.83
216.50	171.50	420.35	53.29	-112.60	124.57	29.64	-32.34
218.50	171.50	290.95	20.89	-82.52	85.12	29.26	-37.90
194.50	173.50	48.94	0.00	8.32	8.36	17.08	42.24
196.50	173.50	83.59	-27.98	7.79	29.04	34.75	82.22
198.50	173.50	119.09	-17.48	11.92	21.15	17.64	72.80
200.50	173.50	155.49	-10.43	15.86	18.99	11.27	61.66
202.50	173.50	243.41	-1.53	23.13	23.18	9.52	46.89
204.50	173.50	440.45	13.45	55.40	57.01	12.94	38.18
206.50	173.50	894.21	90.20	110.60	142.72	15.96	25.40
208.50	173.50	2099.12	419.91	117.69	436.09	20.78	7.83
210.50	173.50	2875.30	820.35	16.35	820.56	28.54	0.64
212.50	173.50	1990.50	307.40	-125.31	331.90	20.77	-11.09
214.50	173.50	921.30	124.94	-154.03	198.35	21.53	-25.48
216.50	173.50	543.15	34.98	-125.43	130.22	23.97	-37.21
218.50	173.50	358.14	-19.45	-95.60	97.56	27.24	-50.75
194.50	175.50	69.36	-12.92	5.99	14.25	20.54	77.56
196.50	175.50	175.49	-42.46	22.05	47.85	27.26	76.28
198.50	175.50	284.07	-39.71	20.54	47.76	16.78	73.13
200.50	175.50	349.22	-43.44	29.57	52.55	15.05	72.88
202.50	175.50	440.62	-28.31	24.14	37.21	8.44	69.78
204.50	175.50	764.67	-6.22	51.00	51.38	6.72	48.48
206.50	175.50	1562.36	50.62	11.52	51.33	3.29	6.49
208.50	175.50	3505.74	78.17	112.96	137.37	3.92	27.60
214.50	175.50	1272.67	87.78	-111.70	142.06	11.16	-25.92
216.50	175.50	838.63	-21.45	-100.92	109.05	17.07	-50.68
218.50	175.50	421.42	-25.85	-90.49	94.10	22.33	-52.97
194.50	177.50	64.31	-26.84	3.40	27.05	32.09	86.40
196.50	177.50	275.03	-87.59	17.59	89.84	25.40	82.71
198.50	177.50	519.72	-100.22	35.77	112.08	21.57	80.70
200.50	177.50	661.33	-113.77	35.27	119.11	18.01	81.39
202.50	177.50	824.49	-72.77	39.42	82.77	10.04	75.78
204.50	177.50	1042.72	-50.00	-31.25	64.13	3.90	-75.42
206.50	177.50	3397.79	326.47	178.49	372.07	10.95	14.33
214.50	177.50	2210.55	215.20	27.73	210.98	9.82	3.07
216.50	177.50	749.78	-17.17	-59.66	62.08	8.28	-53.03
218.50	177.50	466.42	-30.61	-52.72	60.97	15.23	-60.08
194.50	179.50	88.53	-16.00	-0.05	16.06	23.43	-89.92
196.50	179.50	225.49	-60.27	8.35	60.85	26.99	86.06
198.50	179.50	403.28	-110.75	19.27	112.41	24.26	85.07
200.50	179.50	693.80	-119.94	19.13	121.46	17.51	85.47
202.50	179.50	1288.74	-153.75	14.00	154.39	11.98	87.40
204.50	179.50	3215.55	123.29	46.31	131.70	4.10	10.29
214.50	179.50	2619.41	134.00	79.28	156.27	5.54	15.25
216.50	179.50	1038.21	15.18	-25.07	29.31	2.82	-29.40
218.50	179.50	479.62	-1.77	-22.35	22.42	4.67	-47.27
194.50	181.50	43.25	-11.92	2.45	12.17	28.89	84.19
196.50	181.50	102.53	-9.84	2.87	10.25	9.99	81.89

196.50	181.50	220.80	-39.71	-3.36	39.85	18.05	-87.58
200.50	181.50	565.65	-90.24	-14.19	91.35	16.21	-85.54
202.50	181.50	1729.24	-190.43	-46.66	196.54	11.37	-82.85
204.50	181.50	4170.63	-183.81	-239.13	301.61	7.25	-63.78
214.50	181.50	2621.54	124.24	38.71	130.13	4.96	8.65
216.50	181.50	1276.63	3.65	11.85	12.46	0.98	36.04
218.50	181.50	869.38	1.22	2.89	3.14	0.36	33.54
196.50	183.50	67.50	0.55	-0.47	0.72	1.07	-20.27
198.50	183.50	149.25	-13.19	-3.96	13.78	9.23	-81.65
200.50	183.50	516.53	-73.74	-29.46	79.41	15.31	-79.12
202.50	183.50	1723.61	-131.76	-119.00	177.54	10.30	-68.96
204.50	183.50	3436.24	-73.92	-275.22	284.98	8.29	-52.52
206.50	183.50	3845.29	133.84	-247.61	281.47	7.32	-30.81
208.50	183.50	3340.92	240.39	-57.11	252.93	7.57	-6.52
210.50	183.50	2717.57	210.18	-57.97	218.03	8.02	-7.71
212.50	183.50	2160.56	133.89	31.22	137.48	6.36	6.50
214.50	183.50	1746.35	103.30	12.38	104.04	5.96	3.42
216.50	183.50	1317.29	-11.24	32.71	34.59	2.03	54.48
218.50	183.50	1279.15	-12.51	52.30	53.78	4.20	51.73
196.50	185.50	65.56	1.78	-1.55	2.36	3.61	-20.52
198.50	185.50	165.72	-13.50	-12.66	18.51	11.30	-66.41
200.50	185.50	481.25	-48.12	-27.86	55.61	11.56	-74.96
202.50	185.50	1317.71	-58.10	-113.24	126.37	9.59	-58.18
204.50	185.50	2511.60	50.34	-270.47	275.11	11.90	-39.73
206.50	185.50	2544.06	239.42	-263.24	370.86	14.56	-24.90
208.50	185.50	1931.52	231.48	-131.09	266.32	13.79	-14.62
210.50	185.50	1351.85	145.75	-27.95	148.40	10.98	-5.43
212.50	185.50	1272.02	95.52	7.44	95.81	7.53	2.23
214.50	185.50	1450.58	122.31	25.51	124.94	8.58	5.89
216.50	185.50	1271.00	43.26	53.71	68.96	5.43	25.58
218.50	185.50	1169.76	39.77	84.44	93.33	7.84	32.39
196.50	187.50	62.55	-1.14	0.94	1.48	2.56	70.18
198.50	187.50	169.56	-17.89	-15.59	25.80	15.63	-66.96
200.50	187.50	446.65	-13.60	-41.41	43.59	9.75	-54.09
202.50	187.50	966.54	-7.41	-65.96	84.28	8.54	-47.53
204.50	187.50	1600.22	65.12	-174.46	194.12	12.09	-32.00
206.50	187.50	1674.79	205.32	-185.32	276.56	16.51	-21.04
208.50	187.50	1215.23	101.49	-62.93	131.53	14.94	-13.59
210.50	187.50	979.67	124.37	-20.33	126.02	12.66	-4.64
212.50	187.50	1142.62	139.12	-4.54	139.19	12.18	-0.94
214.50	187.50	1286.46	151.43	18.20	152.52	11.86	3.43
216.50	187.50	1080.21	67.67	53.49	86.42	7.94	19.12
218.50	187.50	817.19	19.14	41.88	46.05	5.63	32.73
196.50	189.50	59.10	0.43	-4.37	4.39	7.43	-42.17
198.50	189.50	175.19	-14.09	-15.95	21.28	12.15	-65.73
200.50	189.50	539.41	-21.21	-44.69	49.46	14.57	-57.70
202.50	189.50	857.22	-0.60	-74.71	74.72	11.73	-45.23
204.50	189.50	1020.39	70.52	-95.40	122.30	11.92	-25.64
206.50	189.50	1145.38	152.16	-107.60	188.36	16.27	-17.63
208.50	189.50	862.64	119.76	-62.05	134.88	15.64	-13.70
210.50	189.50	903.17	91.94	-16.38	93.76	10.36	-5.05
212.50	189.50	1241.94	159.86	20.95	161.22	12.98	3.73
214.50	189.50	1304.70	159.00	44.16	165.00	12.09	7.74
216.50	189.50	965.77	98.86	41.95	105.55	11.65	11.71
218.50	189.50	461.06	19.35	14.39	24.11	5.23	16.32
196.50	191.50	46.42	-0.99	-3.19	3.34	7.20	-53.63
198.50	191.50	121.45	-4.71	-21.61	22.12	18.22	-51.15
200.50	191.50	255.10	-5.01	-26.93	27.39	10.62	-50.26
202.50	191.50	442.29	12.09	-42.52	44.20	9.99	-37.00
204.50	191.50	674.18	48.17	-64.16	80.23	11.90	-26.56

208.50	157.50	66.65	19.54	0.44	19.54	29.59	0.64
210.50	157.50	98.69	25.56	-7.43	26.43	26.76	-6.17
212.50	157.50	92.67	27.16	-4.07	27.46	29.63	-4.26
214.50	157.50	56.62	10.00	-12.66	16.33	27.85	-25.99
204.50	159.50	65.36	8.90	12.14	15.05	23.03	26.68
206.50	159.50	111.28	35.26	3.52	35.46	31.66	2.85
208.50	159.50	191.92	69.77	-0.08	69.77	36.36	-0.03
210.50	159.50	251.22	93.71	-9.01	94.14	37.47	-2.75
212.50	159.50	246.45	84.77	-17.98	86.66	35.16	-5.99
214.50	159.50	172.50	47.76	-27.27	54.99	31.88	-14.87
216.50	159.50	82.69	17.72	-14.90	23.15	28.00	-20.03
202.50	161.50	94.03	14.93	0.03	14.93	15.87	0.05
204.50	161.50	159.41	45.45	33.11	56.23	35.27	18.04
206.50	161.50	226.23	66.27	27.80	71.87	31.49	11.38
208.50	161.50	294.95	114.69	14.16	115.56	39.16	3.52
210.50	161.50	310.45	114.28	-5.14	114.39	36.65	-1.29
212.50	161.50	290.37	110.83	-33.75	115.80	39.09	-8.47
214.50	161.50	244.61	91.25	-43.14	100.93	41.26	-12.65
216.50	161.50	156.42	55.56	-34.13	65.21	41.16	-15.78
218.50	161.50	85.11	23.03	-20.04	30.53	46.89	-20.52
200.50	163.50	56.29	12.30	11.02	16.52	28.54	20.93
202.50	163.50	135.12	20.35	31.73	41.23	30.97	25.15
204.50	163.50	245.64	72.51	49.72	87.92	35.79	17.22
206.50	163.50	302.25	91.79	45.08	102.26	33.63	13.08
208.50	163.50	332.58	112.21	18.69	113.76	34.20	4.73
210.50	163.50	307.97	122.24	2.54	122.27	39.70	0.60
212.50	163.50	277.03	103.95	-27.00	107.40	38.77	-7.28
214.50	163.50	235.76	89.27	-54.04	104.36	40.80	-15.60
216.50	163.50	207.28	64.85	-57.43	86.63	41.79	-20.76
218.50	163.50	109.53	20.20	-32.77	38.52	35.17	-29.14
200.50	165.50	71.63	5.24	11.39	12.54	17.49	32.66
202.50	165.50	134.56	19.73	22.95	30.27	22.53	24.66
204.50	165.50	239.28	60.93	47.52	77.27	32.29	18.98
206.50	165.50	338.65	98.91	43.27	107.96	31.88	11.81
208.50	165.50	377.77	134.08	22.40	135.94	35.98	4.74
210.50	165.50	327.17	124.20	-0.95	124.20	37.98	-0.22
212.50	165.50	273.94	97.15	-24.82	100.27	36.66	-7.17
214.50	165.50	260.65	79.50	-63.39	101.67	36.20	-19.28
216.50	165.50	209.10	82.71	-65.04	116.03	44.06	-22.90
218.50	165.50	102.69	37.74	-49.03	61.87	38.03	-26.21
198.50	167.50	55.36	-6.57	9.04	11.35	20.80	61.73
200.50	167.50	80.06	2.59	15.14	15.36	17.44	40.14
202.50	167.50	116.62	15.52	23.75	27.32	23.00	30.16
204.50	167.50	209.54	54.77	45.41	71.14	35.95	19.83
206.50	167.50	354.46	99.76	48.72	111.02	31.32	13.01
208.50	167.50	485.71	161.57	32.23	164.75	35.92	5.64
210.50	167.50	420.74	144.54	2.38	144.56	34.36	0.41
212.50	167.50	306.61	106.97	-31.56	111.33	36.36	-8.22
214.50	167.50	313.01	90.81	-75.19	117.90	37.67	-19.61
216.50	167.50	291.46	76.89	-65.41	116.27	39.89	-25.64
218.50	167.50	186.11	34.69	-56.72	68.20	36.65	-29.71
196.50	169.50	41.35	7.45	4.65	8.89	21.49	16.52
198.50	169.50	70.57	-0.03	12.66	12.66	17.94	45.07
200.50	169.50	100.49	1.25	15.59	15.64	15.57	42.70
202.50	169.50	122.84	6.57	19.05	20.15	16.41	35.49
204.50	169.50	201.43	33.77	29.37	44.78	22.22	20.51
206.50	169.50	425.73	94.36	59.43	111.52	26.19	16.10
208.50	169.50	814.12	261.84	73.44	271.95	33.40	7.83
210.50	169.50	834.39	285.49	-2.44	285.50	34.22	-0.25
212.50	169.50	491.99	144.28	-40.77	149.93	30.47	-7.69

206.50	191.50	839.51	127.56	-72.30	146.63	17.47	-14.77
208.50	191.50	615.35	73.19	-32.59	80.11	13.02	-12.00
210.50	191.50	636.29	60.89	-10.62	61.85	9.72	-5.04
212.50	191.50	905.22	116.20	31.62	122.41	12.42	7.53
214.50	191.50	1096.97	149.89	54.35	159.44	14.51	9.97
216.50	191.50	889.41	97.63	44.99	107.49	15.59	12.37
218.50	191.50	297.30	12.97	20.60	24.52	8.25	29.03
196.50	193.50	64.69	1.42	-14.42	14.49	17.10	-42.20
200.50	193.50	242.65	11.08	-46.65	47.95	19.81	-38.32
202.50	193.50	455.94	37.16	-72.84	81.77	17.93	-31.49
204.50	193.50	588.84	69.11	-70.98	99.07	16.62	-22.88
206.50	193.50	602.57	92.68	-51.73	106.14	17.62	-14.59
208.50	193.50	468.23	82.60	-32.39	86.73	16.17	-10.71
210.50	193.50	489.59	69.60	-1.35	69.61	14.62	-0.55
212.50	193.50	655.23	89.50	15.74	90.87	13.91	4.99
214.50	193.50	754.47	106.77	53.57	121.25	16.07	13.11
216.50	193.50	536.07	69.41	47.66	84.31	15.67	17.29
218.50	193.50	270.25	30.60	28.07	41.52	15.36	21.26
196.50	195.50	65.62	1.65	-7.74	7.92	12.07	-38.98
200.50	195.50	194.09	10.18	-30.63	32.28	16.58	-35.81
202.50	195.50	425.30	62.74	-79.88	101.57	25.88	-25.93
204.50	195.50	560.44	87.39	-77.05	116.51	23.28	-20.70
206.50	195.50	510.98	79.79	-45.82	92.01	18.01	-14.93
208.50	195.50	541.27	112.06	-30.57	115.18	21.46	-7.63
210.50	195.50	542.03	129.10	-14.84	129.95	25.97	-3.28
212.50	195.50	509.70	102.52	21.46	104.74	20.55	5.91
214.50	195.50	522.07	82.82	55.41	99.65	19.69	16.89
216.50	195.50	523.14	114.34	71.83	135.03	25.81	16.07
218.50	195.50	256.77	51.79	34.88	62.44	24.32	16.98
196.50	197.50	45.74	4.23	-2.21	4.77	10.92	-13.78
200.50	197.50	104.62	4.32	-16.92	17.47	16.70	-37.84
202.50	197.50	270.93	46.73	-52.89	70.58	26.05	-24.27
204.50	197.50	360.86	68.72	-67.97	96.66	26.78	-22.35
206.50	197.50	305.76	65.29	-49.47	81.91	21.34	-18.58
208.50	197.50	431.91	100.33	-27.44	104.01	24.08	-7.65
210.50	197.50	460.29	117.72	-4.42	117.80	25.59	-1.07
212.50	197.50	398.51	94.87	13.88	95.88	24.06	4.16
214.50	197.50	380.01	79.70	28.18	84.55	21.90	9.74
216.50	197.50	350.10	95.31	48.21	106.81	29.83	13.42
218.50	197.50	157.46	30.05	16.26	35.16	22.33	15.65
200.50	199.50	46.06	5.63	-7.62	9.48	20.57	-26.77
202.50	199.50	98.66	18.74	-18.00	25.99	26.29	-21.93
204.50	199.50	156.69	34.57	-29.82	45.66	28.73	-20.39
206.50	199.50	192.21	50.53	-22.65	55.37	28.81	-12.07
208.50	199.50	212.65	40.17	-14.77	48.48	22.66	-8.87
210.50	199.50	252.32	59.20	-1.47	59.22	25.49	-0.71
212.50	199.50	205.10	50.45	3.99	50.61	24.68	2.26
214.50	199.50	176.21	40.93	5.54	41.30	23.44	3.85
216.50	199.50	124.65	26.10	7.94	27.28	21.85	8.46
218.50	199.50	66.44	8.30	4.62	9.49	14.29	14.56
204.50	201.50	47.28	15.78	-8.34	16.11	34.07	-15.59
206.50	201.50	64.45	11.14	-10.10	15.04	23.34	-21.11
208.50	201.50	61.44	6.73	-8.61	12.26	19.95	-22.30
210.50	201.50	74.54	13.53	-1.47	13.61	18.25	-3.11
212.50	201.50	66.44	16.05	0.12	16.05	24.15	0.21
214.50	201.50	54.45	12.13	-0.72	12.15	22.32	-1.70

ACKNOWLEDGEMENTS

I would like to thank Dr. S M Scarrott for his encouragement, assistance and unceasing moral guidance offered at all times, and also for his provision of the data. I would also like to express my appreciation to Dr. R G Bingham of the Royal Greenwich Observatory for his tireless enthusiasm and encouragement.

Professor B Bransden is thanked for making the facilities of the department readily available, as is the Durham University Standing Committee for Research Awards for the provision of the studentship. Brian Lander and the staff of the Computer Unit are also thanked for their patience and help.

Finally, I would like to thank Mrs. Mellanby for her excellent typing and my landlady, Ms. S M Byrne, for her patient transcription of my diagrams.